Kinetics of Precipitation Reactions

By
Pedro Eduardo José Rivera Díaz del Castillo
Selwyn College, University of Cambridge

Department of Materials Science and Metallurgy
Pembroke Street, Cambridge CB2 3QZ

A dissertation submitted for the
degree of Doctor of Philosophy at the
University of Cambridge
January 2002

Preface

This dissertation is submitted for the degree of Doctor of Philosophy at the University of Cambridge. The research described herein was conducted under the supervision of Professor H. K. D. H. Bhadeshia in the Department of Materials Science and Metallurgy, University of Cambridge, between October 1998 and January 2002.

This work is to the best of my knowledge original, except where acknowledgements and references are made to previous work. Neither this, nor any substantially similar dissertation has been or is being submitted for any other degree, diploma or other qualification at any other university. This dissertation contains less than 60,000 words.

Part of this work has been presented in the following publications:

Rivera-Díaz-del-Castillo, P. E. J. and Bhadeshia, H. K. D. H. [2001], *Growth of needle and plate shaped particles: theory for small supersaturations, maximum velocity hypothesis*, *Materials Science and Technology*, **17**, 25–29.

Rivera-Díaz-del-Castillo, P. E. J. and Bhadeshia, H. K. D. H. [2001], *Theory for growth of spherical precipitates with capillarity effects*, *Materials Science and Technology*, **17**, 30–32.

Rivera-Díaz-del-Castillo, P. E. J. and Bhadeshia, H. K. D. H. [2002], *Theory for growth of needle–shaped particles in multicomponent systems*, *Metallurgical and Materials Transactions A*, **33A**, in press.

Rivera-Díaz-del-Castillo, P. E. J. [2002], *Precipitate coarseining in multicomponent systems*, *Scripta Materialia*, in press.

P. E. J. Rivera Díaz del Castillo

January 2002

Acknowledgements

I am indebted to Professors D. J. Fray and A. H. Windle for the provision of laboratory facilities in the Department of Materials Science and Metallurgy at the University of Cambridge. I would like to express my sincere thanks to my supervisor Professor Harry Bhadeshia for his guidance and great enthusiasm.

I am indebted to The Mexican National Council of Science and Technology (CONACYT) and the Cambridge Overseas Trust for financial support. I want to express my gratitude to the Committee of Vice–Chancellors and Principals of the Universities of the United Kingdom for the Overseas Research Studentship.

I would also like to thank the past and present members of the Phase Transformations and Complex Properties Research Group for their help and friendship, in particular to Miguel Yescas, Harsha Lalam, Thomas Sourmail, Marimuthu Murugananth, Shingo Yamasaki, Gareth Hopkin, Francisca Caballero, Hiroshi Matsuda, Carlos Capdevila, Toshihiro Tsuchiyama, Frank Tancret, Carlos Garcia, Dominique Carrouge, Pascal Jacques and Nick Tyas. It was an enormous pleasure to work with them.

Finally, I take this opportunity to express my gratitude to my family for their unfailing encouragement and support, specially my parents Jose and Zita. Thanks to Ralucuţa for everything.

Abstract

There have been considerable advances in recent years in the understanding of solid–state phase transformations. This has involved the creation and application of new knowledge over a large range of length scales, leading to descriptions which have predictive power and sufficient complexity to deal with industrial practice. The subject is commonly known as "modelling". The application of modelling to steels of the kind used in industry has also highlighted the shortcomings of kinetic theory. The purpose of the work presented in this thesis was to tackle some of the difficulties by developing new theory and concepts.

The thesis begins with an introduction to previous work and to the importance of precipitation in commercial steels. The theory associated with precipitation reactions is described in Chapter 2, especially for the growth of particles which are spherical, needle–shaped or plate–shaped. It is claimed that the published work does not deal adequately with the growth of such particles in multicomponent systems from the point of view of capillarity and diffusion.

Spherical particles have the unique property that the size, and the radius of the front at which growth occurs, are described by a single parameter. There has never, therefore, been a mathematical solution for the growth of a sphere with capillarity taken into account. This theory is developed in Chapter 3, albeit with a critical approximation, whose effect is explored by numerical simulation. The solution is also extended for multicomponent alloys in both the dilute and concentrated forms (Chapters 5, 6).

For needles and plates, where the tip radii and lengths are separate parameters, exact solutions are possible (even for multicomponent systems), as described in subsequent chapters. There are exciting conclusions, such as in some cases it is not possible to apply a maximum growth criterion to select a tip radius.

The final chapter deals with the application of theory to both precipitation and coarsening phenomena and the thesis concludes with a description of future work and a systematic presentation of the computer software associated with the work.

Table of Contents

Nomenclature

$(A]$, $[A)$	vector **A** expressed as a row or column matrix, respectively
$[A]$	square matrix **A**
A	coefficient for parabolic coordinates in differential equation solution
A_h	coefficient in Hillert growth model
A_i	A coefficient of element i
c	alloy chemical composition
C	system number of components
c_i	concentration field of element i in the matrix
c'	concentration field in the matrix for constant concentration interface
$c^{\alpha\beta}$	solute concentration of α in equilibrium with β
$c^{\alpha\theta}$	solute concentration of α in equilibrium with θ
$c^{\beta\alpha}$	solute concentration of β in equilibrium with α
c^{θ}	solute concentration of θ
$c_i^{\beta\alpha}$, $c_{ri}^{\beta\alpha}$	concentration of solute i in β in equilibrium with α for a flat and a curved interface, respectively
$c_i^{\alpha\beta}$, $c_{ri}^{\alpha\beta}$	concentration of solute i in α in equilibrium with β for a flat and a curved interface, respectively
$\overline{c}$	average concentration of solute in the far field
$\overline{c}_i$	i component average concentration of solute in the far field
c_n^j	matrix concentration in node n at j time interval
$c_{i,n}^j$	i solute matrix concentration in node n at j time interval
C	number of components present in the alloy
c_j^0	j component alloy concentration
$\overline{c}_0^{\alpha\beta}$	initial supersaturation $c_j^0 - c_j^{\alpha\beta}$
$c_r^{\alpha\beta}$	capillarity corrected concentration of α in equilibrium with β
$c_r^{\beta\alpha}$	capillarity corrected concentration of β in equilibrium with α
C_1	proportionality constant to determine effective diffusion distance
C_2	arbitrary constant in the Hillert growth model
D	diffusion coefficient
D_i	diffusion coefficient of element i in the matrix
d	needle thickness
d_p	adimensional half needle thickness for dissolution

$\overline{d}$	average particle distance
D_o	diffusivity
$D_{o\mathrm{C}}, D_{o\mathrm{Mo}}$	diffusivity of C and Mo
E_1	exponential integral function
erfc	complementary error function
f	radius distribution function for precipitate coarsening
f_o	focal distance
f_p	transformed focal distance
f_1	auxiliary function to solve sphere growth
g	spherical precipitate growth rate
g_p	needle and plate lengthening rate
g^*	auxiliary function for needle growth
$g^\diamond$	auxiliary function for plate growth
g_c	growth rate at which growth stops
g^α	atomic Gibbs energy of the α phase
g^β_∞	atomic Gibbs energy of a β phase particle with an infinite radius of curvature
g^β_r	atomic Gibbs energy of a β phase particle with a radius of curvature r
ΔG	energy change when a nucleus is formed
ΔG_v	chemical free energy change (per unit volume) for the formation of a nucleus
G^*	critical free energy to from a nucleus
G^α	molar Gibbs energy of the alpha phase
h	Planck's constant
H	curvature
H_{2m}	Hermitian polynomial
I	nucleation rate per unit volume
IC	interface composition contours
IS	interface saturation contours
IV	interface velocity contours
$I_m$erfc	normalised integral error function
k	Boltzmann's constant
K	coarsening rate constant
k_1, k_2	constants to linearly relate volume fractions
l	needle length
L^o_n	Laguerre polynomial

m	arbitrary constant in the Hillert model
n	exponent of spherical growth constant
n	number of atoms
n_i	number of atoms of component i
N	number of precipitate particles
N_β	number density of nucleation sites for a precipitate β
N_β^l	number density of nucleation sites for a large precipitate β
N_θ	number density of nucleation sites for cementite
$N_\bullet$, $N_\circ$	number density of $\bullet$ and $\circ$ particles per unit length
N_o	initial number of sites in which nucleation occurs
N_0	number of nodes in matrix
N_1, N_2	functions to account for curvature and interface kinetics, respectively
O	area of an interface
O$\{x\}$	correction term of the order of magnitude of x
p	Péclet number
P	pressure
P^α, P^β	pressure of α and β phase, respectively
P	number of phases present in the system
p_i	Péclet number of element i
q^*, q	parameter to measure importance of interface kinetics and diffusion effects in needles and plates, respectively
Q	activation energy for volume diffusion
Q^*	activation energy barrier to the transfer atoms across the interface
r	radius of a particle
r_1, r_2	particle principal radii of curvature
r_i	radius of a flat interface
$\overline{r}$	average particle radius
$\overline{r}_r$	average reference particle radius for coarsening
r^*	critical radius to form a nucleus
r_c	radius at which growth stops
$r_{c,i}$	critical radius to form a nucleus with element i
R	radial distance in the parabolic and spherical coordinate system
$\overline{R}$	average needle interface radius
R_u	universal gas constant

R_{XZ}	radius curvature at any point of the parabola interface
R_1, R_2	complex functions in needle growth model
R_1', R_2'	derivatives of R_1 and R_2 functions
s_{C}, s_{Mo}, s_i	matrix composition shifts of C, Mo and i components
s^{α}	activity coefficient in the matrix
s_r^{α}	activity coefficient when capillarity is present
s_{ri}^{α}, s_i^{α}	i component activity coefficients when capillarity is present and absent, respectively
$\overline{S}_i^{\alpha}$, $\overline{S}_i^{\beta}$	i component partial molar entropy of α and β phase, respectively
S_1, S_2	complex functions in plate growth model
S_1', S_2'	derivatives of S_1 and S_2 functions
t	time
t_c	time for cementite enrichment
T	temperature
t_1, t_2	terms in needle boundary condition
T_1	homogenisation temperature
T_3	tempering temperature
T_S	solidification temperature
T^{α}, T^{β}	Temperature of α and β phase, respectively
u	auxiliary function for needle average radius
v_c, v_d	dissolution velocity for cementite and Mo_2C
V	total volume of the system
V_N	needle volume
V_s	small particle volume
V_l	large particle volume
$\overline{V}_i$	partial molar volume of component i
$\overline{V}^{\beta}$	partial molar volume
V_m	precipitate molar volume
V^{β}	volume transformed to β in a precipitation reaction
V_e^{β}	extended volume of the β phase
v_τ	volume of a transformed region after the induction period of precipitation
v^{β}	atomic volume of β phase
V^{α}	untransformed volume of α during precipitation reaction
w	order of curvature of a particle

x	position at any point in the matrix
x_θ	cementite thickness
x_p, y_p	parabolic transformed variables
x_1, x_2	directions along and perpendicular to the growth direction in Hillert model
X, Y	fixed Cartesian coordinates
y^D	effective diffusion distance for spherical growth
z	transformed volume fraction of all phases present
z^e	extended volume fraction of all phases present
Z	distance along which concentration varies
Z^*	position of the interface
α	matrix
α_j	growth parameter of particles of j dimensions
α_{3i}	i component grow parameter for three dimensional particle
α_j^*	natural growth parameter for j-dimensional growth
β	product of the precipitation reaction
γ	parabolic coordinate for needle precipitate
δ	parabolic coordinate for needle precipitate
Δ	alloy cumulative supersaturation
Δ_0	initial supersaturation prior to coarsening
Δc_k^α, Δc_k^β	$c_k^{\alpha\beta}\{r\} - c_k^{\alpha\beta}$, $c_k^{\beta\alpha}\{r\} - c_k^{\beta\alpha}$
$\Delta c_k^{\alpha\beta}$	$c_k^{\beta\alpha}\{r\} - c_k^{\alpha\beta}\{r\}$
$\Delta \overline{c}_k^{\alpha\beta}$	$\overline{c}_k - c_k^{\alpha\beta}$
Δc_r^β	$c^{\beta\alpha}\{\overline{r}_r\} - c^{\beta\alpha}$
$\Delta \overline{V}_i$, $\Delta \overline{S}_i$	difference between partial molar volume and entropy of α and β phases, respectively
Λ	interactions of solute species in β as curvature changes
Λ_r	reference value of Λ for a given radius r
γ_e	Euler's constant
Γ	capillarity constant
Γ_i	capillarity constant for element i
Γ_D	gamma function
ζ	volume fraction of product transformed
ζ_i	volume fraction of transformed precipitate i
ζ_i^e	extended volume fraction of precipitate i

η	parabolic coordinate for plate precipitate
μ_o	interface kinetics coefficient
μ^j, μ_r^j	chemical potential in j phase for a flat and curved interface, respectively
μ_i^j, μ_{ir}^j	chemical potential of component i in j phase for a flat and curved interface, respectively
$\mu_{o,i}$	interface kinetics coefficient of element i
ν_1	rate at which an individual site becomes a nucleus
ξ	parabolic coordinate for plate precipitate
σ	surface energy of the precipitate–matrix interface
σ^j	surface energy of the j precipitate–matrix interface
τ	induction period for a precipitation reaction
θ	cementite
$\overline{\varphi}$	volume fraction during coarsening
φ_v	limiting value of precipitate volume fraction during coarsening
φ_j	degree of advancement of a moving interface
Ψ	confluent hypergeometric function of the second type
Ω	dimensionless supersaturation
Ω^I	β energy increase as a curvature and change in chemical potential are present
Ω_{si}	spherical supersaturation for component i
Ω_{pi}	plate and needle supersaturation for component i
ϕ	auxiliary function to solve sphere growth problem
Φ	coarsening resistance of the precipitate

CHAPTER ONE

Introduction

1.1 Models for precipitation kinetics

The improvement of commercial alloy properties relies on an accurate prediction of the microstructure. A popular method for alloy strengthening is precipitation hardening. Long tempering heat treatments frequently lead to coarsening, which usually causes a lowering of the alloy yield strength and possibly its embrittlement. Therefore, it is useful to develop models to predict the kinetics of precipitation in order to control and optimise those properties.

In the case of steels, which are the most commonly available structural materials, complex sequences of precipitates may form. An example of such a case is shown in Fig. 1.1 for 2.25Cr1Mo [Baker and Nutting, 1959], where M stands for a metallic component. The variety of precipitates that are present at different stages of tempering can affect the properties of that steel.

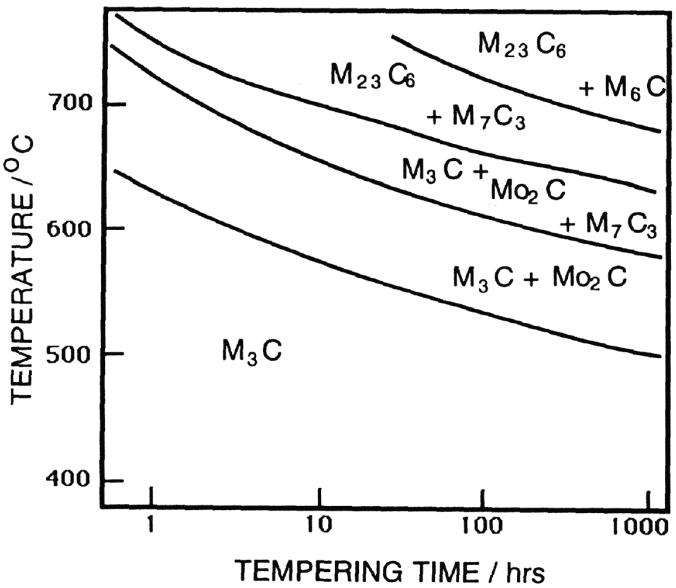

Fig. 1.1: Kinetics of precipitation in 2.25Cr1Mo [Baker and Nutting, 1959].

A number of attempts to predict kinetics of precipitation reactions in steels have been published. Table 1.1 shows a selected review of the modelling done for alloys where a single precipitate was taken into account [Hall *et al.*, 1972; Saito *et al.*, 1988; Akamatsu *et al.*, 1992; Liu and Jonas, 1988; Miyahara *et al.*, 1995; Okamoto and Suehiro, 1998; Gustafson *et*

al., 1998; Lee *et al.*, 1991a,b,c]; it reveals that most works deal with the precipitate as an equilibrium phase and some of them use overall transformation theory based on the extended volume concept [Kolmogorov, 1937; Johnson and Mehl, 1939; Avrami, 1939, 1940, 1941]. In general, the application of these models relies on a number of semi–empirical parameters which do not always have a clear meaning, and thus their validity is restricted to the alloys to which they were applied. Furthermore, all of them can cope with only one precipitation reaction occurring at any instance, as an equilibrium phase. In practice, many reactions may occur simultaneously and non–equilibrium phases are often important (Fig. 1.1). For example, in heat–resistant steels the precipitation and dissolution processes continues during service at elevated temperature as equilibrium is approached. The conventional models listed in Table 1.1 cannot be applied directly to such simultaneous reactions in practical steels.

Olson [1997] has proposed an integral approach for alloy design, which includes simultaneous precipitation and overall microstructure prediction in steels. His method is aimed to design alloys considering a hierarchical analysis ranging from the atomic to the microstructural level; the goal is to predict a number of parameters ranging from interfacial energies to precipitation rate constants, but it requires extensive experimental validation prior to utilisation.

Simultaneous precipitation has recently been modelled by Robson and Bhadeshia [1997b] and Fujita and Bhadeshia [1999, 2001] in power plant and secondary hardening steels, respectively, by the calculation of nucleation and growth kinetics, together with a scheme for overall kinetics. However, their models are not generally capable of predicting particle size and size–distribution for non–spherical precipitates, on which strengthening methods rely. Furthermore, they contain a number of approximations which limit their application.

1.2 Areas of improvement of the theory and aims of this work

The current state of the theory is shown schematically in Fig. 1.2 †, it is seen that important advances in the treatment of overall transformation kinetics have been achieved, and success in treating the multicomponent growth of spherical particles has been obtained. Modelling of needle–shaped particles has been developed, but the theory is unable to predict their aspect ratio, and therefore its shape. Ostwald ripening theory has been applied but assumes no change in precipitate composition. The way these problems have been tackled in the present thesis is listed next.

† The existing model is defined as the fundamental concepts that have been applied commonly in industry. These are presented in Chapter 2.

Reference	System	Conditions	Comments
Hall *et al.*, 1972	Mo_2C in Fe–0.11C–1.95Mo	Isothermal heat treatment	Particle lengthening rate was calculated using Zener–Hillert equation and by adjusting the diffusion coefficient
Saito *et al.*, 1988	NbC in HSLA	Deformation at high temperatures	Volume fraction of NbC was calculated by classical nucleation and growth using KJMA theory
Akamatsu *et al.*, 1992	NbC in HSLA	Deformation at high temperatures	Volume fraction and size of NbC were calculated by classical nucleation and diffusion controlled growth
Liu and Jonas, 1988	TiC in HSLA	Deformation at high temperatures	Precipitation starting time was determined experimentally using a relaxation test
Miyahara *et al.*, 1995	Laves in Fe–10Cr	Tempering	Volume fraction of Laves phase was calculated using the KJMA theory
Okamoto and Suheiro, 1998	Nb(C,N) in HSLA	Isothermal heat treatment	Volume fraction and size of NbC calculated by classical nucleation diffusion–controlled growth and capillarity
Gustafson *et al.*, 1988	(V,Nb)N in Fe–10Cr	Isothermal heat treatment	Size of (V,Nb)N in ripening was calculated by multicomponent diffusion
Lee *et al.*, 1991	Mo_2C in several secondary harde–ning steels	Tempering	Size of Mo_2C in ripening calculated using LSW theory

Table 1.1: List of of models where the kinetics of one precipitate are taken into account. HSLA stands for High Strength Low Alloy Steel, KJMA stands for Kolmogorov–Johnson–Mehl–Avrami theory and LSW stands for Lifshitz–Slyozov–Wagner ripening theory.

Growth of spheres

The theory for precipitate growth is now capable of predicting the thickening of spher-

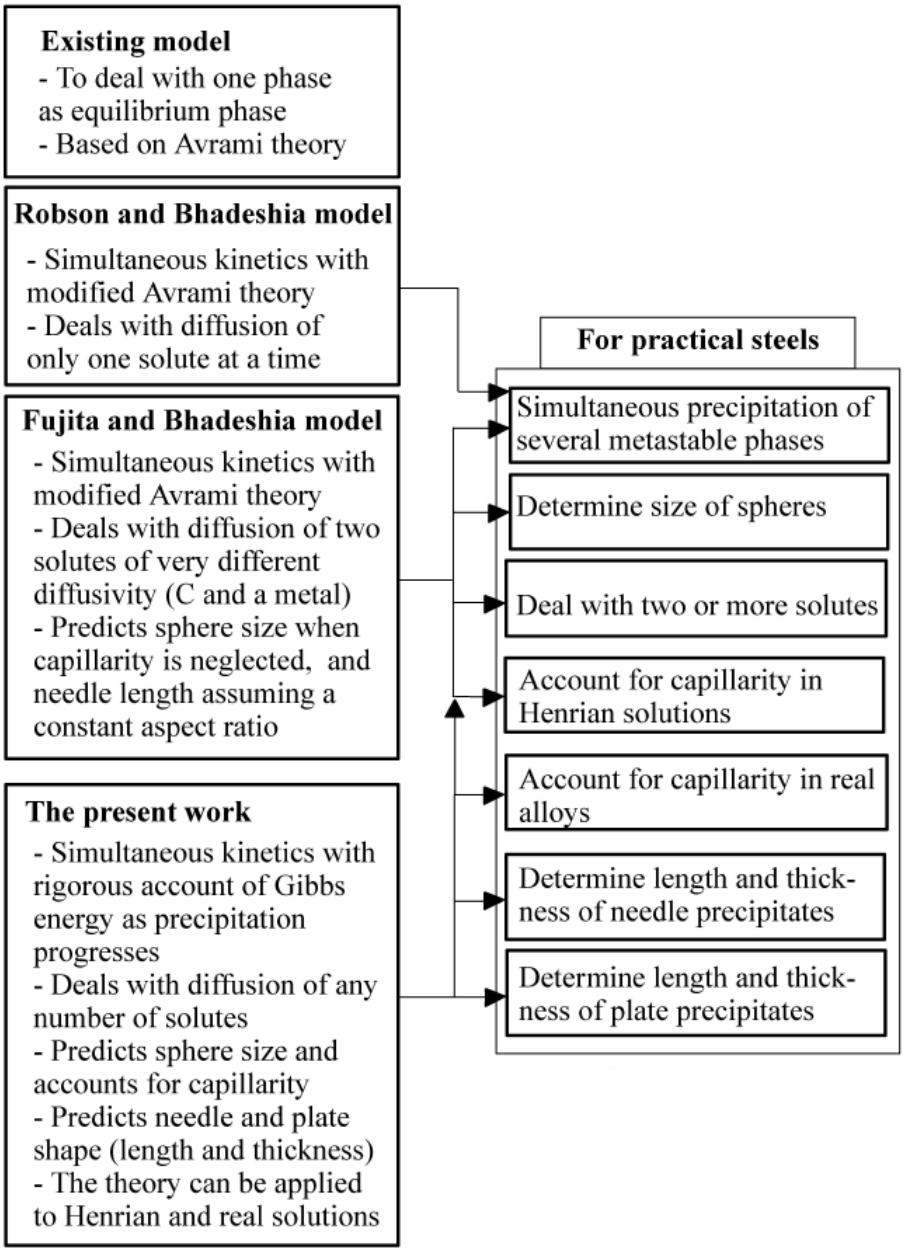

Fig. 1.2: Schematic illustration of activities for modelling precipitation reactions.

ical precipitates with one [Zener, 1949] or several solutes [Coates, 1972, 1973a,b] in Henrian solutions. However it is necessary to account for capillarity during growth. In this work an approximate analytical and a numerical solution are provided to obtain the kinetics of precipitation reactions accounting for multicomponent diffusion and capillarity effects in Henrian and concentrated solutions.

Growth of needle and plate–shaped particles

A number of treatments for needle and plate–shaped precipitate growth are available, the

most comprehensive theory is from Trivedi [1970a,b], who assumes the needles approximate a paraboloid of revolution, and plates a parabolic cylinder. This theory is, however, restricted to the diffusion of one solute in Henrian solutions. In this work it is extended for multicomponent capillarity and interface kinetics effects in Henrian and real solutions.

Ostwald ripening

The Ostwald ripening theory developed by Lifshitz and Slyozov [1961] and Wagner [1961] has been derived under the assumption that no change in composition of the precipitate phase occurs during the coarsening process, this assumption is removed and new relationships are derived.

Model

A new model has been developed to implement some of the new concepts outlined above; this has been applied to the needle–shaped Mo_2C nucleation, growth and coarsening in the secondary hardening steel Fe–0.11C–1.95Mo wt.%. The results obtained include precipitate length, thickness and the number of particles at each stage of growth; each particle is assumed to be in equilibrium with the matrix at any stage of growth.

1.3 Summary

Although a great deal of experimental work has been performed to characterise the precipitation process and although semi–empirical models have been applied successfully, the current stage of the theory demands a great deal of improvement. This developments are essential for a deeper understanding of the precipitation kinetics, especially in commercial alloys.

CHAPTER TWO

Theory for precipitation reactions

2.1 Introduction

Accurate prediction of precipitation kinetics requires the use of thermodynamics, transport theory and statistical methods to determine particle dispersions. These fundamental concepts are presented in this chapter with emphasis on areas where improvement is required.

2.2 Preliminary concepts

An example of a precipitation reaction is when a new phase β is formed from a supersaturated solution α, obtained by rapid cooling of an alloy of composition c, from a temperature T_1 (Fig. 2.1) into the two-phase field.

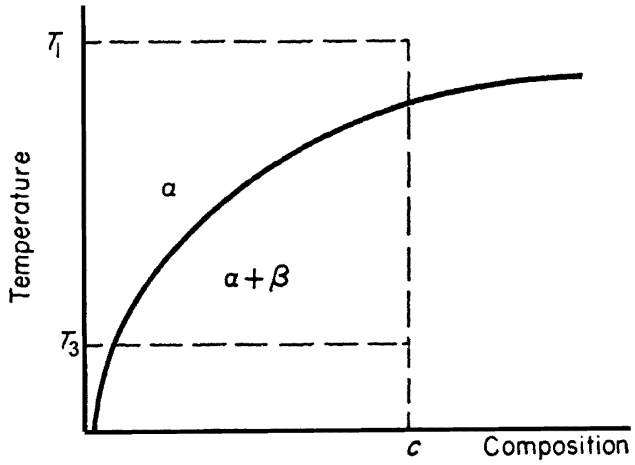

Fig. 2.1: Precipitation of phase β from solid solution α [Cottrell, 1995].

Since α and β have different equilibrium compositions, precipitation causes concentration gradients at the β/α boundaries. The resulting concentration profiles are described in terms of three different concentrations: $c^{\beta\alpha}$, which is the solute concentration in the precipitate in equilibrium with α; $c^{\alpha\beta}$, which is the solute concentration in the matrix in equilibrium with β; and $\overline{c}$, which is the average concentration of solute in the matrix in the "far field" (Fig. 2.2). The abscissa in Fig. 2.2 represents the distance perpendicular to the precipitate boundary.

The presence of the new phase β will modify the mechanical properties of the alloy. When dealing with steels of the type Fe-C-X (where X is a substitutional solute), quenching from

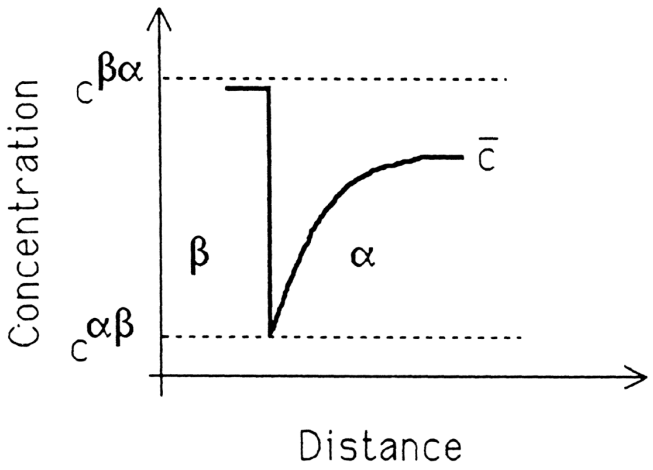

Fig. 2.2: Concentration distribution around precipitate boundary.

the austenite phase field gives supersaturated martensite, which in steels tends to be brittle. Therefore, the alloy is tempered at temperatures around 400°C which leads to the precipitation of iron carbides and an improvement in toughness together with a reduction in strength. To precipitate more stable alloy carbides requires heat treatment at a higher temperature (*e.g.* 600°C). Such carbides appear in power plant steels which can be in service for more than 30 years at temperatures around 600°C. It is thus required to have expressions for precipitate equilibrium; these come from thermodynamics theory.

2.3 Theory of nucleation

2.3.1 The classical theory

Nucleation is the process through which the smallest stable particle of a new phase is formed. The embryo develops by statistical fluctuations involving individual atom additions, and evolves from a monomer (*i.e.* atom) to a critical size configuration known as *critical radius* whose growth leads to a reduction in free energy [Aaronson and Lee, 1978].

Assuming that the precipitate nucleates as a spherical particle of radius r, a fluctuation of structure and composition leads to a change in the free energy by an amount ΔG given by

$$\Delta G = \frac{4}{3}\pi r^3 \Delta G_v + 4\pi r^2 \sigma \tag{2.1}$$

where ΔG_v is the chemical free energy change per unit volume and σ is the surface free energy per unit area of the precipitate–matrix interface. The maximum value of ΔG with r gives the activation free energy G^* to form a nucleus of critical radius r^*:

$$G^* = \frac{16\pi\sigma^3}{3\Delta G_v^2}, \quad r^* = \frac{2\sigma}{\Delta G_v} \tag{2.2}$$

If V_m, R_u and T are defined as the precipitate molar volume, universal gas constant and temperature, respectively, the activation free energy G^* can be expressed in terms of the precipitate and matrix concentrations as $\Delta G_v = (1/V_m) R_u T \ln\{\overline{c}/c^{\alpha\beta}\}$ [Christian, 1975], from which a relationship between r^* and the concentrations can be obtained:

$$\frac{r^* R_u T}{2\sigma V_m} = \frac{1}{\ln\{\overline{c}/c^{\alpha\beta}\}} \tag{2.3}$$

and the rate of nucleation is

$$I = N_\beta \frac{kT}{h} \exp\left\{-\frac{G^* + Q^*}{kT}\right\} \tag{2.4}$$

where Q^* is the activation energy required to transfer atoms across the precipitate interface, N_β is the number density of nucleation sites for the precipitate, h and k are the Planck and Boltzmann constants, respectively.

Equations [2.2–2.4] describe the kinetics of the nucleation process and have been widely used. However, one of the difficulties associated with their application is the choice of interfacial energy σ. A typical critical nucleus size may be in the range 2-50 nm and it could be argued that σ should depend on the particle size itself [Christian, 1975]. In the solid-state σ may reasonably be expected to depend also on the orientation of the interface plane. Detailed information of this kind is simply not available and it is usual therefore to assume a constant value of σ to describe the entire nucleation process. This drastic assumption adds enormous uncertainty to any calculation of nucleation rates, and certainly does not inspire confidence.

However, recent exciting work by Miyazaki and co-workers [1996, 1999] has demonstrated that the approximation may in fact be justified. Miyazaki *et al.* measured by direct observation the nucleus sizes in concentration gradients (*i.e.*, as a function of the driving force) and demonstrated that a single interfacial energy could describe all data irrespective of the particle size by following equation [2.3]. The results were obtained by measuring the critical radii of nucleated particles as a function of supersaturation, and are illustrated in Fig. 2.3, where the solid line represents the normalised radius $r^* R_u T/(2\sigma V_m)$, and the data corresponds to the systems Cu-Ti, Ni-Al, Cu-Co and Ni-Si [Miyazaki, 1999]. The results match equation [2.3] when the proper value of σ is selected.

2.3.2 Surface energy considerations

When atoms are transferred from α to the β phase, there is an additional energy term due to the increase in surface area of the β particles. If dn atoms are transferred from α to β, and the corresponding change in interfacial area is dO, the additional energy term is σdO,

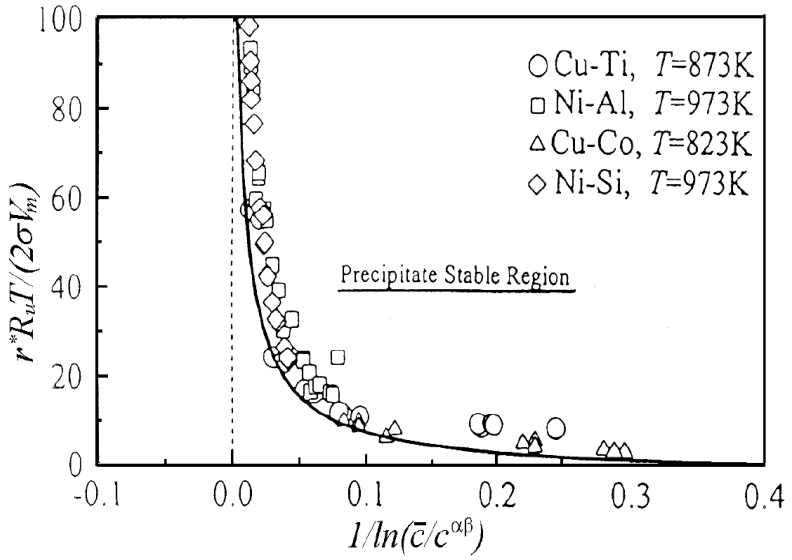

Fig. 2.3: The critical particle sizes scaled with supersaturation of solute atom for four alloy systems on the basis of equation [2.3], after Miyazaki [1999]

where σ is the surface energy per unit area of the α/β interface, and O is the area of the interface. If g^{β}_{∞} is the Gibbs energy per atom that corresponds to the β phase with an infinite radius of curvature at the interface, and g^{α} the Gibbs energy per atom that corresponds to the matrix, there will be an increase in g^{β}_{∞} due to the surface energy term; *i.e.* g^{β}_{∞} will transform to $g^{\beta}_{r} = g^{\beta}_{\infty} + \sigma(dO/dn)$, where g^{β}_{r} stands for the energy of β phase with a curved interface. The new equilibrium compositions are given by the points of contact of the tangent common to the curves of g^{α} and g^{β}_{r} against the concentration of solute c.

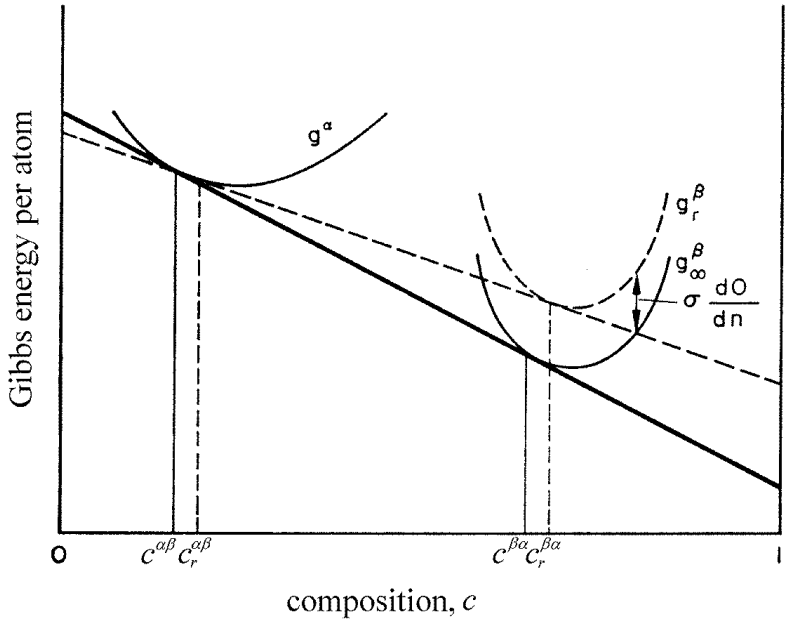

Fig. 2.4: Increase of the Gibbs energy due to the surface energy of the particle [Christian, 1975]

As shown in Fig. 2.4, there will be a change in the equilibrium composition of the matrix as an effect of the curvature. For an infinite radius of curvature, the original composition of the matrix would be $c^{\alpha\beta}$, but interface curvature increases it to $c_r^{\alpha\beta}$. Thus, the change in composition is $\Delta c_r^{\alpha\beta} = c_r^{\alpha\beta} - c^{\alpha\beta}$, which can be expressed using Henry's law [Christian, 1975]:

$$\Delta c_r^{\alpha\beta} = c^{\alpha\beta} \frac{\sigma}{kT} \left(\frac{dO}{dn} \right) \left(\frac{1 - c^{\alpha\beta}}{c^{\beta\alpha} - c^{\alpha\beta}} \right) \tag{2.5}$$

To evaluate the term $(\frac{dO}{dn})$, it is noted that for spherical particles $dO = (2v^\beta/r)dn$, where v^β is the atomic volume of the β phase, and r is the radius of the spherical particle. Thus:

$$\frac{dO}{dn} = \frac{2v^\beta}{r} \tag{2.6}$$

This is an important relation which will be used in subsequent growth theories. A more general case is given by Christian [1975]:

$$\frac{dO}{dn} = v^\beta (r_1^{-1} + r_2^{-1}) \tag{2.7}$$

where r_1 and r_2 are the principal radii of curvature.

The capillarity constant is defined as:

$$\Gamma = \left(\frac{\sigma v^\beta}{kT} \right) \left(\frac{1 - c^{\alpha\beta}}{c^{\beta\alpha} - c^{\alpha\beta}} \right) \left(1 + \frac{d \ln s^\alpha}{d \ln c} \right) \tag{2.8}$$

where s^α is the activity coefficient of the solute in the matrix α. For dilute solutions or solutions which obey Henry's law, s^α is constant, so that Γ becomes

$$\Gamma = \left(\frac{\sigma v^\beta}{kT} \right) \left(\frac{1 - c^{\alpha\beta}}{c^{\beta\alpha} - c^{\alpha\beta}} \right) \tag{2.9}$$

and for sufficiently small values of $c^{\alpha\beta}$

$$\Gamma = \frac{\sigma v^\beta}{kT(c^{\beta\alpha} - c^{\alpha\beta})} \tag{2.10}$$

This form has been used by Trivedi [1970a,b] as reviewed in next sections.

Thus, following Henry's law, the concentration in the matrix adjacent to a spherical particle, including the capillarity effect, is

$$c_r^{\alpha\beta} = \left(1 + \frac{2\Gamma}{r} \right) c^{\alpha\beta} \tag{2.11}$$

A discussion of the concentration change for needles and plate type precipitates will be presented in later sections.

2.4 Theories of diffusion–controlled growth in binary systems

2.4.1 Zener's theory

The presence of a concentration field around the particle (Fig. 2.2) must induce diffusion; the rate of diffusion determines the precipitate growth rate. To describe this processes mathematically, a function $c\{x,t\}$ is defined, this represents the concentration at any point x in the matrix, assuming one dimensional growth along x. Thus, the diffusion equation (Fick's second law) has to be satisfied:

$$\frac{\partial c\{x,t\}}{\partial t} = D\nabla^2 c\{x,t\} \tag{2.12}$$

where, one of the boundary conditions of this equation is $c\{x,0\} = \overline{c}$, where $\overline{c}$ is the average solute concentration in the matrix, and D is the diffusion coefficient. Data for D can often be found in the published literature, *e.g.* for diffusion in iron, Fridberg *et al.* [1969] have published an extensive list of element diffusion coefficients.

A solution to the diffusion equation for precipitate growth in a spherical system was derived by Zener [1949]. Assuming a particle radius increase proportional to $t^{1/2}$ (parabolic growth), and a radial symmetry, the concentration field can be expressed by the function $c\{t,R\}$, where R is the radial distance in a spherical coordinates system. The general diffusion equation is then reduced to

$$\frac{\partial c}{\partial t} = D\left(\frac{\partial^2 c}{\partial R^2}\right) + (j-1)\frac{D}{R}\left(\frac{\partial c}{\partial R}\right) \tag{2.13}$$

where $j = 1, 2, 3$ for one, two or three–dimensional growth. Considering that the interface is at $R = r$, the boundary conditions for equation [2.13] are

$$c\{t,r\} = c^{\alpha\beta}, \quad c\{0,R\} = \overline{c}$$

Zener showed that the concentration varied with distance as follows:

$$c = \overline{c} + (c^{\alpha\beta} - \overline{c})\frac{\varphi_j\{R/(Dt)^{1/2}\}}{\varphi_j\{r/(Dt)^{1/2}\}} \tag{2.14}$$

where φ_j measures the degree of advancement of a moving interface and is given by

$$\varphi_j\{x\} = \int_x^\infty \xi^{1-j} e^{(-\xi^2/4)} d\xi$$

The kinetic equation that describes the advance of the interface is

$$g(c^{\beta\alpha} - c^{\alpha\beta}) = D\left(\frac{\partial c}{\partial R}\right)_{R=r} \tag{2.15}$$

where g is the growth rate of the particle. The solution to equation [2.15] using equation [2.14] is

$$r = \alpha_j (Dt)^{1/2} \tag{2.16}$$

where α_j is an adimensional growth parameter given by

$$(\alpha_j)^j = \frac{2\Omega e^{(-\alpha_j^2/4)}}{\varphi_j\{\alpha_j\}}$$

and Ω is the dimensionless supersaturation given by the relation

$$\Omega = \frac{\overline{c} - c^{\alpha\beta}}{c^{\beta\alpha} - c^{\alpha\beta}}$$

Zener obtained several asymptotic approximations of the value of α_j for one and three dimensions ($j = 1, 3$), $\alpha \gg 1$ and $\alpha \ll 1$ [Zener, 1949].

Another approximation is to consider $\partial c/\partial R$ as constant (Fig. 2.5). As a result of this assumption Zener [1949] obtained a "natural" growth parameter α_j^*, which expresses the growth law for a plane interface. This approximation has a prominent place in literature.

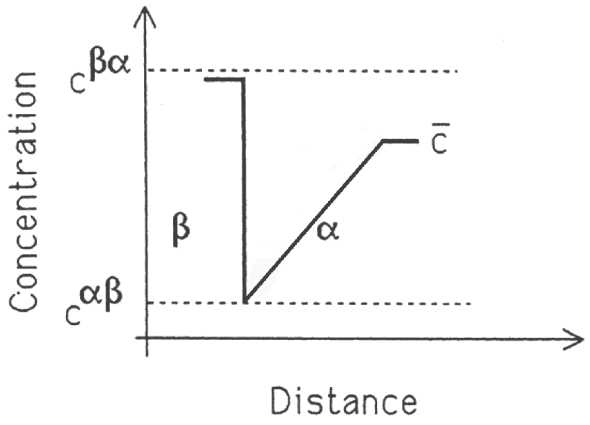

Fig. 2.5: Constant gradient approximation Zener [1949]

2.3.2 Zener model for needles and plates

Another important theory for needles and plates of constant diameter or thickness has been given by Zener–Hillert. In this model, equation [2.15] is simplified as

$$g(c^{\beta\alpha} - c^{\alpha\beta}) = \Delta c \frac{D}{y^D} \tag{2.17}$$

where $\Delta c = \overline{c} - c_r^{\alpha\beta}$ and y^D is an "effective diffusion distance" which is assumed to be proportional to r, *i.e.* $y^D = C_1 r$, where C_1 is a proportionality constant; because solute is partitioned

to the sides of the needle or plate, it is assumed that y^D remains constant with time for a needle or plate of a given thickness. Given that $c_r^{\alpha\beta}$ is the capillarity corrected concentration (equation [2.16]) and defining r_c as the radius at which growth stops

$$r_c = 2c^{\alpha\beta}\Gamma/(\overline{c} - c^{\alpha\beta}) \tag{2.18}$$

the growth rate is written as

$$g = \frac{D\Omega}{C_1 r}\left(1 - \frac{r_c}{r}\right) \tag{2.19}$$

In this model, the needle plate tip radius is fixed during the stages of growth.

The growth rate given by [2.19] is zero for $r = r_c$. The maximum growth rate occurs when $r = 2r_c$, and is given by

$$g = \frac{D\Omega}{4C_1 r_c} \tag{2.20}$$

Zener assumed that the observed velocity will be the maximum possible velocity, given by equation [2.20] [Zener, 1946], and correspondingly that the diameter of a needle or the thickness of a plate will be given by $2r = 4r_c$.

2.4.3 Hillert model

Hillert [1957] improved the solution given by Zener for needles and plates, by considering an origin in the moving boundary using x_1 and x_2 as coordinates in the direction of growth and normal to the plane of the needle or plate respectively (Fig. 2.6). In this case, the diffusion equation can be expressed as

$$D\left[\left(\frac{\partial^2 c}{\partial x_1^2}\right) + \left(\frac{\partial^2 c}{\partial x_2^2}\right)\right] + g\left(\frac{\partial c}{\partial x_1}\right) = 0 \tag{2.21}$$

The solution to the differential equation is

$$c - c^{\alpha\beta} = \int_0^\infty A\{b\}\exp\{(-\varrho x_1)\}\cos\{bx_2\}db \tag{2.22}$$

and the problem is reduced to the determination of the coefficients $A\{b\}$, but the boundary conditions are not compatible with the existence of a steady–state solution. Hillert avoids the difficulty by specifying an internal condition which satisfies the boundary conditions only in the x_2 direction. The concentration in the plane $x_1 = 0$ is assumed to fit the equation

$$c - c^{\alpha\beta} = C_2\exp\{-\pi x_2^2/16m^2\} \tag{2.23}$$

where C_2 and m are arbitrary constants. Although this is a plausible form of the concentration change, no real justification can be given for the assumptions. If it is used to replace the real boundary conditions, the solution obtained is:

$$g = \frac{D\Omega}{2}\frac{c^{\beta\alpha} - c_r^{\alpha\beta}}{c^{\beta\alpha} - \overline{c}}\frac{1}{m}\left(1 - \frac{m_c}{m}\right) \tag{2.24}$$

which is equal to Zener's equation [2.17] if

$$C_1 = \frac{2(c^{\beta\alpha} - \overline{c})}{(c^{\beta\alpha} - c_r^{\alpha\beta})}$$

$$m \simeq r \tag{2.25}$$

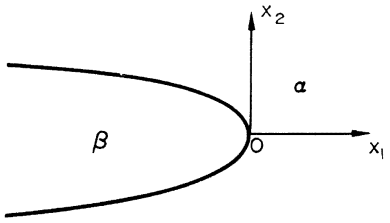

Fig. 2.6: Zener-Hillert growth model [Christian, 1975]

The few theories discussed in this subsection have been used in contemporary computational models to describe the precipitation reactions. Capillarity and surface tension considerations have been included; however, none of those theories are able to integrate successfully those concepts in a single framework. A theory which does the task for needle and plate-type precipitates is the one due to Trivedi, as described in the next section.

2.4.4 Trivedi theory of growth

To overcome the problems that arise from an incorrect selection of boundary conditions, an appropriate coordinate system has to be chosen to solve the diffusion equation [2.12] for needle and plate-like precipitates. The parabolic coordinate system is approximate, since the shapes of needles or plates can be represented by a paraboloid of revolution or a parabolic cylinder, respectively. A schematic representation of the parabolic coordinate system for a needle is shown in Fig. 2.7, in which γ and δ are the orthogonal coordinates, Z/r and R/r are the dimensionless coordinates along which the needle grows or thickens.

The diffusion equation in the parabolic coordinate system is written as

$$\frac{\partial^2 c}{\partial \gamma^2} + \left(\frac{1}{\gamma} + 2p\gamma\right)\frac{\partial c}{\partial \gamma} + \frac{\partial^2 c}{\partial \delta^2} + \left(\frac{1}{\delta} - 2p\delta\right)\frac{\partial c}{\partial \delta} = 0 \tag{2.26}$$

from which Ivanstov [1947] and Horvay and Cahn [1961] obtained a rigorous solution for an isoconcentrate needle. The concentration can thus be expressed as:

$$c' - \overline{c} = (c^{\alpha\beta} - \overline{c})\frac{E_1\{p\gamma^2\}}{E_1\{p\}} \tag{2.27}$$

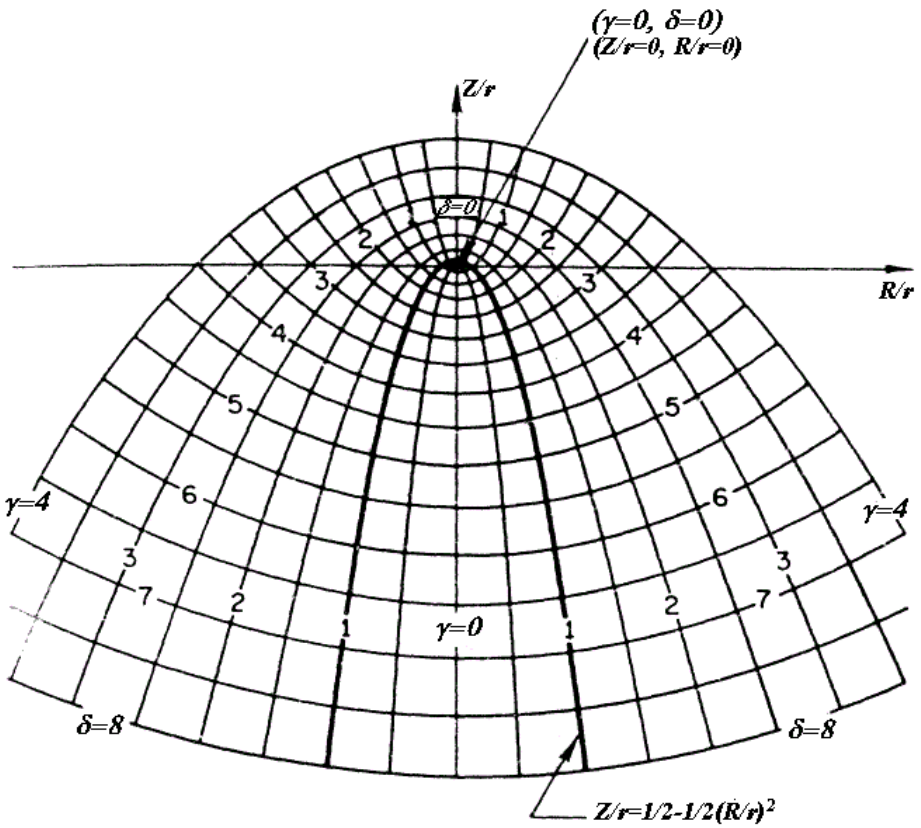

Fig. 2.7: Parabolic coordinate diagram and precipitate interface [Kotler and Tarshis, 1969]

where c' is the concentration field of the matrix for the case in which the interface has a constant concentration equal to $c^{\alpha\beta}$, E_1 is the exponential integral function [Abramowitz, 1965] and $p = g_p r/2D$ is the Péclet number.

Temkin [1960] and Bolling and Tiller [1961] pointed out the non–isothermal nature of the dendrite along the surface of the parabola as the curvature changes or, equivalently, the composition change along the surface, and presented a solution for small Péclet numbers, which was later extended by Kotler and Tarshis [1969] with an approximate heat flow (or mass balance) equation.

Trivedi [1970a,b] accounted for the concentration change and interface kinetics in needle and plate–like precipitates. The assumptions of this model are: (1) elastic strain energy and anisotropy of surface properties are neglected, (2) diffusion of solute inside the precipitate is negligible, (3) the concentration in the matrix is such that the capillarity of dilute solutions is applicable, (4) the diffusion coefficient and the partial molar volume of solute are independent of concentration, (5) the steady–state shape of the interface near the growing tip of the needle can be approximated by a paraboloid of revolution.

Growth of precipitate needles with diffusion of one solute

The boundary is defined at $\gamma = 1$ (Fig. 2.7), where the coordinates are the result of the transformation suggested by Kotler and Tarshis [1969]:

$$\frac{Z}{r} = \frac{(\gamma^2 - \delta^2)}{2}, \quad \frac{R}{r} = \gamma\delta \tag{2.28}$$

as the surface of the needle is described by the equation

$$\frac{Z}{r} = \frac{1}{2} - \frac{1}{2}\left(\frac{R}{r}\right)^2 \tag{2.29}$$

and the boundary condition (which allows for variation of solute concentration along it) is given by:

$$c\{1,\delta\} - c^{\alpha\beta} = \left(\frac{c^{\alpha\beta}\Gamma}{r}\right)\frac{(2+\delta^2)}{(1+\delta^2)^{3/2}} + \frac{g_p}{\mu_o}\frac{1}{(1+\delta^2)^{1/2}} \tag{2.30}$$

where Γ (equation [2.10]) is the capillarity constant, r is the radius of curvature of the needle tip, g_p is the velocity of the needle tip and μ_o is the interface kinetics coefficient for uniform attachment kinetics, which is a measure of the mobility of the atoms as they transfer from the matrix to the precipitate in the presence of a driving force.

The general solution to the diffusion equation [2.26] is:

$$c\{\gamma,\delta\} - c' = \sum_{i=0}^{\infty} A\frac{e^{-p\gamma^2}\Psi\{i+1,1,p\gamma^2\}}{e^{-p}\Psi\{i+1,1,p\}}L_i^o\{p\delta^2\} \tag{2.31}$$

where Ψ is the confluent hypergeometric function of the second type [Zhang, 1999], and L_i^o is a Laguerre polynomial [Abramowitz, 1965]. The coefficient A is evaluated using the boundary condition given by equation [2.30], and its expression is

$$A = \frac{c^{\alpha\beta}\Gamma}{r}e^p\left[2pI_{2i+1}\mathrm{erfc}\sqrt{p} + \sqrt{p}\frac{\Gamma_D\{i+\frac{1}{2}\}}{\Gamma_D\{i+1\}}I_{2i}\mathrm{erfc}\sqrt{p}\right] + \frac{g_p}{\mu_o}e^p\sqrt{p}\frac{\Gamma_D\{i+\frac{1}{2}\}}{\Gamma_D\{i+1\}}I_{2i}\mathrm{erfc}\sqrt{p} \tag{2.32}$$

where $I_m\mathrm{erfc}\{x\}$ is the normalised error function, and Γ_D is the gamma function [Abramowitz, 1965].

In analogy to the treatments of the previous section, once an expression for the concentration is obtained, it becomes possible to solve the flux balance equation. Considering the concentration changes due to capillarity and interface kinetics, the equivalent equation to [2.15] in the parabolic coordinate system is:

$$2p\left[c^{\beta\alpha} - \left(c^{\alpha\beta} + 2\frac{c^{\alpha\beta}\Gamma}{r} + \frac{g_p}{\mu_o}\right)\right] = \left(\frac{\partial c}{\partial\gamma}\right)_{\substack{\gamma=1\\ \delta=0}} \tag{2.33}$$

where $\left(\frac{\partial c}{\partial \gamma}\right)_{\substack{\gamma=1 \\ \delta=0}}$ is obtained from equation [2.31]. The solution of equation [2.33] can be expressed as

$$\Omega = pe^{p} E_1\{p\}\left[\underbrace{1}_{i} + \underbrace{\frac{g_p}{g_c}\Omega R_1\{p\}}_{ii} + \underbrace{\frac{r_c}{r}\Omega R_2\{p\}}_{iii}\right] \tag{2.34}$$

where $g_c = \mu_o(\overline{c} - c^{\alpha\beta})$, $r_c = 2c^{\alpha\beta}\Gamma/(\overline{c} - c^{\alpha\beta})$ and R_1, R_2 are complex functions of p which have been obtained numerically by Trivedi and are shown in Fig. 2.8.

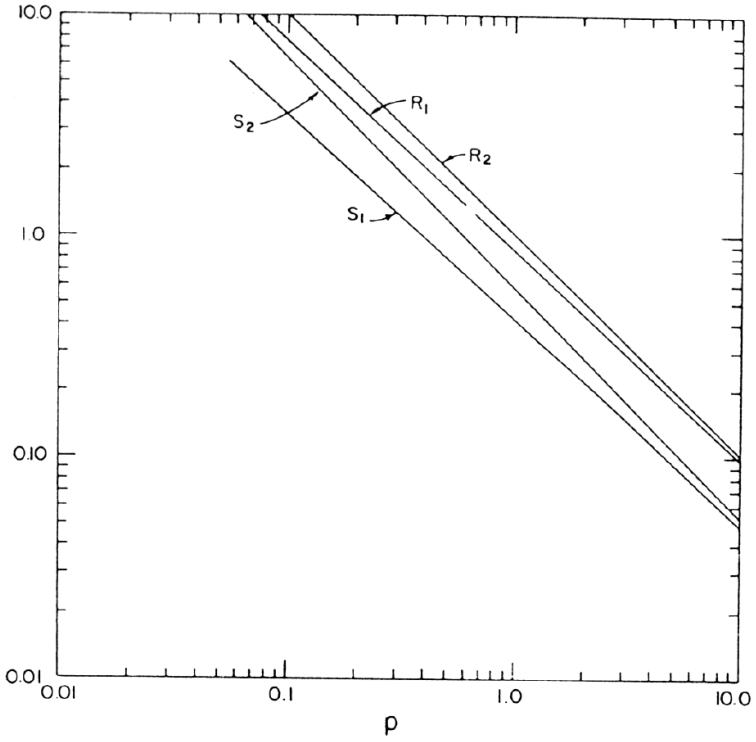

Fig. 2.8: Values of S_1, S_2, R_1 and R_2 Trivedi [1970a]

Growth of precipitate plates with diffusion of one solute

The methodology to solve this problem is essentially the same than for needles, but some small differences arise from the selection of the parabolic coordinate system, because the steady state shape of the interface near the growing plate tip is approximated by a parabolic cylinder. The rest of the assumptions for needle precipitates hold.

Instead of the transformations stated in [2.28], the transformations $x = (X - g_p t)/r$ and $y = Y/r$ are used, where t stands for time, and X, Y are the fixed Cartesian coordinates.

The diffusion equation is thus:

$$\frac{\partial^2 c}{\partial \xi^2} + \frac{\partial^2 c}{\partial \eta^2} + 2p\left[\xi\frac{\partial c}{\partial \xi} - \eta\frac{\partial c}{\partial \eta}\right] = 0$$

where the parabolic coordinates (ξ,η) are now the result of the transformations

$$\xi^2 = \sqrt{x^2+y^2} + x, \quad \eta^2 = \sqrt{x^2+y^2} - x$$

The general solution of the diffusion equation is [Trivedi, 1970b]:

$$c - c' = \sum_{m=0}^{\infty} A_{2m} \frac{I_{2m}\mathrm{erfc}\{\sqrt{p}\xi\}}{I_{2m}\mathrm{erfc}\{\sqrt{p}\}} H_{2m}\{\sqrt{p}\eta\} \tag{2.35}$$

where H_{2m} represents a Hermite polynomial,

$$A_{2m} = \frac{2c^{\alpha\beta}\Gamma}{r}\frac{p^{3/2}}{\pi}\frac{(-1)^m}{(2m)!}\Gamma_D\left(m+\frac{1}{2}\right)\Gamma_D\left(m+\frac{3}{2}\right)\Psi\left(m+\frac{3}{2},2,p\right)$$

$$+\frac{g_p}{\mu_o}\frac{p^{1/2}}{\pi}\frac{(-1)^m}{(2m)!}\Gamma_D\left(m+\frac{1}{2}\right)\Gamma_D\left(m+\frac{1}{2}\right)\Psi\left(m+\frac{1}{2},1,p\right) \tag{2.36}$$

where Γ_D and Ψ are the gamma function, and the confluent hypergeometric function of the second kind, respectively.

Similarly, the flux balance equation is obtained as:

$$2p\left[c^{\beta\alpha} - \left(c^{\alpha\beta} + \frac{c^{\alpha\beta}\Gamma}{r} + \frac{g_p}{\mu_o}\right)\right] = \left(\frac{\partial c}{\partial \xi}\right)_{\substack{\xi=1\\ \eta=0}}$$

The final relation is [Trivedi, 1970b]:

$$\Omega = \sqrt{\pi p}e^p\mathrm{erfc}\{\sqrt{p}\}\left[\underbrace{1}_{iv} + \underbrace{\frac{g_p}{g_c}\Omega S_1\{p\}}_{v} + \underbrace{\frac{r_c}{r}\Omega S_2\{p\}}_{vi}\right] \tag{2.37}$$

where S_1 and S_2 are complex functions of p, which are plotted in Fig. 2.8, and

$$r_c = c^{\alpha\beta}\Gamma/(\overline{c} - c^{\alpha\beta}) \tag{2.38}$$

where Γ is the capillarity constant (equation [2.10]), but [2.38] is different from the needle r_c by a factor of $\frac{1}{2}$. This is due to the fact that a parabolic cylinder has a single radius of curvature at the tip, whereas the paraboloid of revolution has two radii.

Discussion of Trivedi's theory

Equations [2.34] and [2.37] possess three terms in the right hand side; terms i, iv represent the solution to the kinetics equation when interface kinetics and capillarity effects are absent, while terms ii, v and iii, vi account for them, respectively.

Purdy [1971] and Simonen and Trivedi [1977] have compared Trivedi's theory against experiment by measuring the lengthening rate of α needles in ordered β' Cu-Zn. Purdy [1971]

assumed $\mu_o = \infty$ and a value for σ, and calculated r_c with equation [2.8] (non-ideal solution). His results match experimental measurements very well. Simoen and Trivedi [1977] performed measurements over an extensive range of temperature, and found their results approximately match experiments.

2.5 Theories of growth in multicomponent systems

When a variety of components diffuse into a spherical particle, equation [2.13]

$$\frac{\partial c_i}{\partial t} = \frac{D_i}{R^2}\frac{\partial}{\partial R}\left\{ R^2 \frac{\partial c_i}{\partial r} \right\} \tag{2.39}$$

has to be satisfied simultaneously for $i = 1, 2, ..., C$ components; the terms c_i and D_i stand for the concentration gradient and diffusion coefficient of component i. The solution to the system given by [2.39] has been presented by Coates [1972, 1973a,b] for a ternary alloy. He particularly considered the case where the two solutes have different diffusivities. In order to conserve the conditions at the interface, it becomes necessary to define two growth rate constants α_{31} and α_{32} representing components 1 and 2 respectively:

$$r = \alpha_{31}\sqrt{D_1 t} \qquad \text{and} \qquad r = \alpha_{32}\sqrt{D_2 t} \tag{2.40}$$

with $\alpha_{32} = \sqrt{D_1/D_2}\alpha_{31}$; *i.e.* they are dependent only on the ratio of the diffusion coefficients of both species.

The solution to equation [2.39] is thus given by the simultaneous solution of

$$\Omega_i = \frac{1}{2}\alpha_{3i}^3 \exp\left\{\frac{1}{4}\alpha_{3i}^2\right\}\left[\frac{1}{\alpha_{3i}}\exp\left\{-\frac{\alpha_{3i}^2}{4}\right\} - \frac{\sqrt{\pi}}{2}\mathrm{erfc}\left\{\frac{\alpha_{3i}}{2}\right\}\right] \tag{2.41}$$

for $i = 1,\ 2$, where Ω_i is the supersaturation referred to component i and can be expressed as

$$\Omega_i = \frac{\overline{c}_i - c_i^{\alpha\beta}}{c_i^{\beta\alpha} - c_i^{\alpha\beta}} \tag{2.42}$$

where $\overline{c}_i$ is the average composition of component i in the alloy, and $c_i^{\alpha\beta}$, $c_i^{\beta\alpha}$ are the concentrations of component i in α in equilibrium with β, and β in equilibrium with α, respectively.

In order to illustrate the influence of different diffusing coefficient ratios D_2/D_1, on an isothermal section of a ternary phase diagram, Coates introduced the concepts of interface–composition (IC) and interface–velocity (IV) contours [1972]. All alloys $(\overline{c}_1, \overline{c}_2)$ with a composition lying on an IC contour would involve precipitate growth with interface compositions

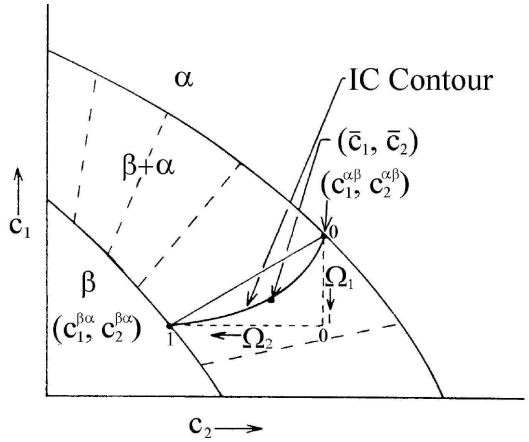

Fig. 2.9: Schematic representation of an IC contour in a ternary system [Coates, 1972].

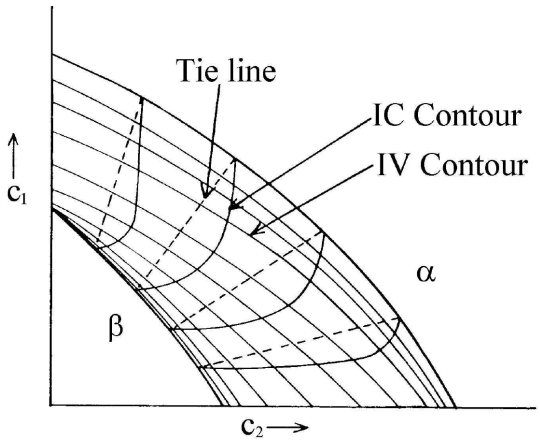

Fig. 2.10: Schematic representation of an IV contour in a ternary system [Coates, 1972].

$c^{\beta\alpha}$ and $c^{\alpha\beta}$ defined by the same tie–line (Fig. 2.9). On the other hand, the parabolic growth parameters α_{31} and α_{32} are identical for all alloys which lie on an IV contour (Fig. 2.10).

IC and IV contours can be obtained by proposing a value of α_{31}, and obtaining $\alpha_{32} = \sqrt{D_1/D_2}\alpha_{31}$, and using them to solve equation [2.41] for $i = 1,\ 2$.

IC contours for a given tie–line are plotted for a variety of diffusivity ratios in Fig. 2.11; as $D_2/D_1 \to \infty$, the IC contour tends to become composed of two straight segments defined by $\Omega_2 = 0$ and $\Omega_1 = 1$. In the region where $\Omega_2 \simeq 0$, $\overline{c}_2 - c_2^{\alpha\beta} \simeq 0$, the fast diffuser is keeping pace with the slow diffuser by virtually eliminating the driving force ($\overline{c}_2 - c_2^{\beta\alpha} \simeq 0$) for the diffusion of the fast diffuser; the rate is then determined by the slow diffuser. For $\Omega_1 \simeq 1$, $\overline{c}_1 \simeq c_1^{\beta\alpha}$ so that the slow diffuser can keep pace with the fast diffuser by increasing the concentration gradient of component 1.

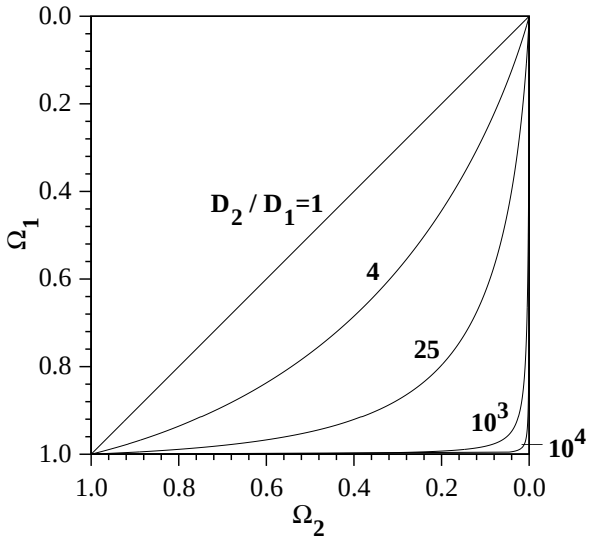

Fig. 2.11: IC Contours for different ratios of diffusivities [Coates, 1972].

2.6 Theories of coarsening

The earliest application of quantitative ideas to the coarsening process of metallic precipitates was by Greenwood [1956]; a few years later, the most widely used theory was developed independently by Lifshitz and Slyozov [1961] and Wagner [1961] (LSW theory). Marqusee and Ross [1983] presented an alternative analysis using a time scaling technique to derive the power law time dependence and distribution function for the size of the particles of the new phase; their results were extended by Umanstev and Olson [1993] for multicomponent systems. The solution method they used was to define a particle radius distribution function $f\{r,t\}$ to which they applied the continuity equation

$$\frac{\partial f}{\partial t} + \frac{\partial}{\partial r}\left\{ f \frac{\partial r}{\partial t} \right\} = 0 \tag{2.43}$$

which has to be satisfied along with the flux balance equation [2.15] and a mass balance equation. Their results are for small volume fractions of transformed phase, and can be expressed [Marqusee and Ross, 1983] as

$$\overline{r}^3\{t\} = (2/3)^2 Kt + \mathrm{O}\{1\}, \quad K = 2\sigma V_m/\Phi \tag{2.44}$$

$$\Delta\{t\} = (3\sigma V_m)^{2/3}\Phi^{1/3}t^{-1/3} + \mathrm{O}\{t^{-2/3}\} \tag{2.45}$$

$$N\{t\} = (3\overline{\varphi}\Phi/4\pi\sigma)t^{-1} + \mathrm{O}\{t^{-4/3}\} \tag{2.46}$$

where $\overline{r}$ is the average precipitate radius,

$$\Delta\{t\} = \sum_{i=1}^{n} c_i^{\beta\alpha}(\mu_i^{\alpha}\{\overline{c}_i\} - \mu_i^{\alpha}\{c_i^{\alpha\beta}\}) \tag{2.47}$$

is the cumulative supersaturation of the alloy, V_m is the volume of the precipitate phase, $N\{t\}$ is the number of precipitate particles and $\overline{\varphi}$ the limiting value of the precipitate volume fraction. The scalar parameter Φ is defined as

$$\Phi = \sum_{j=2}^{n} \sum_{i=1}^{n} c_i^{\beta\alpha} \frac{\mu_{ij}^{\alpha}}{D_j} (c_j^{\beta\alpha} - c_j^{\alpha\beta}) \tag{2.48}$$

where $\mu_{ij}^{\alpha} = \left(\frac{\partial \mu_i}{\partial c_j}\right)_{T,P,c_k}$, characterises the coarsening resistance of the precipitate, and depends upon diffusion mobilities and thermodynamic interactions between species.

Referring to equations [2.44–2.46], these are reduced to those obtained by Lifshitz and Slyozov [1961] when the terms O$\{1\}$, O$\{t^{-2/3}\}$ and O$\{t^{-4/3}\}$ are neglected.

Morral and Purdy [1994] have added the effects of off–diagonal terms of the diffusivity, producing expressions consistent with [2.44–2.46], where the coarsening rate coefficient is given by:

$$K = \frac{2\sigma V_m}{(\Delta c^{\alpha\beta}][G][D]^{-1}[\Delta c^{\alpha\beta})} \tag{2.49}$$

In the notation used here a matrix **A** can be expressed as (A), [A] or [A), which refer to a row, square or column matrix, respectively; thus $[G]$ is a square matrix containing the elements

$$G_{ij} = \frac{\partial^2 G^{\alpha}}{\partial c_i \partial c_j} = [G]$$

$[D] = D_{ij}$ is the square diffusivity matrix and $(\Delta c^{\alpha\beta}] = (c^{\beta\alpha} - c^{\alpha\beta}]$. Through insertion of equation [2.49] in [2.44] Morral and Purdy recognised that the particle coarsening is independent of the solution thermodynamics of the matrix phase for the multicomponent phase. It depends, as for binaries, primarily on surface tension, tie–line length and on the diffusion matrix.

The coarsening kinetic equations developed so far neglect changes in chemical potential of the precipitate phase, and its composition shifts. New theory has to be produced to account for these, and the effects it produces on the calculated thickening rates need further assessment.

2.7 The Avrami theory

Once the precipitates grow and reach a considerable size, impingement starts, raising mutual interference between the growth of independent particles. One of the first successful approaches to describe such processes was given by Avrami *et al.* [Christian, 1975]. This treatment introduces the concept of extended volume which is widely used in precipitation kinetics modelling. It considers, as well, the dependence of the growth rate on the particle shape and the nucleation rate.

In order to produce expressions to describe the precipitation kinetics when mutual interference between the particles is present, it is first recognised that the growth curves for a transformed product are similar to Fig. 2.12; they are characterised by an induction period τ at the intersection of the linear region and the abscissa (time axis). At time $t = \tau$, the first products will form, and thereafter, the size of the nucleus formed will increase continuously. Defining I as the nucleation rate per unit volume, and g as the growth rate, and assuming that the particle will grow at the same rate in all directions, for $t > \tau$, the volume of a β region is $v_\tau = \frac{4\pi}{3} g^3 (t - \tau)^3$. In the whole assembly, during the initial stages of transformation, when $V^\beta \ll V^\alpha$ the interference of neighbouring particles can be neglected, so the volume increment $dV^\beta = v_\tau I V^\alpha d\tau$. In this case, V^α, the volume of the matrix, is almost equal to V, thus the total volume transformed at time t is

$$V^\beta = \frac{4\pi}{3} \int_{\tau=0}^{t} I g^3 (t - \tau)^3 d\tau \tag{2.50}$$

Equation [2.50] can be integrated assuming that I does not vary with time, and the result is

$$\zeta = V^\beta / V = (\pi/3) I g^3 t^4 \tag{2.51}$$

where ζ represents the volume fraction transformed at time t. The rate of transformation according to this equation rises rapidly in the initial stages.

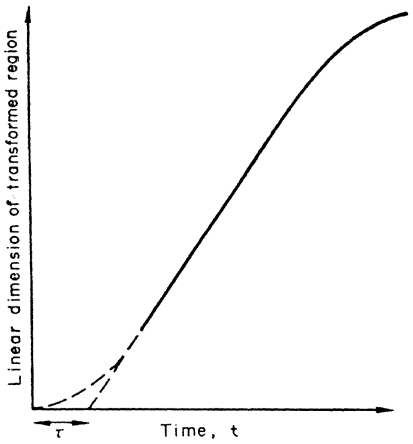

Fig. 2.12: Schematic growth curve for a product region [Christian, 1975]

In real cases, however, it is necessary to consider the mutual interference of regions growing from separate nuclei. When the regions touch, they develop a common interface, over which growth ceases, although it continues normally elsewhere. During the time $d\tau$, when $IV^\alpha d\tau$

new transformed regions are nucleated, $IV^{\beta}d\tau$ regions would have nucleated in the transformed portion of the assembly. Then, the *extended* volume of the transformed material V_e^{β} is

$$dV_e^{\beta} = v_{\tau} I(V^{\alpha} + V^{\beta})d\tau \Rightarrow V_e^{\beta} = \frac{4\pi}{3} \int_{\tau=0}^{t} g^3 I(t-\tau)^3 d\tau \tag{2.52}$$

which accounts for the transformed volumes occurring in α and those regions of β had not transformation previously occurred there. The extended volume can thus be visualised as a series of volume elements having the same limiting surface as the actual transformed volume but growing "through" each other. The extended volume is represented in Fig. 2.13 where a new region (say b) may be formed in regions which are already transformed (say c and d).

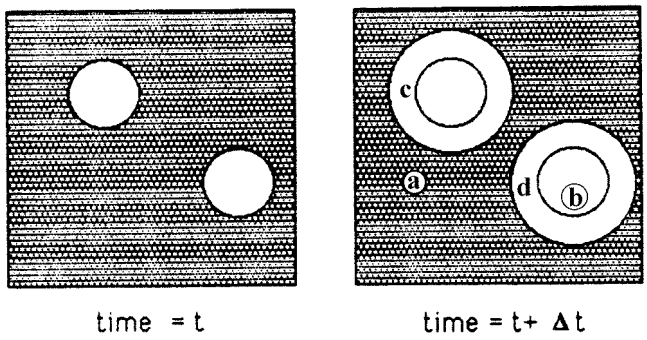

Fig. 2.13: Two precipitates have nucleated together and grown to a finite size in the time t. New regions c and d are formed as the original particles grow, but a and b are new particles, of which b has formed in a region which is already β [Robson, 1997d]

It is necessary to find a relation between the extended volume V_e^{β} and the real transformed volume V^{β}. Consider any small random region of which a fraction $(1 - V^{\beta}/V)$ remains untransformed at time t. During a further time dt, the extended volume of β in the region will increase by dV_e^{β}, and the true volume by dV^{β}. Of the new elements of volume which make up dV_e^{β}, a fraction $(1 - V^{\beta}/V)$ on the average will lie in previously untransformed material, and thus contribute to dV^{β}, while the reminder of dV_e^{β} will be in already transformed material. Therefore

$$dV^{\beta} = (1 - V^{\beta}/V)dV_e^{\beta} \Rightarrow V_e^{\beta} = -V\ln\{1 - V^{\beta}/V\} \tag{2.53}$$

Substituting into [2.52], we obtain

$$-\ln\{1-\zeta\} = \frac{4\pi}{3} g^3 \int_{0}^{t} I(t-\tau)^3 d\tau \tag{2.54}$$

Assuming that I is constant:

$$\zeta = 1 - e^{(-\pi g^3 I t^4/3)} \tag{2.55}$$

I will not in general be constant; it is possible that nucleation occurs only at certain preferred sites in the assembly, which are gradually exhausted. If there are N_o sites per unit volume of the α phase at the beginning, and N_r remaining after time t, the number disappearing in a further time interval dt is $dN_r = -N_r \nu_1 dt$, where the frequency ν_1 gives the rate at which an individual site becomes a nucleus. Thus $N_r = N_o e^{(-\nu_1 t)}$, and the nucleation rate per unit volume is

$$I = -\frac{dN}{dt} = N_o \nu_1 e^{(-\nu_1 t)} \tag{2.56}$$

Substituting I into equation [2.54] and integrating by parts, Avrami obtained the expression:

$$\zeta = 1 - \exp\left\{(8\pi N_o g^3/\nu_1^3)\left[e^{-\nu_1 t} - 1 + \nu_1 t - \frac{\nu_1^2 t^2}{2} + \frac{\nu_1^3 t^3}{6}\right]\right\} \tag{2.57}$$

A generalisation of Avrami's theory has been carried out recently by Kasuya *et al.* [1999]. Redefining the variables as

$$\zeta_i = \frac{V_i}{V}, \quad \zeta_i^e = \frac{V_i^e}{V}, \quad z = \sum_{j=1}^{\mathrm{P}} \zeta_j \quad \text{and} \quad z^e = \sum_{j=1}^{\mathrm{P}} \zeta_j^e \tag{2.58}$$

where V_i ($i = 1$ to P) is the real volume of the product phase i, and V_i^e is its extended volume.

From the same analysis as before (equation [2.53])

$$d\zeta_i = (1 - z) d\zeta_i^e \tag{2.59}$$

the real volume change can be calculated using the relationship:

$$\zeta_i = \int \frac{dv_i^e}{dz^e} \exp\{z^e\} dz^e \tag{2.60}$$

Kasuya *et al.* obtained analytical solutions of equation [2.60] for special cases where the extended volumes of the different phases (ζ_i^e for $i = 1$ to P) can be related. Thus, for $n = 2$ and treating ζ_1^e as an independent variable, if ζ_1^e and ζ_2^e are related linearly according to $\zeta_2^e = k_1 \zeta_1^e - k_2$, where k_1 is a positive constant and k_2 is zero or a positive constant. Equation [2.60] can now now be integrated; since ζ_2^e cannot be negative. For $0 \leq \zeta_1^e \leq \frac{k_2}{k_1}$

$$\zeta_1 = 1 - \exp\{-\zeta_1^e\} \quad \text{and} \quad \zeta_2 = 0 \tag{2.61}$$

and for $\zeta_1^e > \frac{k_2}{k_1}$

$$\zeta_1 = 1 - \frac{k_2}{k_1} \exp\left\{\frac{k_2}{k_1}\right\} - \frac{1}{k_1 + 1} \exp\left\{-(k_1 + 1)\zeta_1^e + k_2\right\} \tag{2.62}$$

Examples of precipitation phenomena with simultaneous reactions related linearly can be found in ferritic steels [Kasuya *et al.* al., 1999]. Kinetic predictions on secondary hardened steels for power plants with those linear relations have been carried out by Robson and Bhadeshia [1997b].

Kasuya *et al.* obtained as well analytical relationships for ζ_1 and ζ_2, when ζ_1^e and ζ_2^e are related parabolically, however, no example of such relationship seems to appear in actual transformations. Anyway, equation [2.60], when solved numerically, provides a general methodology to calculate the real volume from the extended volume for any number of phases.

2.8 Summary

Well established theories of precipitate nucleation, growth and coarsening have been reviewed in this chapter. The thermodynamic equilibrium relationships describing the initial and final states of the precipitation process are defined; and the Avrami theory of soft impingement has been introduced. The necessity to develop new theory to extend the reviewed concepts to multicomponent alloys where simultaneous reactions occur has been indicated. Such theory is presented in the next chapters, and incorporated into a new model to predict the kinetics of complex alloys.

Addendum

Mullins, W. W. and Sekerka, R. F. (*J. Appl. Phys.* **34** [1963] 323) have provided a quasi steady state solution for spherical growth with capillarity. They solved equation [2.12] assuming $\partial c/\partial t = 0$, which is equivalent to Laplace's equation. Coriell, S. R. and Parker, R. L. (*Crystal Growth*, ed. Peiser, H. S., Pergamon Press, Oxford 1967 p. 703) have even extended this solution to account for interface kinetic effects. Their solutions are similar to the analytical solution presented in Chapter 3, equation [3.12].

CHAPTER THREE

Spherical growth with capillarity effect

3.1 Introduction

During precipitation processes, there is usually a combination of many kinds of particles with a variety of shapes, ranging from needles and plates to spheres. Many of the precipitates approximate to a spherical shape. Although attempts have been made to estimate the kinetics of spherical particle precipitation in power plant steels [Robson and Bhadeshia, 1997a,b] there is no analytical solution for the growth of a sphere with capillarity included, since for spheres the radius of curvature also defines the size of the particle [Zener, 1949]. The Gibbs–Thompson capillarity effect is due to the curvature of the interface, which influences the equilibrium compositions at the particle/matrix boundary. A consequence is that small particles will grow less rapidly than large particles even when the far–field concentration is identical for all particles. Some quite elegant work by Miyazaki and co–workers [1996, 1999] has shown experimentally that the capillarity effect is seminal in the development of precipitation reactions.

Thus, although Zener [1946] recognised the importance of capillarity, and even though capillarity features strongly in the theories for the growth of needles and plates [Trivedi, 1970a,b], the author is not aware of any corresponding theory for spherical precipitates; in this chapter an approximate analytical solution for ideal solutions will be presented, and its range of validity will by assessed numerically. Some of the equations presented in Chapter Two are repeated here for the sake of clarity.

3.2 Approximate analytical solution

For spherical particles, Fick's second law can be written in the spherical coordinate system as:

$$\frac{\partial c}{\partial t} = \frac{D}{R^2}\frac{\partial}{\partial R}\left\{R^2\frac{\partial c}{\partial R}\right\} \tag{3.1}$$

Since the concentration field in the matrix is a function of time and the radial coordinate, this can be written as $c = c\{t, R\}$,

$$c\{0, R\} = \overline{c} \tag{3.2}$$

$$c\{t,r\} = c^{\alpha\beta} + \frac{2c^{\alpha\beta}\Gamma}{r} \tag{3.3}$$

where Γ is the capillarity constant given by [Christian, 1975]

$$\Gamma = \left(\frac{\sigma v^{\beta}}{kT}\right)\left(\frac{1 - c^{\alpha\beta}}{c^{\beta\alpha} - c^{\alpha\beta}}\right) \tag{3.4}$$

The boundary condition of equation [3.2] indicates that, as the precipitation starts at $t = 0$, the concentration everywhere will be equal to the average concentration of the alloy; equation [3.3], which has been defined in analogy to capillarity corrected concentrations of needle and plate–like precipitates [Trivedi, 1970a,b], accounts for the concentration change as the particle approaches to a critical radius r_c which can be expressed as

$$r_c = \frac{2c^{\alpha\beta}\Gamma}{\overline{c} - c^{\alpha\beta}} \tag{3.5}$$

This is obtained by solving equation [3.3] for $c\{t, r_c\} = \overline{c}$.

As the particle radius approaches the critical radius $r = r_c$, the concentration in the matrix at the boundary tends towards the average concentration so that growth becomes impossible [Christian, 1975]. This situation can be shown schematically in Fig. 3.1, where Fig. 3.1a represents the case where the interface is flat, Fig. 3.1b shows the case where $r = 2r_c$, and Fig. 3.1c presents the case where $r = r_c$.

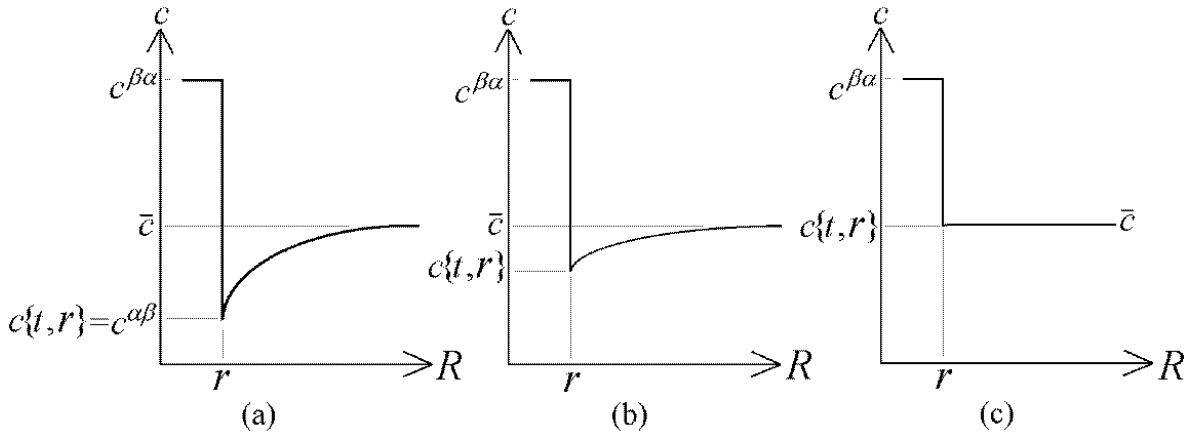

Fig. 3.1: Schematic representation of the concentration gradient as capillarity effect is present. (a) Flat interface; (b) curved interface with $r = 2r_c$; (c) curved interface with $r = r_c$.

Dimensional arguments [Christian, 1975] and experimental observations [Fujita, 2001] of spherical precipitate growth, have shown that the particles display a parabolical rate. The

solution to equation [3.1] given by Zener applies a similarity transformation [Zwillinger, 1998] where the radius varies parabolically with time:

$$r = \alpha_3 \sqrt{Dt} \tag{3.6}$$

where α_3 is a dimensionless growth parameter. The concentration $c\{t, r\}$ that satisfies equation [3.1] and the boundary conditions given by equations [3.2, 3.3] is then:

$$c\{t, R\} = \overline{c} + \left[\left(c^{\alpha\beta} + \frac{2c^{\alpha\beta}\Gamma}{r}\right) - \overline{c}\right] \frac{\phi\{R/\sqrt{Dt}\}}{\phi\{\alpha_3\}} \tag{3.7}$$

where

$$\phi\{\alpha_3\} = \frac{1}{\alpha_3} \exp\left\{-\frac{\alpha_3^2}{4}\right\} - \frac{\sqrt{\pi}}{2} \mathrm{erfc}\left\{\frac{\alpha_3}{2}\right\} \tag{3.8}$$

where erfc is the error function. By substitution in equation [3.1], it is to be noted that the solution given by equation [3.7] is valid only when $\phi\{\alpha_3\}$ is constant, and thus if α_3 is. The forthcoming derivations were done following this assumption.

The rate at which solute is incorporated into the growing precipitate must equal that arriving by diffusion to the interface. Therefore,

$$g\left[c^{\beta\alpha} - \left(c^{\alpha\beta} + \frac{2c^{\alpha\beta}\Gamma}{r}\right)\right] = D \left.\frac{\partial c}{\partial R}\right|_{R=r} \tag{3.9}$$

where $g = dr/dt$ is the particle growth rate. The concentration gradient given by equation [3.7] can now be substituted in [3.9], from which an expression for α_3 can be obtained. After some algebra, the next equation is obtained.

$$f_1\left[1 - \Omega\frac{r_c}{r}\right] = \Omega - \Omega\frac{r_c}{r} \tag{3.10}$$

where f_1 is a complex function of α_3 given by

$$f_1 = \frac{1}{2}\alpha_3^3 \exp\left\{\frac{1}{4}\alpha_3^2\right\}\phi\{\alpha_3\}$$

Provided that the phase diagram is known, equation [3.10] is now a function of α_3 only, which can be expressed as:

$$\Omega = \frac{f_1}{1 + (r_c/r)(f_1 - 1)} \tag{3.11}$$

which was solved numerically as shown in Figs. 3.2 and 3.3 for large and small growth parameters, respectively. The computer program that provided these values is shown in Appendix 1.

Approximately spherical particles precipitate at small supersaturation values in many alloys, such as secondary hardening steels [Robson and Bhadeshia, 1997a,b]. It is desirable

therefore to obtain a simple asymptotic relationship for equation [3.11] as $\Omega \ll 1$. Fig. 3.3 shows that $\alpha_3 \to 0$ as $\Omega \to 0$. Using the Taylor's series expansion of $\exp\{\frac{1}{2}\alpha_3^2\}$ around zero, and expanding $\mathrm{erfc}\{\frac{1}{2}\alpha_3\}$ as $\alpha_3 \to 0$ [Abramowitz, 1965] it can be seen that $f_1\{\alpha_3\} \simeq \frac{1}{2}\alpha_3^2$. Thus:

$$\alpha_3 = \sqrt{\frac{2\Omega(1-\frac{r_c}{r})}{1-\Omega\frac{r_c}{r}}} \quad \text{for} \quad \Omega \ll 1 \tag{3.12}$$

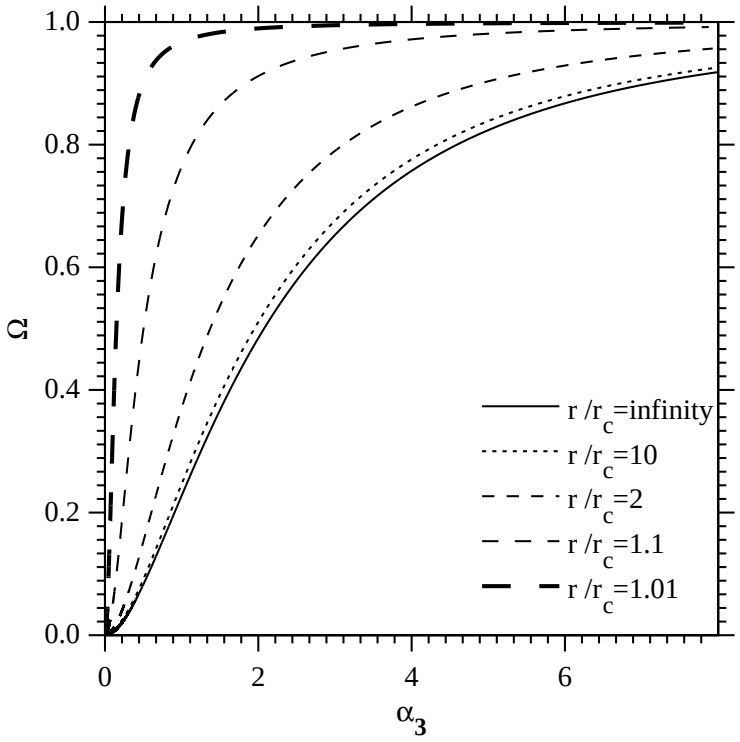

Fig. 3.2: Variation of the growth parameter as a function of the supersaturation and normalised radius.

In order to assess the effect of the particle radius on the growth rate, the value of α_3 against the tip radius for given values of Ω is plotted in Figs. 3.4 and 3.5 at large and small supersaturations, respectively. The solid lines adjacent to each dotted line in Fig. 3.5 represent the values calculated using equation [3.12] for the respective supersaturation.

The capillarity correction on the parabolic growth parameter (α_3) is shown in Figs. 3.4 and 3.5. It can be seen that for small values of r/r_c, there are differences of up to an order of magnitude when compared with a model without the correction. Naturally, when $r \gg r_c$, equation [3.11] reduces to Zener's equation.

Figs. 3.4 and 3.5 show that α_3 varies with r/r_c, which contradicts one of the original assumptions. The error arises when equation [3.7] is inserted in [3.1], giving an additional term in the left hand side ($\partial c/\partial t$) because α_3 actually varies with time. However, the change

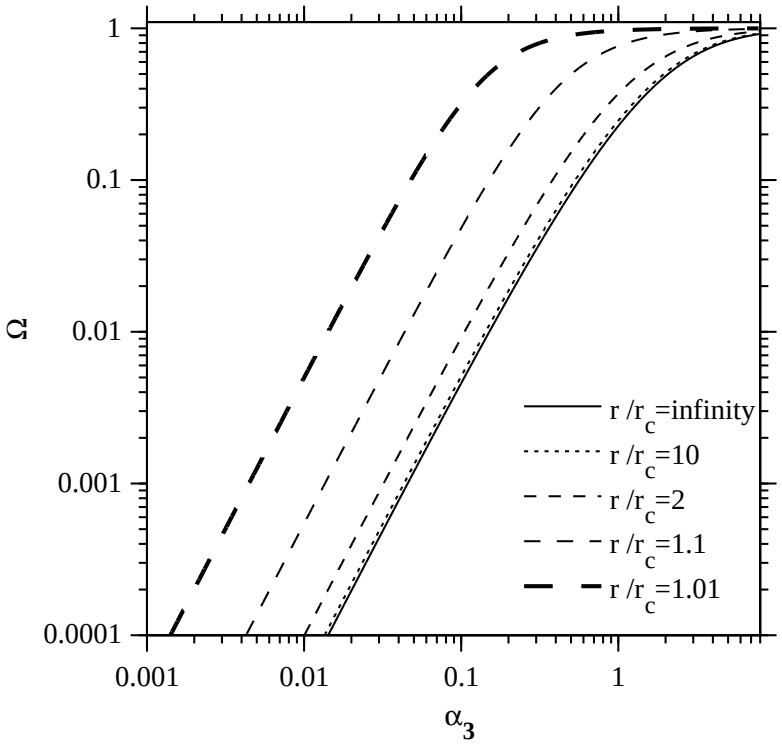

Fig. 3.3: Variation of the growth parameter as a function of the supersaturation and normalised radius. The emphasis here is on small values of Ω.

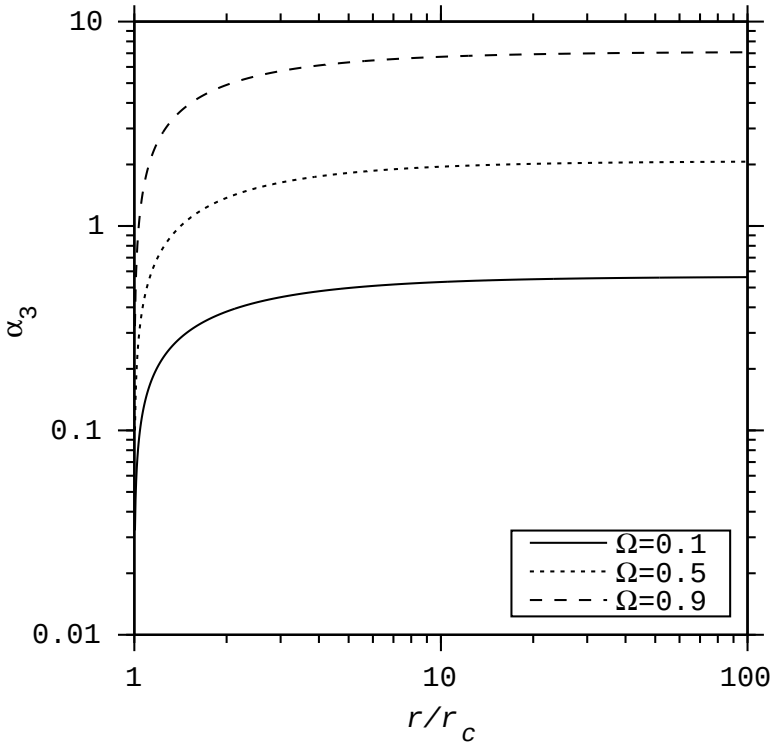

Fig. 3.4: Variation of the growth parameter with the particle radius at large supersaturations.

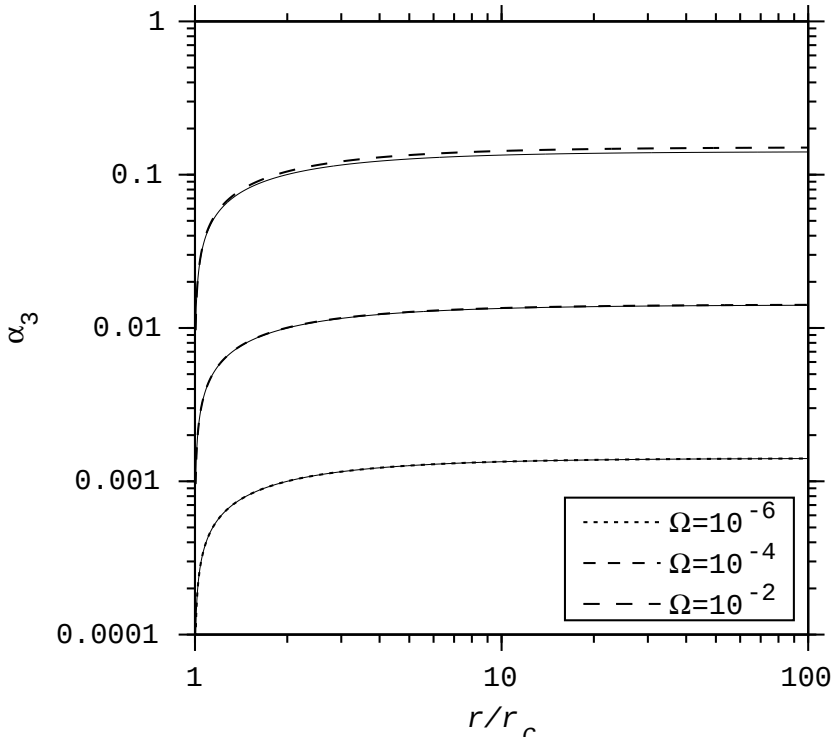

Fig. 3.5: Variation of the growth parameter with the particle radius at small supersaturations.

of α_3 with time is expected to be quite sluggish, at least when capillarity is prominent, so this error might be small.

The author is not aware of an analytical method to rigorously solve equation [3.1] with boundary conditions [3.2, 3.3], but given that the behaviour of the solution seems plausible, it is desirable to measure its accuracy. This was done by numerically solving equation [3.1] as presented in next section.

3.3 Numerical solution

Tanzilli and Heckel [1968] have presented a numerical solution for sphere growth in the absence of capillarity. Thus, equation [3.1] can be expressed as

$$\frac{c_n^{j+1} - c_n^j}{\Delta t} = \frac{N_0 - n}{L - r} \times \frac{c_{n+1}^j - c_{n-1}^j}{2} \times g^{j+1}$$

$$+D \times \frac{c_{n+1}^j - 2c_n^j + c_{n-1}^j}{(L-r)^2/N_0^2} + \frac{D}{r + \frac{(n)(L-r)}{N_0}} \times \frac{c_{n+1}^j - c_{n-1}^j}{(L-r)/N_0} \qquad (3.13)$$

where $n = 0, 1, 2, ..., N_0$ are the nodes that divide the matrix phase in N_0 elements each of length ΔR (Fig. 3.6), j is a time interval, c_n^j is the concentration in n at the time interval j,

Δt is the increment in time, L is the zero mass transfer boundary at the matrix, i.e. where $c_{N_0} = c_{N_0+1}$, and g^{j+1} the interface velocity at the time interval $j+1$. The time increment was set to satisfy the restriction for stable and non–oscillatory solutions to be

$$\Delta t \leq 0.25 \frac{\Delta R^2}{D} \tag{3.14}$$

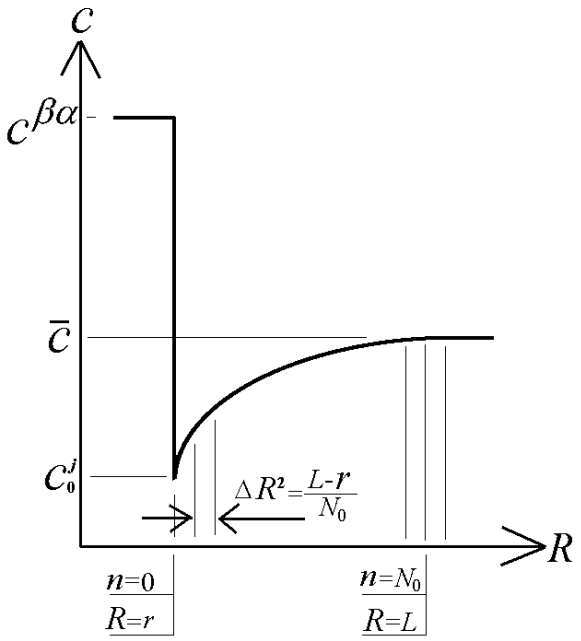

Fig. 3.6: *Definition of finite-difference terminology.*

When capillarity effects are considered, the mass transfer equation [3.9] is similarly expressed as

$$\frac{r^{j+1} - r^j}{\Delta t} = \frac{D}{c^{\beta\alpha} - c_0^j} \times \frac{-c_2^j + 4c_1^j - 3c_0^j}{2(L-r)/N_0} \tag{3.15}$$

where r^j is the particle radius at time interval j and

$$c_0^j = \overline{c} - (\overline{c} - c^{\alpha\beta})\left(1 - \frac{r_c}{r^j}\right) \tag{3.16}$$

where r_c is given by equation [3.5], c_0^j the solute concentration at the matrix interface (Fig. 3.6), which is equivalent to the boundary conditions met by setting the initial concentrations of all the nodes equal to $\overline{c}$ at $t = 0$ except c_0, which is calculated assuming an initial particle radius of $r/r_c = 1.01$. Equations [3.13, 3.15, 3.16] were thus simultaneously solved and their results are shown in Fig. 3.7, where the variation of the growth parameter α_3 is plotted as a function of r/r_c for a variety of compositions (Fig. 3.7a); α_3 was scaled with a starting radius of $r^0 = 1.01$ and Ω with values of $c^{\beta\alpha} = 1$ and $c^{\alpha\beta} = 0$. The variation of the interface velocity g with r/r_c is shown in Fig. 3.7b. The convergence of equations [3.13, 3.15, 3.16] was achieved when as Δt

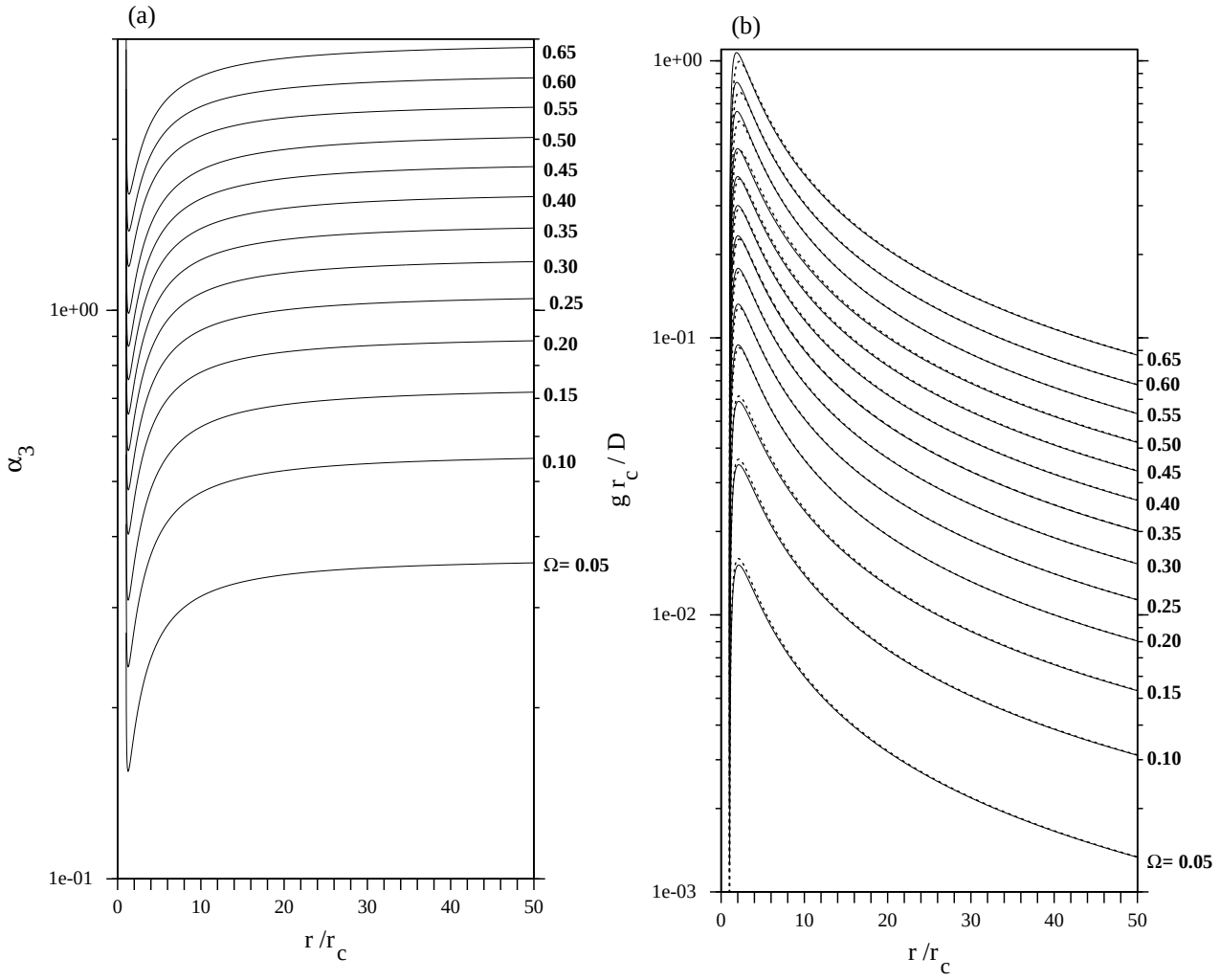

Fig. 3.7: *Finite difference solution for* (a) α_3 *and* (b) g. *The dotted lines represent calculations using the analytical solution.*

was decreased to a convenient value, a negligible change in g^j was produced, and the value of N_0 was such that $c_{N_0} \simeq \overline{c}$. The program that was developed to perform such calculations is shown in Appendix 2.

In Fig. 3.7a α_3 approaches asymptotically the value predicted by Zener's theory; this is expected as for large r/r_c the capillarity effect becomes less important. Consistent with this, the velocity (Fig. 3.7b) approaches a value given by $g = D\alpha_3^2/(2r)$ at large radii, while it approaches zero for small values as the driving force for growth vanishes due to capillarity.

The accuracy of the predictions given by the analytical solution is illustrated in Fig. 3.7b where g is plotted with dotted lines against r/r_c for the indicated values of Ω. The approximate values given by the analytical method adequately predict the velocity trends; in the range of solutions observed, the maximum error was of the order of 11%; thus the analytical solution may be used for calculations where large precision is not required.

Fig. 3.7 shows that the largest correction for α_3, when capillarity is present, is for $1 < r/r_c < 10$. At this stage the particles are quite small, and the inaccuracy that arises from using the analytical solution is very low, thus this can be applied to account for capillarity in alloys such as steels with an error comparable to the resolution of most electron microscopes.

3.4 Summary

An approximate analytical solution for the growth of spherical particles with capillarity has been presented. The theory developed can be applied to dilute ideal solutions. It has been shown that the error involved in the approximation is small, and its application to calculate the kinetics of spherical growth is plausible for many cases.

CHAPTER FOUR

Growth of needle and plate–shaped precipitates

4.1 Introduction

There is a variety of models dealing with the diffusion–controlled growth of precipitates with shapes approximating those of needles or plates. These models have been reviewed in the second chapter. The most comprehensive theory is due to Trivedi [1970a,b], in which the needle is assumed to be in the form of a paraboloid of revolution and the plate as a parabolic cylinder (Fig. 4.1a,b). The solutions he obtained for specified conditions are shape–preserving when the tip radius is several times the critical value (equation[3.5]) and in this context they allow rigorously for changes in capillarity and interface kinetics effects as the curvature of the interface varies along the parabolic surfaces.

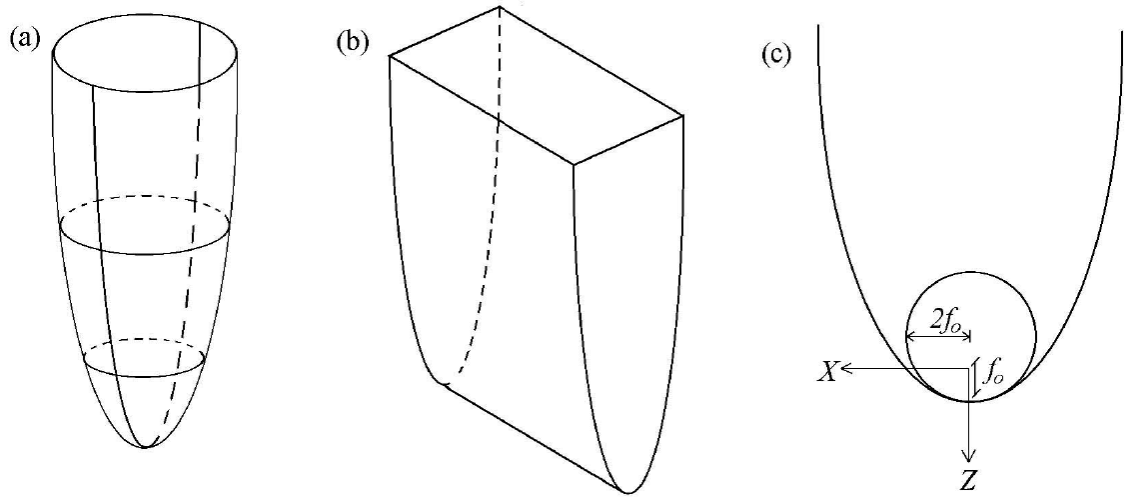

Fig. 4.1: Shapes used to represent needle and plate like precipitates. (a) Paraboloid of revolution; (b) parabolic cylinder; (c) radius of the parabola tip.

Consistent with many experimental observations, the theory predicts constant lengthening rates because the needle or plate tip advances into fresh parent phase as solute is partitioned. However, the numerical components of the solutions obtained by Trivedi [1970a,b] are limited to large values of supersaturation. In practice, many precipitation reactions in technologically important applications occur at small supersaturations [Robson and Bhadeshia, 1997c]. The method and equations that Trivedi used to solve this problem are shown in section 2.4.4,

whereas the fine points of his mathematical treatment are introduced in the forthcoming sections, the extension to low supersaturations is then presented, where simple asymptotic relationships were derived to predict the kinetics at this regime.

4.2 Theory for needle growth

The equation relating the Péclet number $p = g_p r/2D$ to the dimensionless supersaturation Ω is given by:

$$\Omega = p \exp\{p\} E_1\{p\} \left[\underbrace{1}_{i} + \underbrace{\frac{g_p}{g_c} \Omega R_1\{p\}}_{ii} + \underbrace{\frac{r_c}{r} \Omega R_2\{p\}}_{iii} \right] \tag{4.1}$$

where g_p is the lengthening rate, r is the radius of curvature at the tip of the paraboloid, and D is the diffusion coefficient of the solute in the matrix phase. $r = 2f_o$, where f_o is the focal distance (Fig. 4.1c), which is defined uniquely for a parabola lengthening along the Z direction, and thickening along the X direction [Horvay and Cahn, 1961]. $g_c = \mu_o(\overline{c} - c^{\alpha\beta})$ is the velocity of a flat interface during interface controlled growth, i.e., when almost all the free energy is dissipated in the transfer of atoms across the interface, so that the concentration difference in the matrix vanishes; and μ_o is the interface kinetics coefficient.

For curved interfaces, the growth rate is a function of the interface curvature via the Gibbs–Thomson effect. The curvature at which the growth rate becomes zero is $1/r_c$. The functions $R_1 = \frac{1}{2p} N_1\{p\} - 1$ and $R_2 = \frac{1}{4p} N_2\{p\} - 1$ were evaluated numerically by Trivedi [1970b] to deal with the fact that the curvature of the interface varies along the surface of the paraboloid of revolution.

The values of $N_1\{p\}$ and $N_2\{p\}$ are [Trivedi, 1970a]

$$N_1\{p\} = 2p^{3/2} \exp\{p\} \sum_{n=0}^{\infty} \frac{\Gamma_D\{n+\frac{1}{2}\}}{\Gamma_D\{n+1\}} I_{2n}\mathrm{erfc}\{\sqrt{p}\} \frac{\Psi\{n+1;2;p\}}{\Psi\{n+1;1;p\}} \tag{4.2}$$

$$N_2\{p\} = 2p^{3/2} \exp\{p\} \sum_{n=0}^{\infty} 2\sqrt{p} I_{2n+1}\mathrm{erfc}\{\sqrt{p}\} \frac{\Psi\{n+1;2;p\}}{\Psi\{n+1;1;p\}} + N_1\{p\} \tag{4.3}$$

where Γ_D, I_{2n}erfc, and Ψ are the gamma, normalised integral error [Abramowitz, 1965], and confluent hypergeometric function of the second type [Zhang, 1996], respectively.

Referring to equation [4.1], the term i is the Ivanstov [1947] solution where the capillarity and interface kinetics are neglected; terms iii and ii account respectively for those effects.

Equation [4.1] does not give a unique answer for the growth rate g_p which depends on the tip radius r. For solid–state transformations one might adopt Zener's assumption [Zener, 1946,

Bhadeshia, 1985a,b] that the the radius of curvature is that which gives rise to the maximum growth rate. This is obtained by differentiating equation [4.1] with respect to r and setting $\partial g_p/\partial r = 0$, which gives

$$0 = \left(g^*\{p\}\right)^2 \frac{r_c}{r}\left(2\frac{p}{q^*}R_1'\{p\} - \frac{1}{p}R_2\{p\} + R_2'\{p\}\right) + \frac{g^*\{p\}}{p} + g^*\{p\} - 1 \tag{4.4}$$

where $g^*\{p\} = p\exp\{p\}E_1\{p\}$ and $q^* = \frac{\mu_o(\overline{c}-c^{\alpha\beta})}{2D/r_c}$ is a parameter which indicates the relative magnitudes of the interface kinetics and the diffusion effect. Equation [4.1] can be expressed as well using the parameter q^*:

$$\Omega = g^*\{p\}\left[1 + 2\frac{r_c}{r}\frac{p}{q^*}\Omega R_1\{p\} + \frac{r_c}{r}\Omega R_2\{p\}\right] \tag{4.5}$$

The values of the functions R_1, R_2 and R_1' and R_2' were given by Trivedi [1970b] for $p \geq 0.1$; they are used to solve simultaneously equations [4.4] and [4.5], which give in turn a unique solution for p and $\frac{r}{r_c}$ as a function of Ω.

4.3 Theory for plate growth

Trivedi's model for a parabolic cylinder takes a similar form:

$$\Omega = \sqrt{\pi p}\exp\{p\}\mathrm{erfc}\{\sqrt{p}\}\left[\underbrace{1}_{iv} + \underbrace{\frac{g_p}{g_c}\Omega S_1\{p\}}_{v} + \underbrace{\frac{r_c}{r}\Omega S_2\{p\}}_{vi}\right] \tag{4.6}$$

where $S_1\{p\} = \frac{1}{2p}M_1\{p\} - 1$ and $S_2\{p\} = \frac{1}{2p}M_2\{p\} - 1$ account for the change in curvature along the parabolic cylinder [Trivedi, 1970b]. The terms iv, v and vi account for the boundary iso–concentrate solution, interface kinetics, and capillarity effects, respectively.

The functions $M_1\{p\}$ and $M_2\{p\}$ can be expressed as

$$M_1\{p\} = \frac{2p}{\pi}\sum_{n=0}^{\infty}\Gamma_D\{n+\tfrac{1}{2}\}\frac{I_{2n+1}\mathrm{erfc}\{\sqrt{p}\}}{I_{2n}\mathrm{erfc}\{\sqrt{p}\}}\Psi\{n+\tfrac{1}{2};1;p\} \tag{4.7}$$

$$M_2\{p\} = \frac{4p^2}{\pi}\sum_{n=0}^{\infty}\Gamma_D\{n+\tfrac{3}{2}\}\frac{I_{2n+1}\mathrm{erfc}\{\sqrt{p}\}}{I_{2n}\mathrm{erfc}\{\sqrt{p}\}}\Psi\{n+\tfrac{3}{2};2;p\} \tag{4.8}$$

Similarly, equation [4.6] is differentiated with respect to to r, allowing $\partial g_p/\partial r = 0$ to account for maximum growth rate. The resulting equation is

$$0 = \left(g^\diamond\{p\}\right)^2 \frac{r_c}{r}\left[\frac{p}{q}S_1'\{p\} - \frac{1}{p}S_2\{p\} + S_2'\{p\}\right] + \frac{g^\diamond\{p\}}{2p} + g^\diamond\{p\} - 1 \tag{4.9}$$

where $g^\diamond\{p\} = \sqrt{\pi p}\exp\{p\}\mathrm{erfc}\{\sqrt{p}\}$ and $q = 2q^*$. Equation [4.6] can be expressed in terms of q to give

$$\Omega = g^\diamond\{p\}\left[1 + \frac{r_c}{r}\frac{p}{q}\Omega S_1\{p\} + \frac{r_c}{r}\Omega S_2\{p\}\right] \tag{4.10}$$

The values of the functions S_1, S_2 and S_1', S_2' were provided by Trivedi [1970b] for $p \geq 0.1$ and are used to solve simultaneously equations [4.9] and [4.10] from which p and $\frac{r}{r_c}$ are obtained.

4.4 Extension for low supersaturations

To solve simultaneously equation [4.4] with [4.5], and [4.9] with [4.10] for small supersaturations, the functions R_1, R_2, S_1 and S_2 must be evaluated for $p \leq 0.1$. Thus, a numerical method was developed to obtain N_1, N_2, M_1 and M_2 for $p \leq 0.1$, the resulting values are shown graphically in Fig. 4.2; the functions R_1, R_2, S_1 and S_2 can now be evaluated and are shown in Fig. 4.3. The computer programs that cast the values plotted in Figs. 4.2 and 4.3 are presented in Appendix 3.

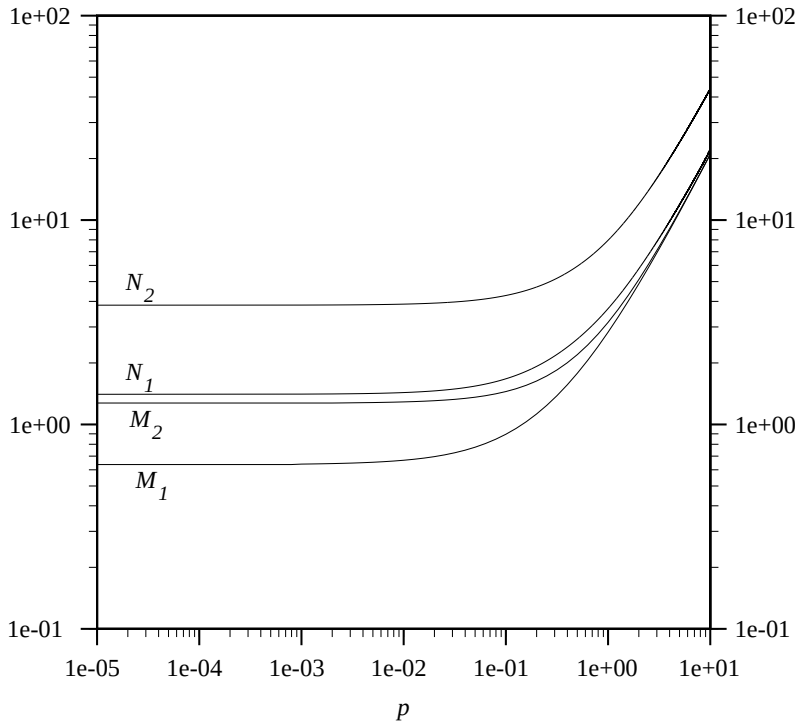

Fig. 4.2: Values of functions N_1, N_2, M_1, M_2

Trivedi's solution for p and r/r_c can now be extended to small supersaturation values of $\Omega < 0.2$ for needles (Figs. 4.4, 4.5) and $\Omega < 0.4$ for plates (Figs. 4.6, 4.7) through simultaneous solution of equations [4.4–5] and [4.9–10]. Computer programs were written to perform the task, and are presented in Appendix 4. The results show that as the supersaturation decreases, the values of p and $\frac{r}{r_c}$ approach asymptotically to a curve; this effect is shown for very small supersaturation values in Figs. 4.8, 4.9 for needles and in Figs. 4.10, 4.11 for plates.

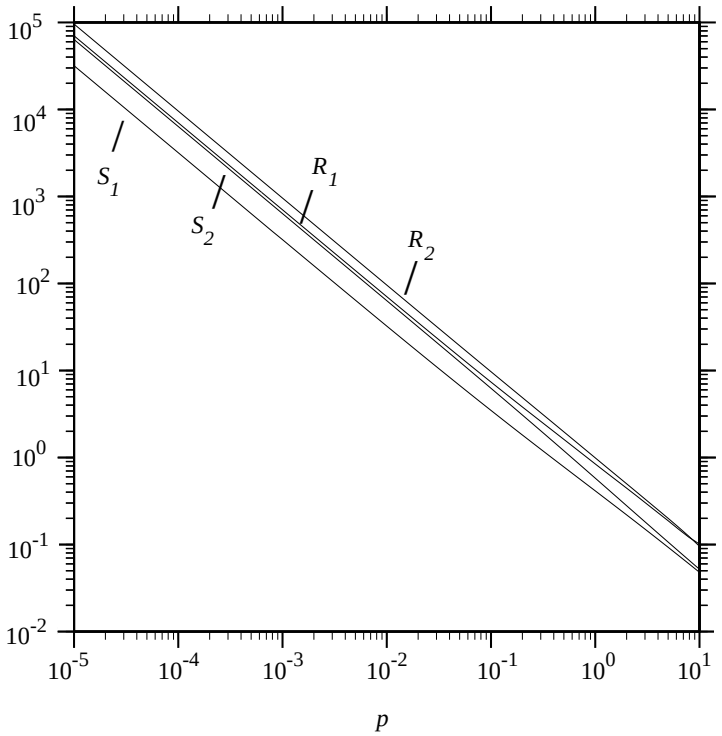

Fig. 4.3: Values of functions R_1, R_2, S_1, S_2

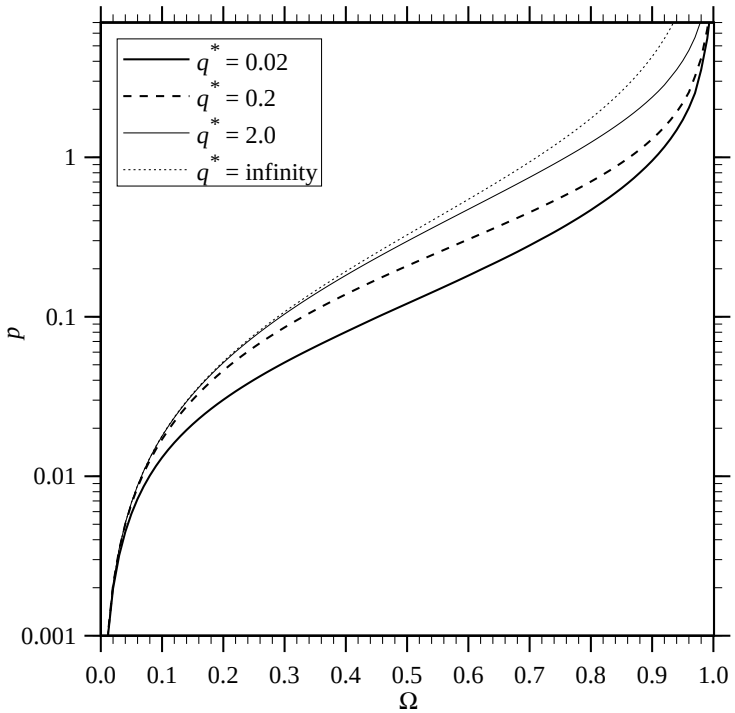

Fig. 4.4: Péclet number for needle maximum growth rate

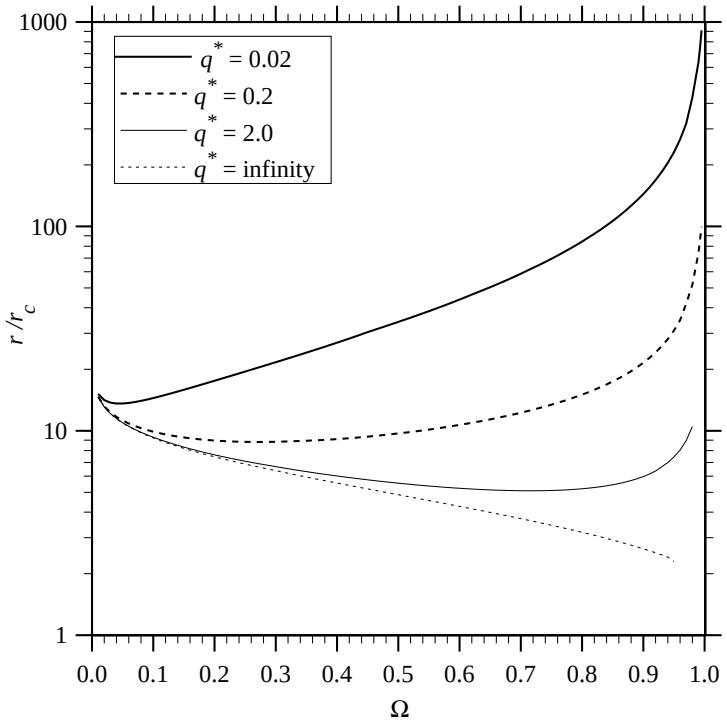

Fig. 4.5: Tip radius for needle maximum growth rate

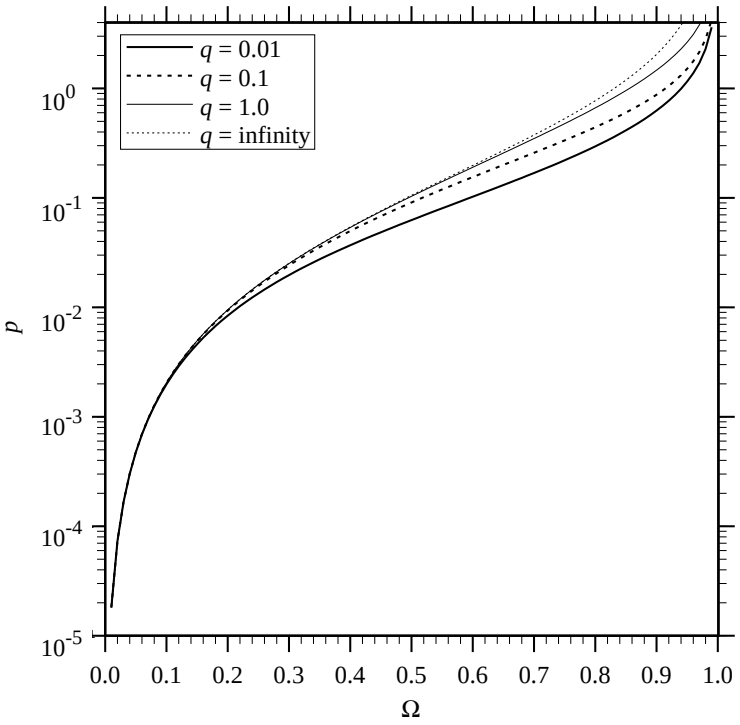

Fig. 4.6: Péclet number for plate maximum growth rate

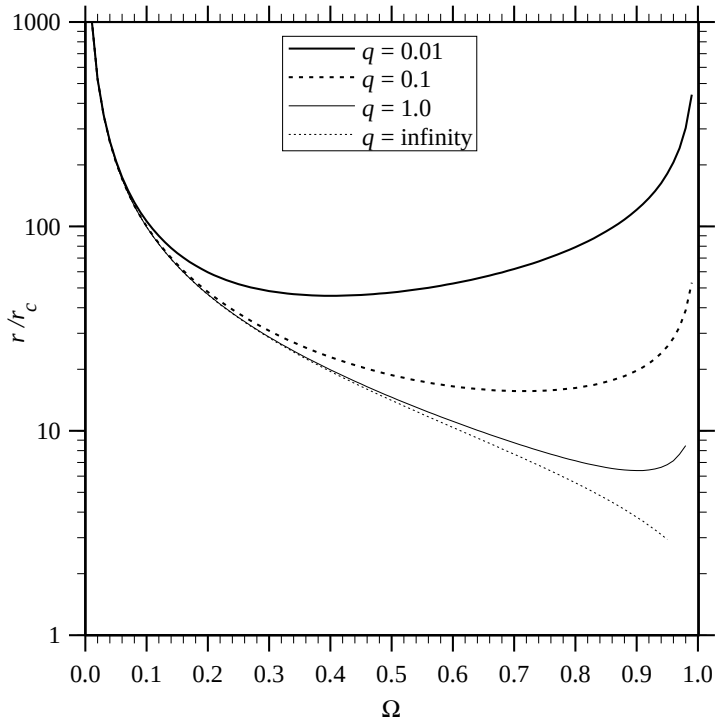

Fig. 4.7: Tip radius for plate maximum growth rate

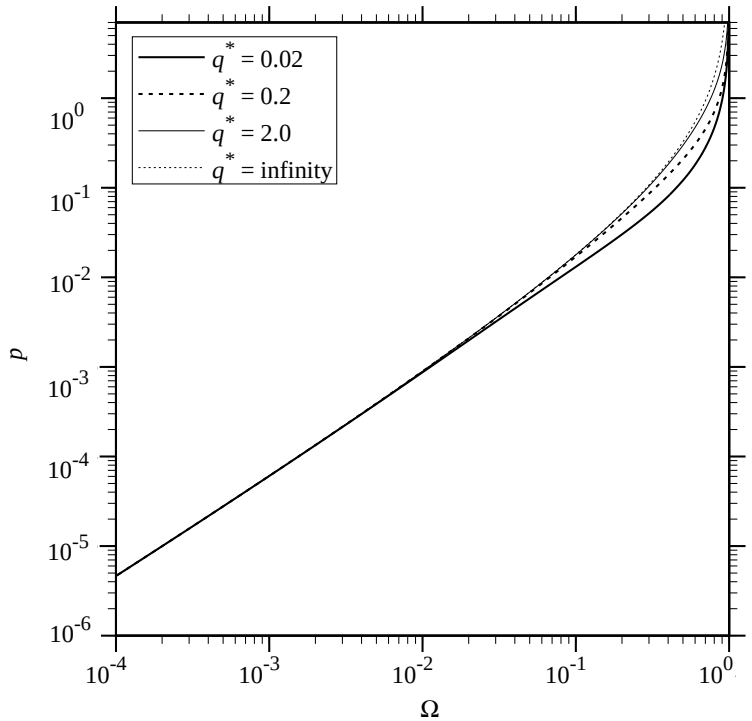

Fig. 4.8: Péclet number for the maximum growth rate of a needle as a function of the supersaturation. Low supersaturation values.

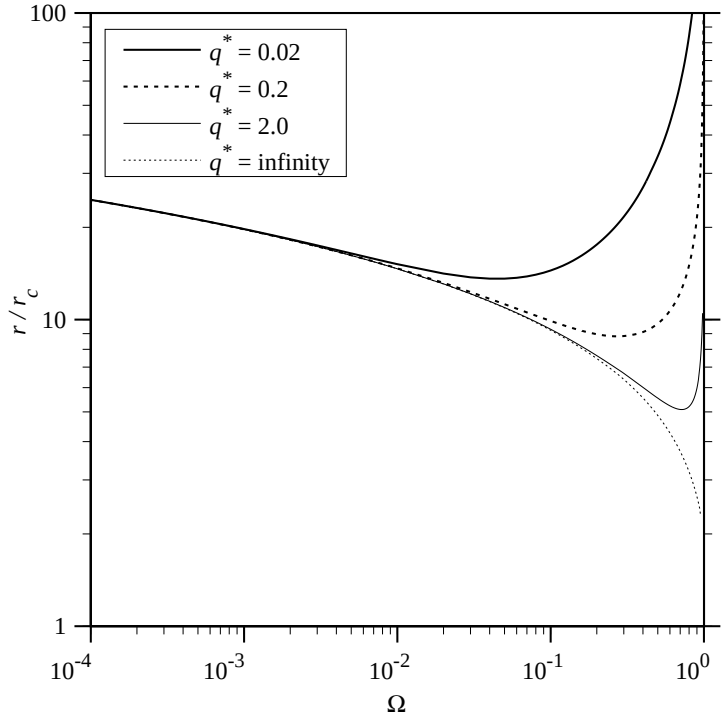

Fig. 4.9: Tip radius for the maximum growth rate of a needle as a function of the supersaturation. Low supersaturation values.

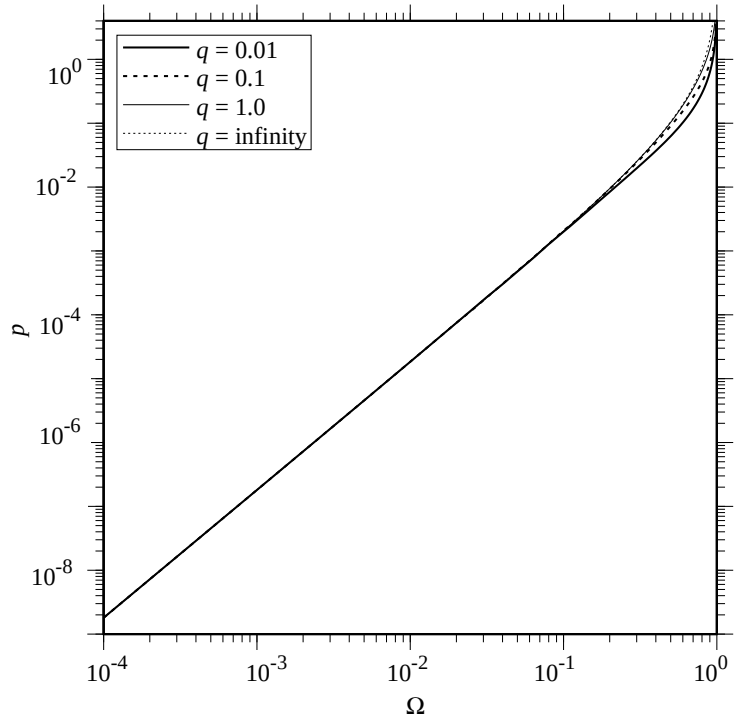

Fig. 4.10: Péclet number for the maximum growth rate of a plate as a function of the supersaturation. Low supersaturation values.

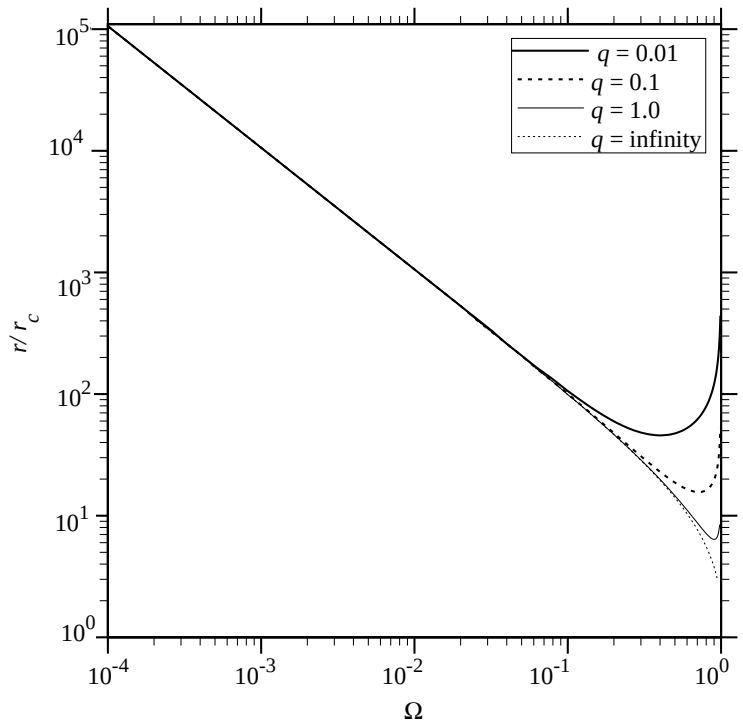

Fig. 4.11: Tip radius for plate for the maximum growth rate of a plate as a function of the supersaturation. Low supersaturation values.

The low supersaturation behaviour displayed by Figs. 4.8–11 suggests simple relationships to express Péclet number and tip radius for needles and plates in the low supersaturation regime. This was investigated by expressing the transcendental functions in equations [4.4–5] and [4.9–10] for low values of p, as described next.

Needles

Equations [4.5] and [4.4] can be expressed as follows:

$$\frac{r}{r_c} = \frac{g^*\{p\}\Omega}{\Omega - g^*\{p\}}\left[2\frac{p}{q^*}R_1\{p\} + R_2\{p\}\right] \tag{4.11}$$

$$\frac{r}{r_c} = \frac{\left(g^*\{p\}\right)^2}{\frac{g^*\{p\}}{p} + g^*\{p\} - 1}\left[-2\frac{p}{q^*}R_1'\{p\} + \frac{1}{p}R_2\{p\} - R_2'\{p\}\right] \tag{4.12}$$

The asymptotic expansion of E_1 is expressed as [Abramowitz, 1965]

$$E_1\{p\} = -\gamma_e - \ln\{p\} - \sum_{n=1}^{\infty}\frac{(-1)^n p^n}{nn!}$$

where $\gamma_e = .5772156649...$ is Euler's constant and $k = \exp\{\gamma_e\}$, thus for $p \to 0$ $E_1\{p\} \simeq -\ln\{kp\}$, so $g^*\{p\} \simeq -p\ln\{kp\}$. Furthermore, as $p \to 0$, $N_1\{p\} \to 1.4050$ and $N_2\{p\} \to 3.8410$ [Trivedi, 1970a]. Equations [4.11] and [4.12] can be equated, and for $p \to 0$

$$\frac{g^*\{p\}\Omega}{\Omega - g^*\{p\}} \to \frac{-p\ln\{kp\}\Omega}{\Omega + p\ln\{kp\}}$$

$$\frac{\left(g^*\{p\}\right)^2}{\frac{g^*\{p\}}{p}+g^*\{p\}-1} \rightarrow \frac{-p^2\ln\{kp\}}{1+(ln\{kp\})^{-1}}$$

$$2\frac{p}{q^*}R_1\{p\}+R_2\{p\} \rightarrow \frac{3.8410}{4p}$$

$$-2\frac{p}{q^*}R_1'\{p\}+\frac{1}{p}R_2\{p\}-R_2'\{p\} \rightarrow \frac{3.8410}{2p^2}$$

Thus, the dominant factor is the capillarity effect (term *iii* in equation [4.1]). After some algebra, the resulting equation can be expressed as

$$\Omega = \frac{2p(\ln\{kp\})^2}{1-\ln\{kp\}} \tag{4.13}$$

while from equation [4.11], in the limit of $p \rightarrow 0$, the needle tip radius expression becomes

$$\frac{r}{r_c} = -\frac{3.8410}{4}\frac{\Omega\ln\{kp\}}{\Omega+p\ln\{kp\}} \tag{4.14}$$

Plates

For plate–shaped precipitates, equations [4.10] and [4.9] can be expressed as

$$\frac{r}{r_c} = \frac{g^\diamond\{p\}\Omega}{\Omega-g\{p\}}\left[\frac{p}{q}S_1\{p\}+S_2\{p\}\right] \tag{4.15}$$

$$\frac{r}{r_c} = \frac{\left(g^\diamond\{p\}\right)^2}{\frac{g^\diamond\{p\}}{2p}+g^\diamond\{p\}-1}\left[-\frac{p}{q}S_1'\{p\}+\frac{1}{p}S_2\{p\}-S_2'\{p\}\right] \tag{4.16}$$

The asymptotic expansion of erfc is expressed as [Abramowitz, 1965]:

$$\text{erfc}\{\sqrt{p}\} = 1-\text{erf}\{\sqrt{p}\} = 1-\frac{2}{\sqrt{\pi}}\exp\{-p\}\sum_{n=0}^{\infty}\frac{2^n}{1\cdot 3\cdots(2n+1)}p^{2n+1}$$

thus, for $p \rightarrow 0$, $\text{erfc}\{\sqrt{p}\} \rightarrow 1-\frac{2}{\sqrt{\pi}}\sqrt{p}$, so $g\{p\} \simeq \sqrt{\pi p}$. Furthermore, as $p \rightarrow 0$, $M_1\{p\} \rightarrow \frac{2}{\pi}$ and $M_2\{p\} \rightarrow \frac{4}{\pi}$ [Trivedi, 1970b]. Equations [4.15] and [4.16] can be equated, and for $p \rightarrow 0$

$$\frac{g^\diamond\{p\}\Omega}{\Omega-g^\diamond\{p\}} \rightarrow \frac{\sqrt{\pi p}\Omega}{\Omega-\sqrt{\pi p}}$$

$$\frac{\left(g^\diamond\{p\}\right)^2}{\frac{g^\diamond\{p\}}{2p}+g^\diamond\{p\}-1} \rightarrow 2\sqrt{\pi}p^{3/2}$$

$$\frac{p}{q}S_1\{p\}+S_2\{p\} \rightarrow \frac{2}{\pi p}$$

$$-\frac{p}{q}S_1'\{p\}+\frac{1}{p}S_2\{p\}-S_2'\{p\} \rightarrow \frac{4}{\pi p^2}$$

Thus, the dominant factor is the capillarity effect (term *vi* in equation [4.6]). After some algebra, the resulting equation can be expressed as

$$p = \frac{9}{16\pi}\Omega^2 \tag{4.17}$$

while from equation [4.5], in the limit of $p \to 0$, the plate tip radius expression becomes

$$\frac{r}{r_c} = \frac{32}{3}\frac{1}{\Omega} \tag{4.18}$$

4.5 Discussion and summary

The analysis presented here provides the values of p and $\frac{r}{r_c}$ for small supersaturations, when the interface kinetics and capillarity effects are present. The results reveal the influence of each effect and provide useful values for further calculations.

Equations [4.13–14] and [4.17–18] are useful in computing the growth rate and tip radius for needles or plates for small supersaturations, *e.g.* the precipitation of needle–type particles in secondary hardening steels. Some of these calculations were performed by Fujita and Bhadeshia [1999], and Robson and Bhadeshia [1997a,b]; they used the Zener theory [1949] reviewed by Christian [1975], which predicts the growth rate for needle precipitates in which a hemispherical needle tip controls the particle growth, but without equilibrium along the interface as the curvature changes. Such theory predicts a constant value of $\frac{r}{r_c} = 2$ regardless of the magnitude of Ω, and $p = \frac{\Omega}{4}$. Fig. 4.9 shows a difference of one order of magnitude compared to that model, while Fig. 4.8 shows a value of $p \simeq 2.5$ bigger than previous approximation.

To summarise, it is now possible to use Trivedi's models to treat the precipitation of plates or needles in circumstances where the supersaturation is quite small. Simple asymptotic relationships have been obtained to calculate the growth rate and tip radius at small supersaturations, and have been shown not to depend on the magnitude of the interface kinetics effect, as less driving force is available for volume diffusion, decreasing the lengthening velocity and the resistance of atoms to transfer across the interface.

CHAPTER FIVE

Growth in multicomponent systems

5.1 Introduction

Having developed the necessary theory for spherical growth with capillarity, and needle and plate growth for low supersaturations with interface kinetics and capillarity, it becomes possible to analyse the behaviour of multicomponent alloys. The present chapter provides such an analysis along with the necessary theory to treat the case. Novel conclusions have been obtained, for example that the maximum velocity hypothesis cannot be sustained in the multicomponent scenario.

5.2 Thermodynamics of multicomponent systems with capillarity

In order to obtain the composition shifts in a multicomponent system, it is necessary to obtain expressions for the Gibbs energy and chemical potential shifts due to capillarity for each component. In analogy to the Gibbs energy increase per atom presented in section 2.3.2, the change in free energy per mole of precipitate phase Δg^{β} can be expressed as

$$\Delta g^{\beta} = \sigma \frac{dO}{dn} \tag{5.1}$$

where the second term implies the rate at which the interfacial area O changes on the addition of n moles of solute. The resulting change in the chemical potential of the solute in α is:

$$\mu_r^{\alpha} - \mu^{\alpha} = \frac{1 - c_r^{\alpha\beta}}{c_r^{\beta\alpha} - c_r^{\alpha\beta}} \sigma \frac{dO}{dn} \tag{5.2}$$

where μ_r^{α} and μ^{α} are the chemical potentials for curved and flat interfaces respectively; $c_r^{\beta\alpha}$ and $c_r^{\alpha\beta}$ are the capillarity corrected concentrations at the interface. The chemical potential shift can be expressed as:

$$\mu_r^{\alpha} - \mu^{\alpha} = R_u T \ln\left(\frac{s_r^{\alpha} c_r^{\alpha\beta}}{s^{\alpha} c^{\alpha\beta}}\right) \tag{5.3}$$

were s_r^{α} and s^{α} are the activity coefficients when capillarity is present, and is neglected, respectively. When expressions [5.2] and [5.3] are equated, equation [2.11] is obtained if the solution is dilute enough to obey Henry's law.

Henry's law is assumed in the following derivation of capillarity in multicomponent solutions. The energy shift referred to component i can then be expressed as

$$\sigma \frac{dO}{dn_i} = \sigma \frac{2\overline{V}_i}{r} \tag{5.4}$$

where n_i is the mole number of component i and $\overline{V}_i$ its partial molar volume. It follows that in a multicomponent solution,

$$\mu_{ri}^{\alpha} - \mu_i^{\alpha} = \frac{1 - c_{ri}^{\alpha\beta}}{c_{ri}^{\beta\alpha} - c_{ri}^{\alpha\beta}} \sigma \frac{2\overline{V}_i}{r} \tag{5.5}$$

$$\mu_{ri}^{\alpha} - \mu_i^{\alpha} = R_u T \ln\left(\frac{s_{ri}^{\alpha} c_{ri}^{\alpha\beta}}{s_i^{\alpha} c_i^{\alpha\beta}}\right) \tag{5.6}$$

where μ_{ri}^{α}, μ_i^{α}, $c_{ri}^{\alpha\beta}$, $c_{ri}^{\beta\alpha}$, s_{ri}^{α} and s_i^{α} hold the same meanings as before, but are referred to component i. When Henry's law can be applied, and if it is assumed that the solution is sufficiently dilute to avoid interactions between the different solutes, equations [5.5] and [5.6] reduce to

$$c_{ri}^{\alpha\beta} = c_i^{\alpha\beta}\left(1 + \frac{2\Gamma_i}{r}\right) \qquad \text{with} \qquad \Gamma_i = \left(\frac{\sigma \overline{V}_i}{R_u T}\right)\left(\frac{1 - c_i^{\alpha\beta}}{c_i^{\beta\alpha} - c_i^{\alpha\beta}}\right) \tag{5.7}$$

and the critical radius becomes

$$r_{ci} = \frac{2 c_i^{\alpha\beta} \Gamma_i}{\overline{c}_i - c_i^{\alpha\beta}} \tag{5.8}$$

Naturally, the value of r_{ci} must be identical for all species of solute.

5.3 Multicomponent spherical growth

Multicomponent growth of spherical particles requires the solution of Fick's second law (equation [2.39]) for each i component, along with the mass conservation condition at the interface, which can be expressed for each component as:

$$g\left[c_i^{\beta\alpha} - c_i^{\alpha\beta}\{t, r\}\right] = D_i \left.\frac{\partial c_i}{\partial R}\right|_{R=r} \tag{5.9}$$

The boundary conditions to be applied are:

$$c_i\{0, r\} = \overline{c}_i \qquad \text{and} \qquad c_i\{t, r\} = c_i^{\alpha\beta} + \frac{2 c_i^{\alpha\beta} \Gamma_i}{r} \tag{5.10}$$

using the approximate solution method given in Chapter 3, it is obtained for each component

$$\Omega_i = \frac{f_{1i}}{1 + \frac{r_{ci}}{r}(f_{1i} - 1)} \qquad \text{where} \qquad f_{1i} = \frac{\alpha_{3i}^3}{2} \exp\left\{\frac{1}{4}\alpha_{3i}^2\right\}\left[\frac{1}{\alpha_{3i}} \exp\left\{\frac{-\alpha_{3i}^2}{4}\right\} - \frac{\sqrt{\pi}}{2} \text{erfc}\left\{\frac{\alpha_{3i}}{2}\right\}\right] \tag{5.11}$$

Equation [5.11] can be solved for any number of diffusing components, using the procedure as follows. The problem is to determine the precipitate growth rate from an alloy of a known composition. The equilibrium values of the components are not independent since they are all connected by a tie–line of the phase diagram. From Gibbs phase rule, when T and P are set, it follows that the equilibrium concentrations of $C-2$ components (C is the number of components of the alloy) can be varied, and the values of all others obtained from the phase diagram, permitting all the supersaturations Ω_i to be calculated, and values of α_{3i}, $i = 1,\ 2,\ ,...,\ m$ to be obtained from equation [5.11]. It is required that the equations arising from substituting $i = 1,\ 2,...,\ C$ in equation [5.11] must produce the same particle growth rate, a condition which is met when

$$\alpha_{31}\sqrt{D_1} = \alpha_{32}\sqrt{D_2} = ... = \alpha_{3C}\sqrt{D_C} \tag{5.12}$$

Thus, the problem is reduced to finding a set of compositions $c_1^{\alpha\beta}$, $c_2^{\alpha\beta}$,...,$c_{C-2}^{\alpha\beta}$ from which equation [5.12] is satisfied, and the growth rate is obtained from

$$\frac{dr}{dt} = \frac{1}{2}\alpha_{3i}\sqrt{\frac{D_i}{t}} \tag{5.13}$$

for any value of i.

Effects in growth rate

Capillarity has the effect of reducing the driving force for transformation; it should therefore be revealed in plots of interface–velocity contours. Figure 5.1 shows that with respect to a particular alloy labelled as 'x' in the phase diagram, the IV contours n $= -8,\ -7,...,\ 7,\ 8$ ($\alpha_{32} = 0.04(2)^{\mathrm{n}}$) shift towards greater supersaturations as capillarity is introduced. When the diffusion ratio is large, it is apparent that an IV contour which lies in a regime where there is no long–range partitioning of the slow diffuser, can be shifted into a regime where such partitioning is necessary. This situation is shown in Fig. 5.2, in which the alloy labelled 'x' slows down from a velocity given by n$\simeq$ 5, when capillarity can be neglected (Fig. 5.2a), to n$\simeq$ 1 when it is relevant (Fig. 5.2c).

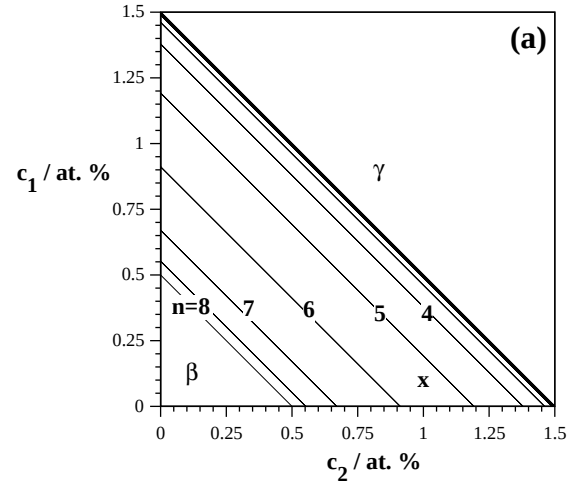

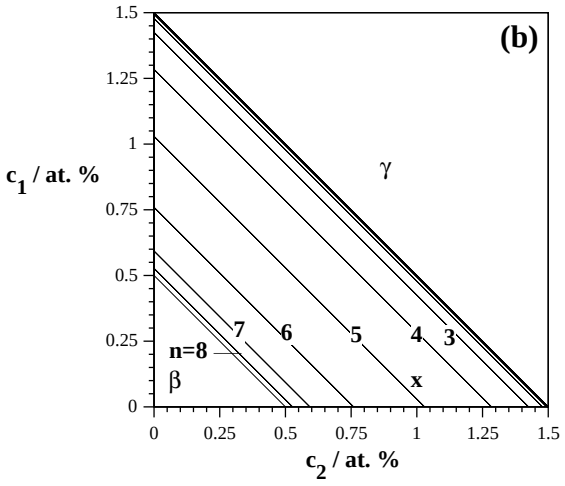

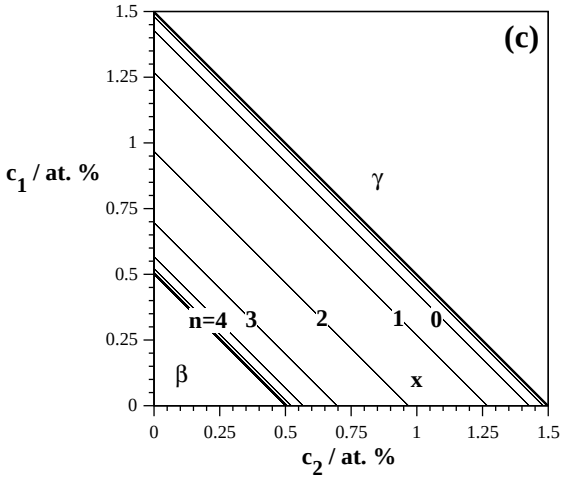

Fig. 5.1: IV Contours for $D_1/D_2 = 1$, (a) capillarity is neglected (b) $r/r_c = 2$, (c) $r/r_c = 1.01$.

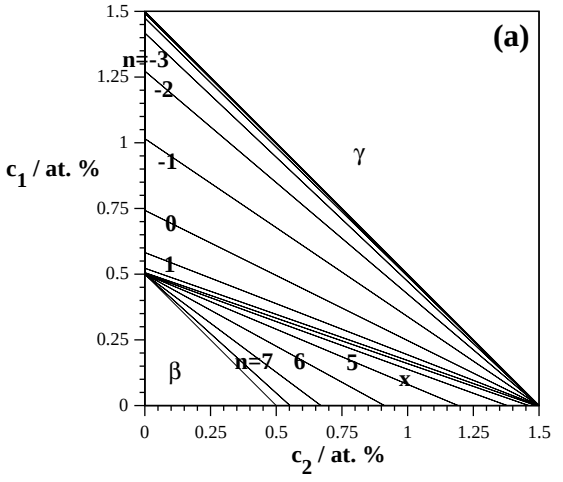

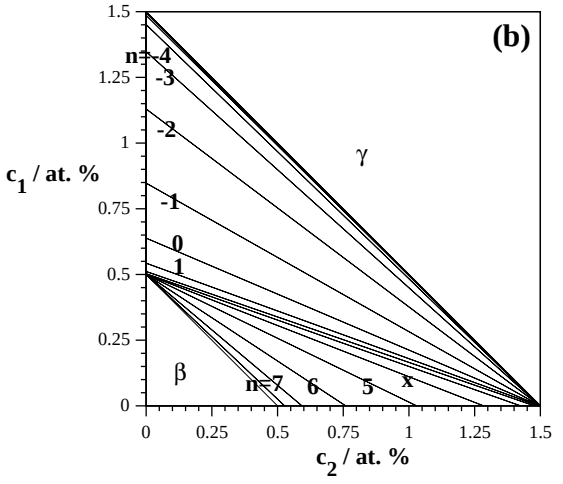

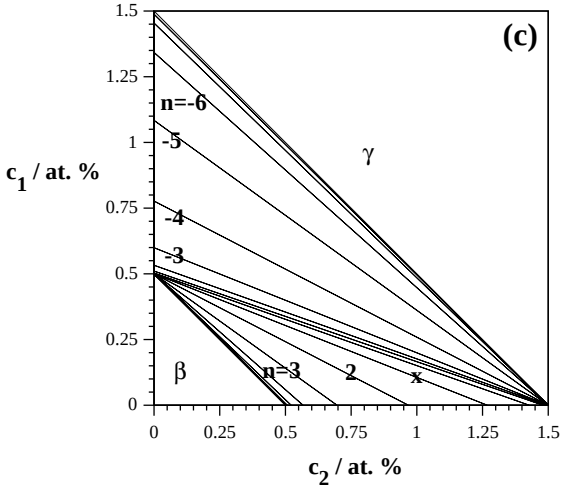

Fig. 5.2: IV Contours for $D_1/D_2 = 10^4$, (a) capillarity is neglected (b) $r/r_c = 2$, (c) $r/r_c = 1.01$.

5.4 Multicomponent needle growth

The solution to the multicomponent growth of needles comes from the solution of Fick's second law which is substituted in the mass balance equation, each of these must be expressed in parabolic coordinates for each component:

$$\frac{\partial^2 c_i}{\partial \gamma^2} + \left(\frac{1}{\gamma} + 2p_i\gamma\right)\frac{\partial c_i}{\partial \gamma} + \frac{\partial^2 c_i}{\partial \delta^2} + \left(\frac{1}{\delta} - 2p_i\delta\right)\frac{\partial c_i}{\partial \delta} = 0 \tag{5.14}$$

$$2p_i\left[c_i^{\beta\alpha} - \left(c_i^{\alpha\beta} + 2\underbrace{\frac{c_i^{\alpha\beta}\Gamma_i}{r}}_{t_1} + \underbrace{\frac{g_p}{\mu_{oi}}}_{t_2}\right)\right] = \left(\frac{\partial c_i}{\partial \gamma}\right)_{\substack{\gamma=1\\ \delta=0}} \tag{5.15}$$

where $p_i = g_p r/2D_i$ is the Péclet number of component i. These equations have to be solved under the next boundary condition

$$c_i(1,\delta) - c_i^{\alpha\beta} = \underbrace{\left(\frac{c_i^{\alpha\beta}\Gamma_i}{r}\right)}_{t_1}\frac{(2+\delta^2)}{(1+\delta^2)^{3/2}} + \underbrace{\frac{g_p}{\mu_{oi}}}_{t_2}\frac{1}{(1+\beta^2)^{1/2}} \tag{5.16}$$

It is observed that the isoconcentrate boundary solution corresponds to the case when t_1 and t_2 are neglected; and when only t_2 is neglected the effect of capillarity with no interface kinetics is present. Due to the complexity of the solution, the analysis of its behaviour is divided in three cases of increasing difficulty: isoconcentrate boundary, capillarity, and capillarity and interface kinetics.

5.4.1 Isoconcentrate boundary

The solution of equation [5.14] using boundary condition [5.16] and substituted in [5.15] with $t_1 = t_2 = 0$ gives Ivanstov equation for $i = 1, 2, ..., C$ components:

$$\Omega_i = p_i \exp\{p_i\} E_1\{p_i\} \tag{5.17}$$

Since g_p and r can only have single values, simultaneous solution of equation [5.17] for $i = 1, 2, ..., C$ demands

$$p_1 D_1 = p_2 D_2 = ... = p_C D_C \tag{5.18}$$

Consider now a ternary system, such as a steel. The influence of a difference in the diffusivities of two components (for example carbon and a substitutional solute) can be seen by varying p_2 and obtaining $p_1 = \frac{D_2}{D_1}p_2$, and plotting the results in the form of Coates interface–composition (IC) contours for several values of D_2/D_1. Such results are shown in Fig. 5.3. Thus, as discussed in Chapter 2, a needle–shaped particle with an isoconcentrate interface

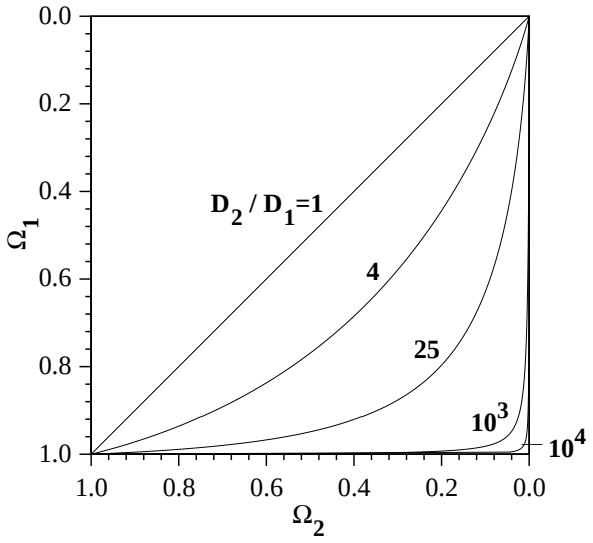

Fig. 5.3: Needle-shaped isoconcentrate particle IC contours for different ratios of diffusivities in a ternary system.

behaves much the same as a sphere but with p_1, p_2 given by the solution of equations [5.17–18]. It is, however, not possible to determine unique values for g_p and r, and the maximum velocity hypothesis is not feasible.

5.4.2 The effect of capillarity

When capillarity is taken into account during needle growth, the corresponding solution of equations [5.14–16] is with $t_2 = 0$, from which mass balance demands for each diffusing component

$$\Omega_i = p_i \exp\{p_i\} E_1\{p_i\} \left[1 + \frac{r_c}{r} \Omega_i R_2\{p_i\} \right] \tag{5.19}$$

for $i = 1, 2, ..., C$ diffusing components. The use of the maximum velocity hypothesis gives

$$0 = \left(g^*\{p_i\} \right)^2 \frac{r_c}{r} \left(-\frac{1}{p} R_2\{p_i\} + R_2'\{p_i\} \right) + \frac{g^*\{p_i\}}{p_i} + g^*\{p_i\} - 1 \tag{5.20}$$

for $i = 1, 2, ..., C$, which gives a system of $2C$ equations in which r and g_p are over determined. The problem will thus be inverted to seek solutions consistent with equations [5.18–19].

Binary systems

First consider a particle growing at $r/r_c = 10$ in a binary system, the corresponding values of p as a function of Ω given by equation [5.19] are shown in Fig. 5.4a. It is seen that a minimum in Ω is present when the critical radius r_c and the needle tip radius $r = 10 \times r_c$ are maximum, as shown in Fig. 5.4b, where r_c was calculated assuming $c^{\beta\alpha} = 0.95$, $c^{\alpha\beta} = 0.05$ and $\frac{\sigma v^\beta}{kT} = 1 \times 10^{-10}$m from the classical theory

$$r_c = \frac{2c^{\alpha\beta}}{\overline{c} - c^{\alpha\beta}} \left(\frac{\sigma v^\beta}{kT} \right) \left(\frac{1}{c^{\beta\alpha} - c^{\alpha\beta}} \right)$$

Note that for a given value of Ω, there are two solutions for p, it is assumed by Trivedi [1970a,b] that growth occurs at the value of p that produces the maximum lengthening rate.

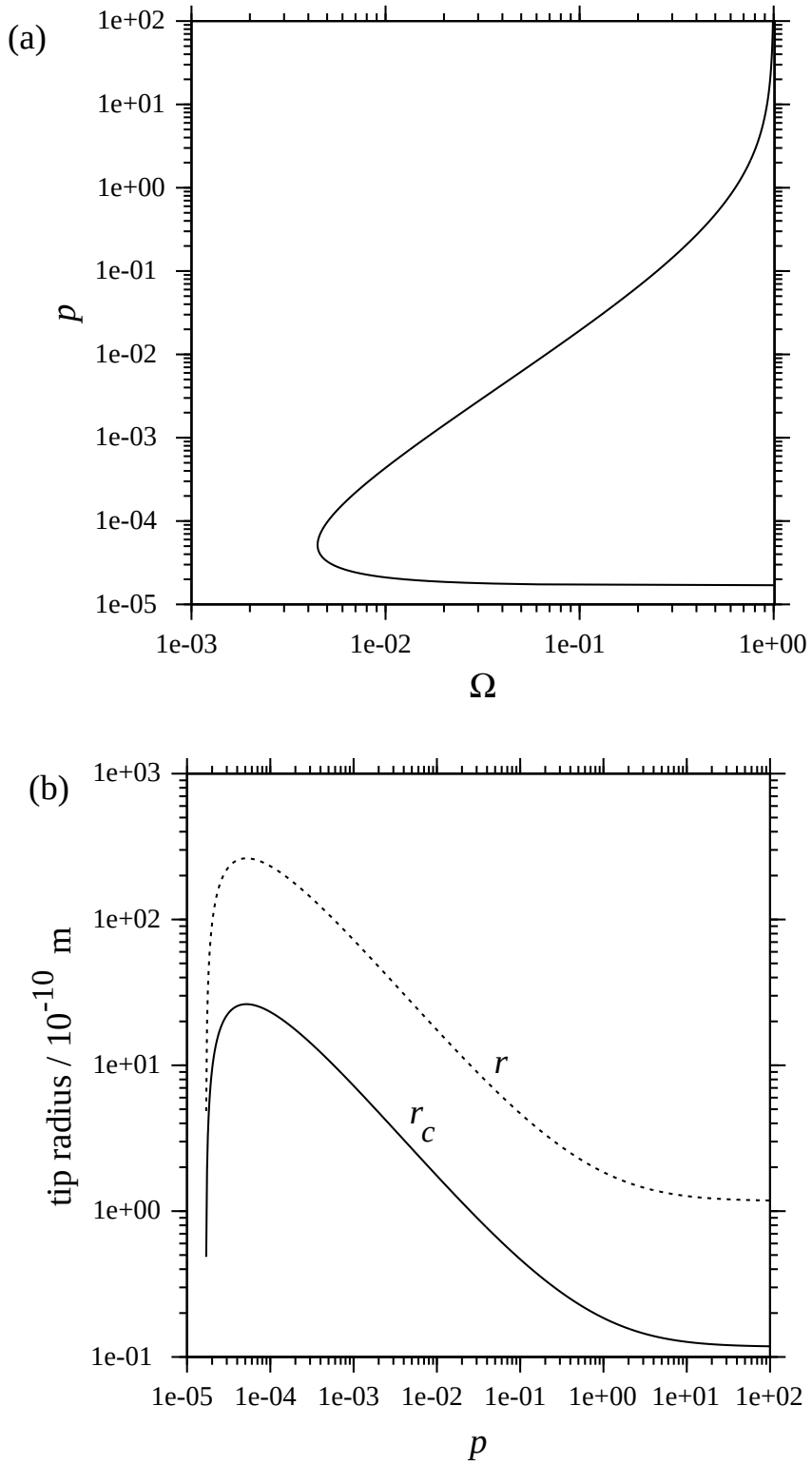

Fig. 5.4: Variation of (a) supersaturation and (b) critical and needle tip radius with p for $r/r_c = 10$.

Fig. 5.5 shows a generic plot of equation [5.19], showing the variation of p with Ω and r/r_c in a binary system. With $r/r_c = \infty$ the plot represents the Ivanstov solution, where r and g_p cannot be defined uniquely. When $r/r_c = 10$ capillarity plays a role in the growth process, Ω is no longer a function that grows monotonically with p; as r/r_c approaches to 1, capillarity becomes prominent, and the growth process has to occur at large supersaturations.

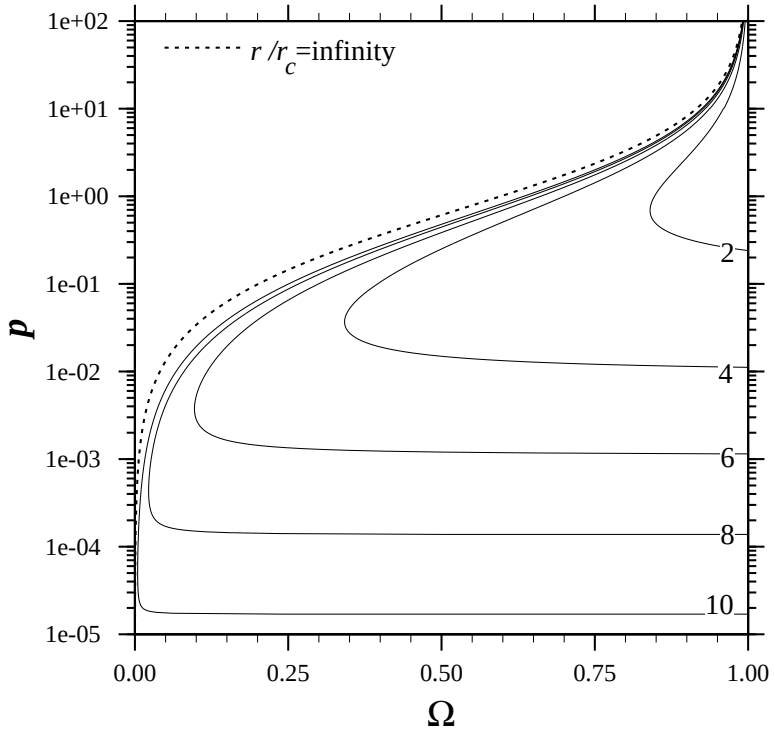

Fig. 5.5: Supersaturation as a function of the Péclet number and tip radius ratio.

Multicomponent systems

The Coates' concept of interface–composition contours as represented in Fig. 5.3 cannot be applied directly when capillarity is included in the calculations. In Fig. 5.3, the Ω_i term defines the compositions at the growing interface via equation [5.17], and at the same time represents the dimensionless supersaturations. Whereas Ω_i continue to represent the supersaturations when capillarity is incorporated into the theory, the compositions at the interface are no longer $c^{\alpha\beta}$ and $c^{\beta\alpha}$ (equation [5.17]) but rather the values the values $c_r^{\alpha\beta}$ and $c_r^{\beta\alpha}$ as modified by capillarity. Therefore, the plots corresponding to Fig. 5.3 are best called interface–saturation (IS) contours rather than interface composition contours; as will be seen later, it is necessary to make this distinction in order to avoid confusion.

The effects of capillarity in multicomponent growth can be observed in IS contours, which in the present context illustrate the locus of points where growth under local equilibrium is possible. In the absence of capillarity, growth with local equilibrium is always possible, as illustrated in Fig. 5.3. Fig. 5.6a shows for a ternary system, the permitted values for Ω_1 and Ω_2 as p_2 is varied for $r/r_c = 6$. Consistent with the binary case (Fig. 5.5), there is a minimum value of Ω_2 for the fast diffuser; larger values of Ω_1 are required when D_2/D_1 is increased, because the slow diffuser requires more driving force to keep pace with the fast diffuser. As capillarity is increased, less energy is available for diffusional growth, demanding larger supersaturations as shown in Fig. 5.6b for $r/r_c = 2$; this effect is reduced for larger values of r/r_c (Fig. 5.6c).

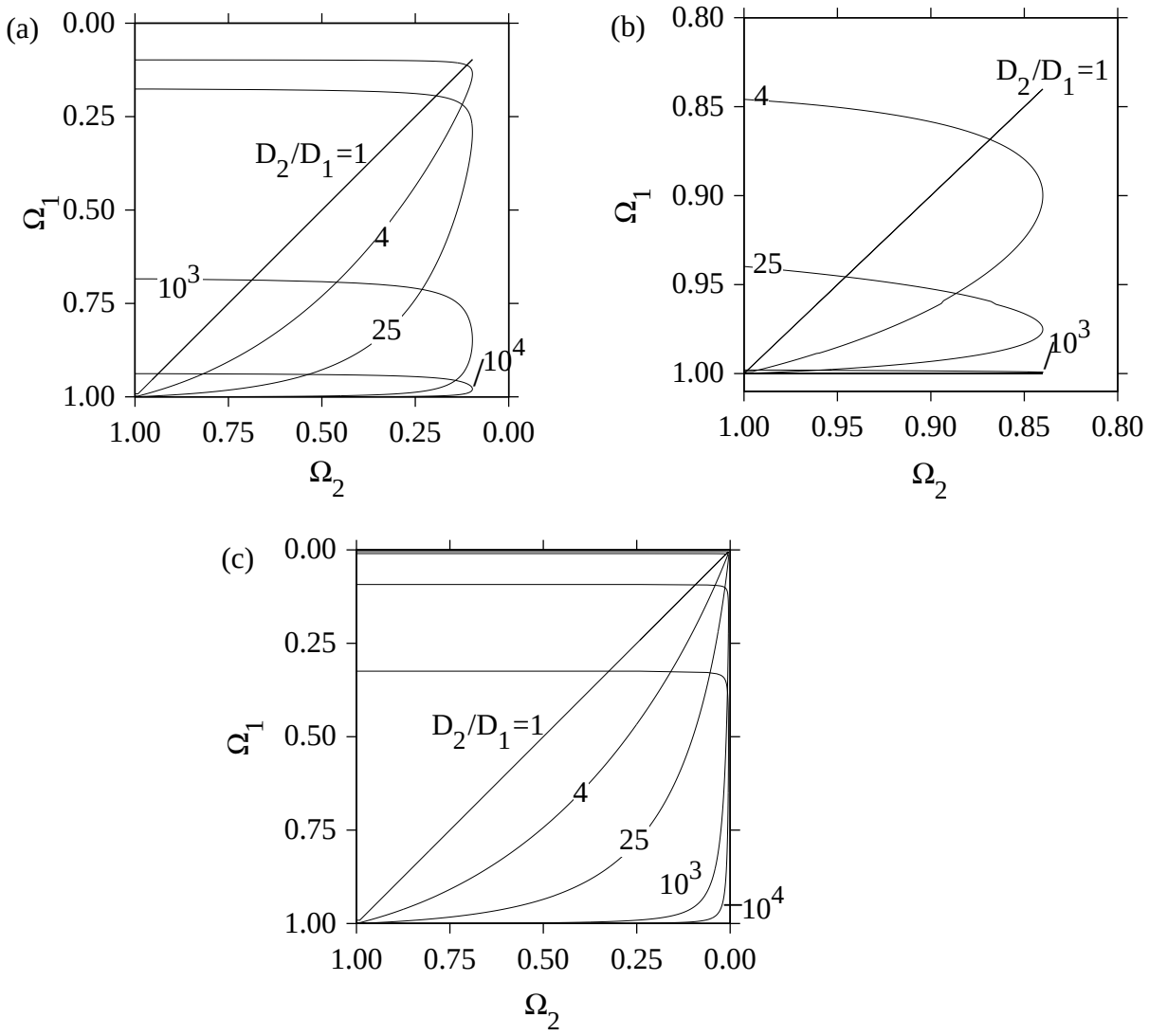

Fig. 5.6: IS contours for needle growth in a ternary system for r/r_c = (a) 6, (b) 2, (c) 10. Note that the scale in Fig. 5.6b is different from 5.6a and 5.6c.

To find a solution to equations [5.18–19], consider an alloy of composition $\overline{c}_i$. In a multicomponent system, the critical radius can be calculated from equation [5.8], which requires that

$$\frac{c_1}{\overline{c}_1 - c_1^{\alpha\beta}} \frac{\overline{V}_1^{\beta}}{c_1^{\beta\alpha} - c_1^{\alpha\beta}} = \frac{c_2}{\overline{c}_2 - c_2^{\alpha\beta}} \frac{\overline{V}_2^{\beta}}{c_2^{\beta\alpha} - c_2^{\alpha\beta}} = ... = \frac{c_C}{\overline{c}_C - c_C^{\alpha\beta}} \frac{\overline{V}_C^{\beta}}{c_C^{\beta\alpha} - c_C^{\alpha\beta}} \tag{5.21}$$

for $i = 1, 2, .., C$ components. Once a tie–line that satisfies equation [5.21] is found, the value of r_c can be obtained.

Consider a ternary system, choosing the appropriate equilibrium tie–line that satisfies equation [5.21], the values of $c_1^{\alpha\beta}$, $c_1^{\beta\alpha}$, $c_2^{\alpha\beta}$, $c_2^{\beta\alpha}$ can be obtained, and thus Ω_1 and Ω_2 and r_c calculated. Provided that the value of the diffusion coefficients of the two solutes is known, D_2/D_1 can be calculated. Then the value of r/r_c can be varied until an IS contour intersects the point Ω_1, Ω_2. This procedure is shown in Fig. 5.7 for $D_2/D_1 = 10^3$, where the point $\Omega_1 = 0.1$, $\Omega_2 = 0.05$ is intersected only by the IS contour produced with $r/r_c = 10$.

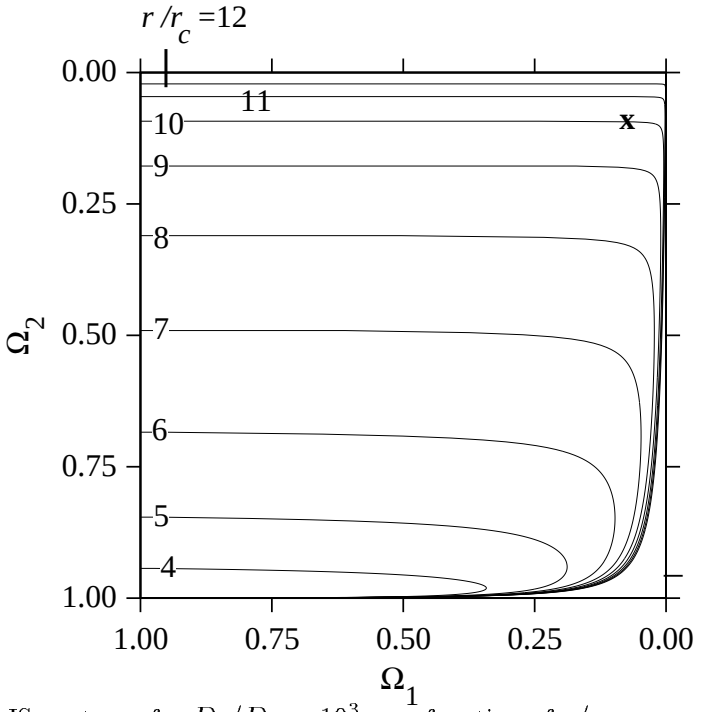

Fig. 5.7: IS contours for $D_2/D_1 = 10^3$ as a function of r/r_c.

For any set of supersaturations Ω_1, Ω_2, there is only one possible IS contour that can be intersected (Fig. 5.7), implying that the value of r/r_c is unique. Furthermore, being that each point of such IS contour is associated to a unique value of p_2 and $p_1 = \frac{D_2}{D_1} p_2$, these are uniquely defined as well. r_c can be obtained from the equilibrium compositions and then the velocity is determined through $g_p = 2p_1 D_1/r = 2p_2 D_2/r$.

5.4.3 The effect of interface kinetics

Assuming no interaction between components, the velocity of a flat interface can be expressed as $g_c = \mu_{oi}(\overline{c}_i - c_i^{\alpha\beta})$ for $i = 1, 2, ..., C$ components, where μ_{oi} is the interface kinetics coefficient of component i. The relative magnitudes of interface kinetics and diffusion effect are given by

$$q_i^* = \frac{\mu_{oi}(\overline{c}_i - c_i^{\alpha\beta})}{2D_i/r_c} \tag{5.22}$$

Thus, equation [5.19] can be modified to include interface kinetics as

$$\Omega_i = g^*\{p_i\}\left[1 + 2\frac{r_c}{r}\frac{p_i}{q_i^*}\Omega_i R_1\{p_i\} + \frac{r_c}{r}\Omega_i R_2\{p_i\}\right] \tag{5.23}$$

For small values of r/r_c, the solution of equation [5.23] for a single diffusing component is shown in Fig. 5.8 for the indicated values of q^*. It is to be noted that as the interface kinetics effect is increased, the permitted values of p are reduced for a given supersaturation and r/r_c. This is because at greater velocities more energy is dissipated in atom transfer across the interface, reducing the lengthening rate.

To assess the effect of multicomponent interface kinetics it is first recognised that

$$q_1^* D_1 = q_2^* D_2 = ... = q_C^* D_C \tag{5.24}$$

which has to be simultaneously solved with equations [5.18] and [5.23] to satisfy mass balance at the interface.

The supersaturations that simultaneously satisfy equations [5.18, 5.23, 5.24] can be expressed as IS contours for $C = 2$. Fig. 5.9 provides an example of such contours for $q_2^* = 0.02$, r/r_c=8, this shows that the addition of interface kinetics effect limits the value of Ω_1 and Ω_2 when these approach 1 due to all the energy will be depleted by this effect.

The overall effect of interface kinetics is to reduce the particle lengthening velocity, and limit this to a maximum value as $\Omega_i \to 1$. The procedure to obtain the lengthening rate and tip radius for a given composition is identical to the one explained previously, but using the appropriate values of q_i^* to produce the IS contours.

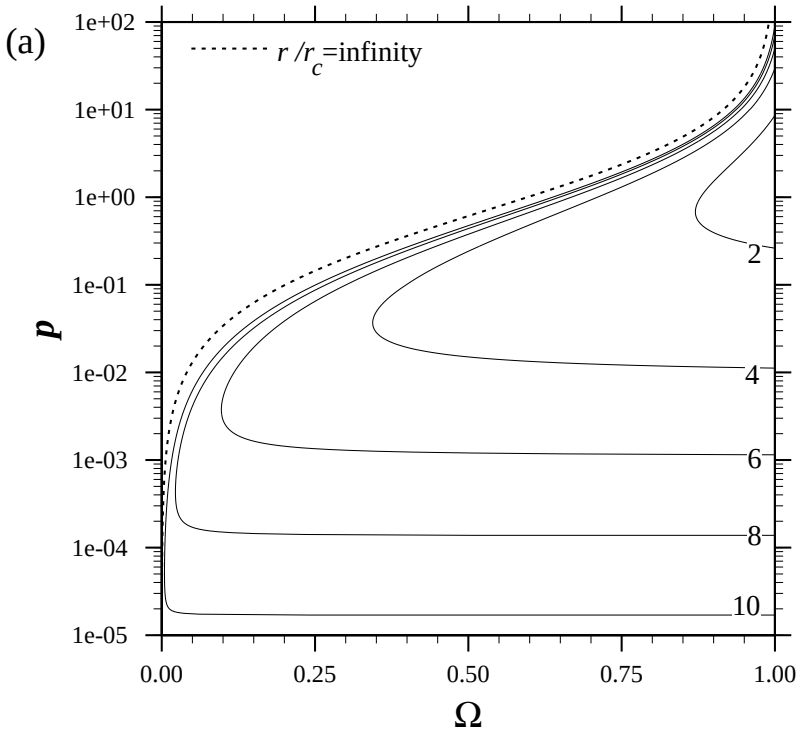
(a)
r /r_c =infinity
2
4
6
8
10
p
Ω
1e+02
1e+01
1e+00
1e-01
1e-02
1e-03
1e-04
1e-05
0.00
0.25
0.50
0.75
1.00

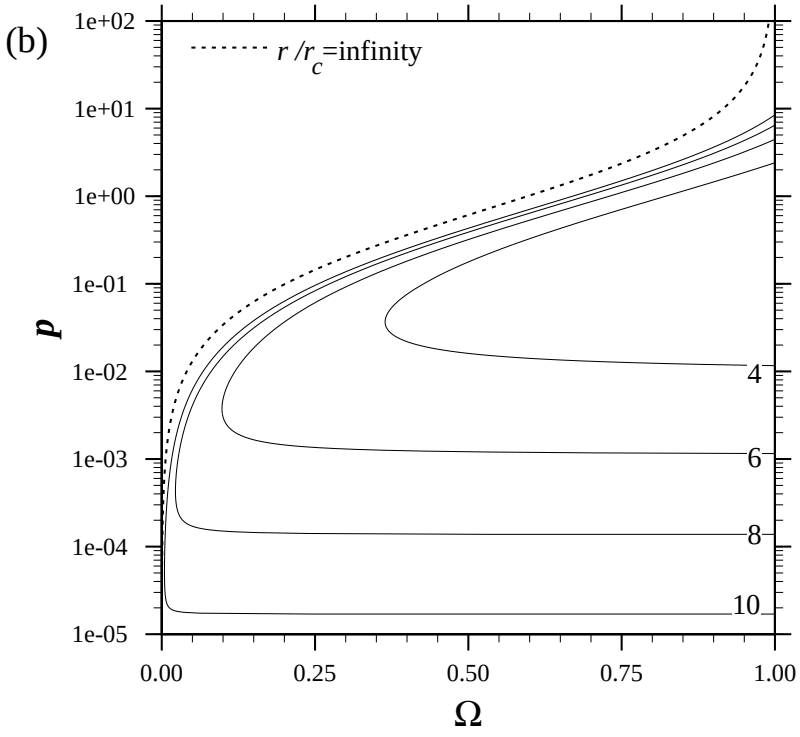
(b)
r /r_c =infinity
4
6
8
10
p
Ω
1e+02
1e+01
1e+00
1e-01
1e-02
1e-03
1e-04
1e-05
0.00
0.25
0.50
0.75
1.00

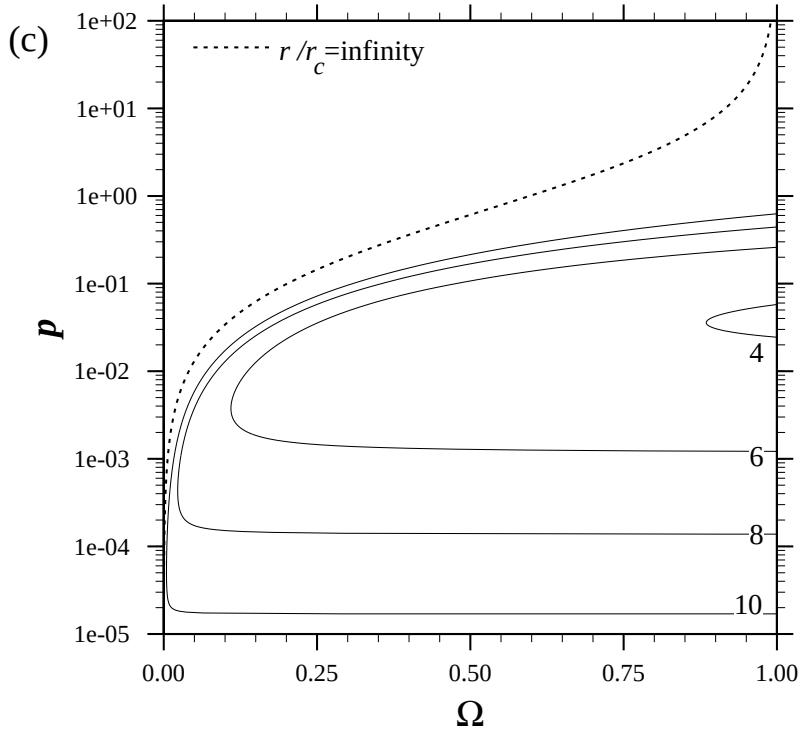

Fig. 5.8: Solutions for single solute for $q^* =$ (a) 20, (b) 2, (c) 0.2 in needle growth

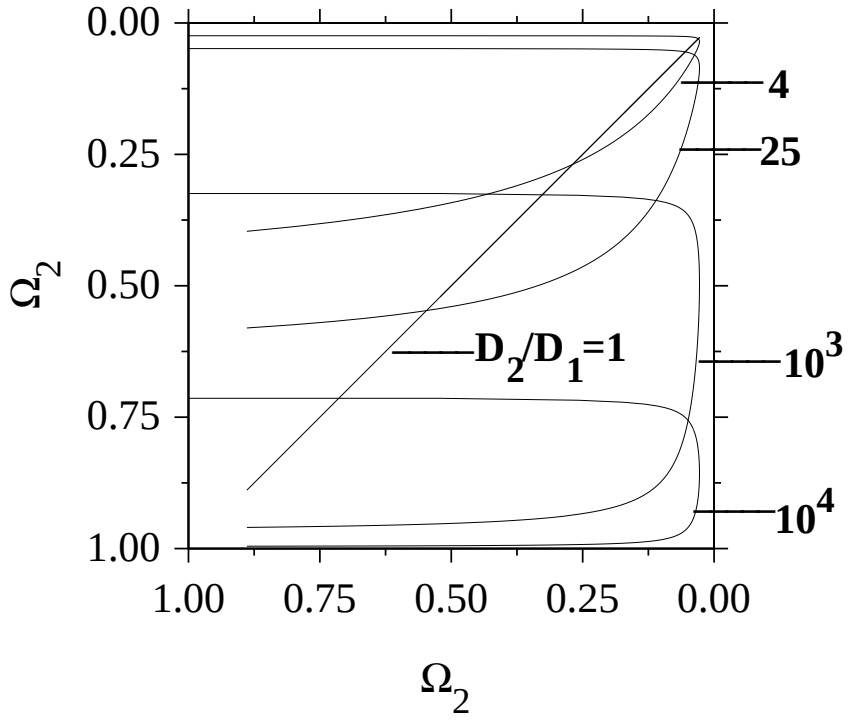

Fig. 5.9: Needle IS contours for $q^* = 0.02$ and $r/r_c = 8$

5.5 Multicomponent plate growth

In analogy to needle growth, mass balance of a plate–shaped particle growing in a multicomponent dilute Henrian solution requires the satisfaction of equation [2.37] for each component, if local equilibrium is assumed at the interface. This is expressed for $i = 1, 2, ..., C$ components as:

$$\Omega_i = \sqrt{\pi p_i}\exp\{p_i\}\mathrm{erfc}\{\sqrt{p_i}\}\left[1 + \frac{g_p}{g_c}\Omega_i S_1\{p_i\} + \frac{r_c}{r}\Omega_i S_2\{p_i\}\right] \tag{5.25}$$

The relative effects of capillarity and interface kinetics are best observed when the parameter

$$q_i = \frac{\mu_i(\overline{c}_i - c_i^{\alpha\beta})}{D_i/r_c} \tag{5.26}$$

is introduced in equation [5.25], this measures the relative magnitudes of interface kinetics and diffusion effects of each component for plate growth with an interface kinetics coefficient given by μ_i. Using q_i, equation [5.25] is expressed as

$$\Omega_i = g^{\diamond}\{p_i\}\left[1 + \frac{r_c}{r}\frac{p_i}{q_i}\Omega_i S_1\{p_i\} + \frac{r_c}{r}\Omega_i S_2\{p_i\}\right] \tag{5.27}$$

where $g^{\diamond}\{p_i\} = \sqrt{\pi p_i}\exp\{p_i\}\mathrm{erfc}\{\sqrt{p_i}\}$

Assuming no interaction between components, the critical velocity at which the concentration difference in the matrix vanishes $g_c = \mu_i(\overline{c}_i - c_i^{\alpha\beta})$ is equal for any component i, this requires

$$q_1 D_1 = q_2 D_2 = ... = q_C D_C \tag{5.28}$$

The analysis performed for needles can now be reproduced for plates.

5.5.1 Isoconcentrate boundary

When capillarity and interface kinetic effects are neglected, equation [5.25] is reduced to

$$\Omega_i = \sqrt{\pi p_i}\exp\{p_i\}\mathrm{erfc}\{\sqrt{p_i}\} \tag{5.29}$$

The solution for $i = 2$ solutes using Coates' IC contours, is shown in Fig. 5.10 for a variety of values of D_2/D_1. It is observed that the behaviour of plates with an isoconcentrate boundary is similar to spheres, and qualitatively identical to that of needles.

5.5.2 The effect of capillarity and interface kinetics

When capillarity and interface kinetic effects are introduced, C equations given by [5.27] have to be solved simultaneously. Additionally, the use of the maximum velocity hypothesis will require to satisfy

$$0 = \left(g^{\diamond}\{p_i\}\right)^2\frac{r_c}{r}\left[\frac{p_i}{q_i}S_1'\{p_i\} - \frac{1}{p_i}S_2\{p_i\} + S_2'\{p_i\}\right] + \frac{g^{\diamond}\{p_i\}}{2p_i} + g^{\diamond}\{p_i\} - 1 \tag{5.30}$$

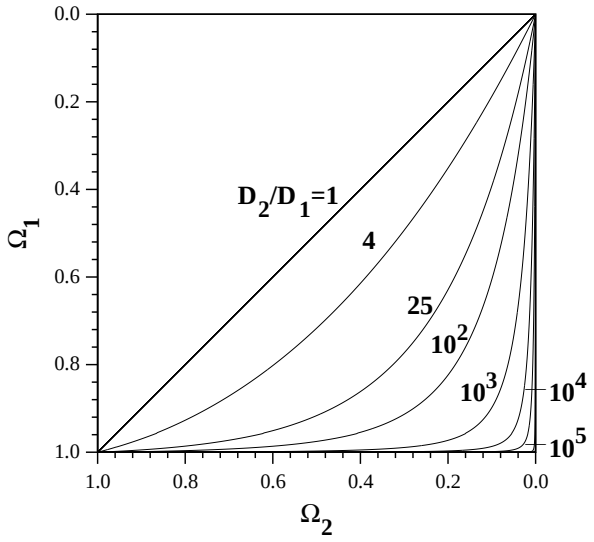

Fig. 5.10: IC contours for plate particles.

which casts a system of $2C$ equations in which the two variables g_p and r are over–determined. In analogy to the analysis for needles, the problem is thus inverted to seek the solutions provided by equation [5.27] in a single solute system, and then extend this to multicomponent systems. Fig. 5.11 shows the values of p as a function of supersaturation for several values of r/r_c; when interface kinetics effects are neglected ($q = \infty$ in Fig. 5.11a), and increasing this to $q = 10,\ 1,\ 0.1$ in Figs. 5.11b,c,d, respectively. The behaviour of the solution resembles that of needles; this is confirmed by the IS contours shown in Figs. 5.12a,b, which are plotted for $q = 10,\ 1$ with $r/r_c = 100$.

It is to be noted that the specific values of r and g_p will differ between needles and plates for given values of supersaturation; in fact, for a given supersaturation, the expected values of r/r_c are lower for needle than for plate–shaped particles. This is generic effect is demonstrated in Fig. 5.13 where p is plotted against Ω in a binary system where interface kinetic and capillarity effects are neglected, the values of p for needles are lower for needles than for plates, implying that for a given lengthening velocity their radius will be smaller.

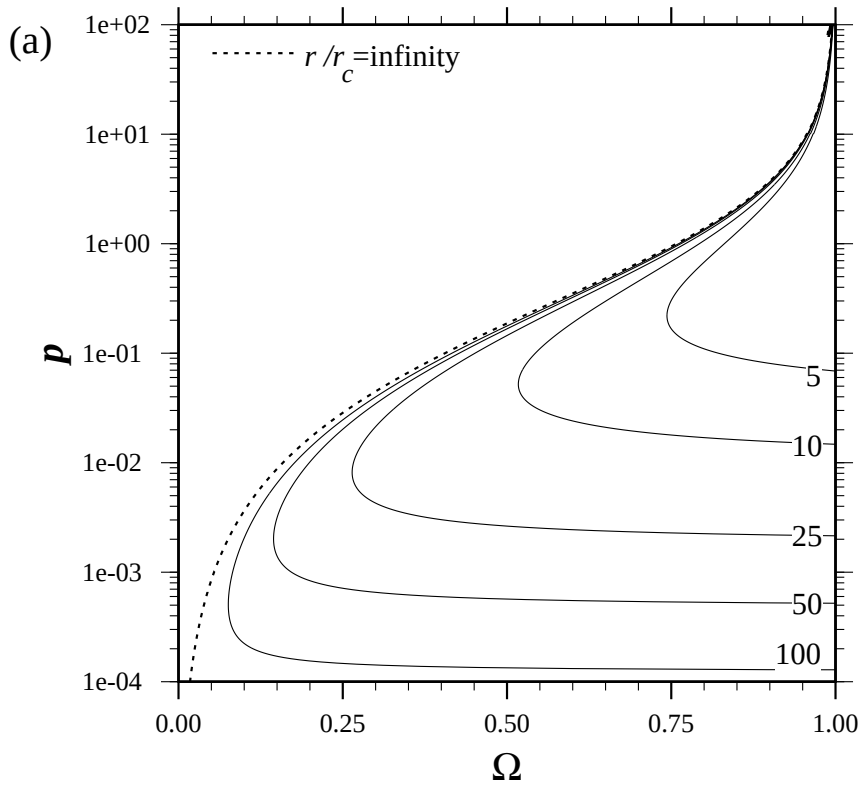
(a)
r /r_c=infinity
1e+02
1e+01
1e+00
1e-01
1e-02
1e-03
1e-04
p
5
10
25
50
100
0.00
0.25
0.50
0.75
1.00
Ω

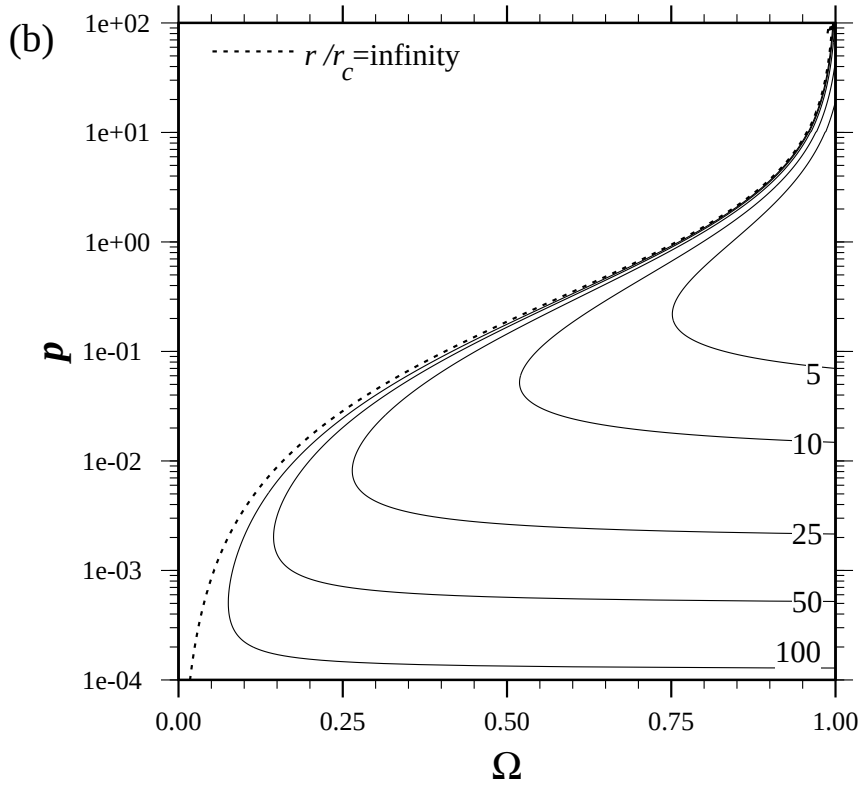
(b)
r /r_c=infinity
1e+02
1e+01
1e+00
1e-01
1e-02
1e-03
1e-04
p
5
10
25
50
100
0.00
0.25
0.50
0.75
1.00
Ω

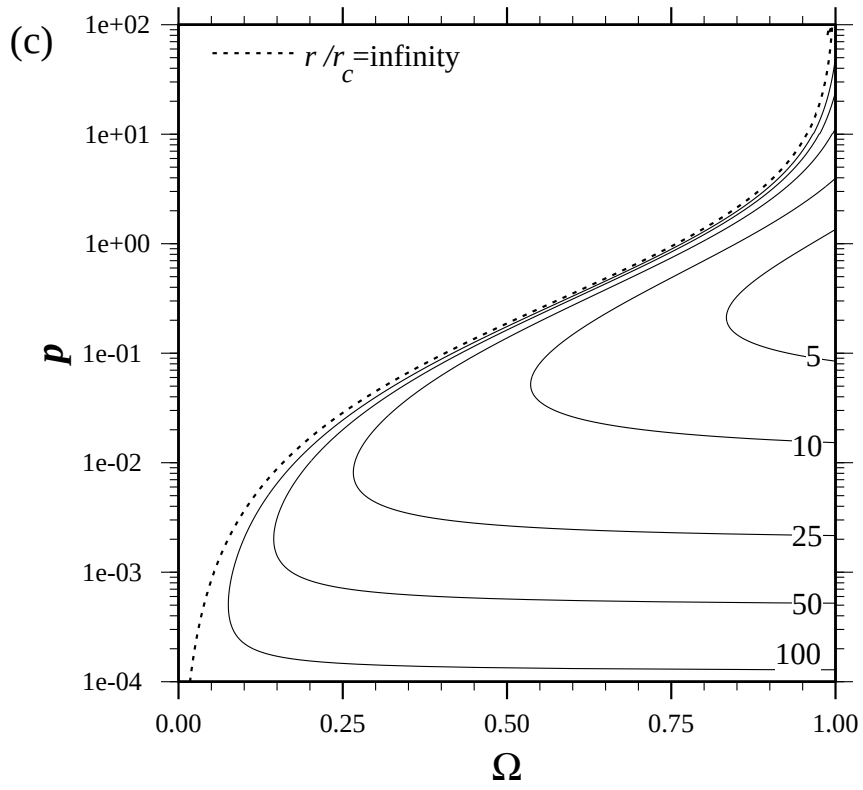

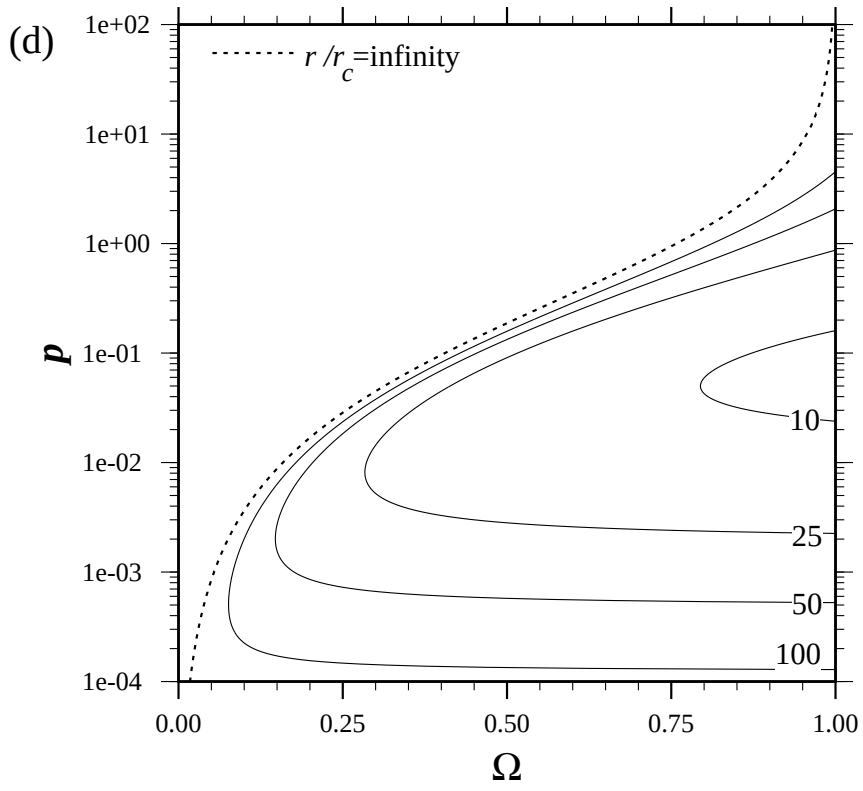

Fig. 5.11: Plate Péclet number as a function of supersaturation for $q =$ (a) ∞, (b) 10, (c) 1, (d) 0.1.

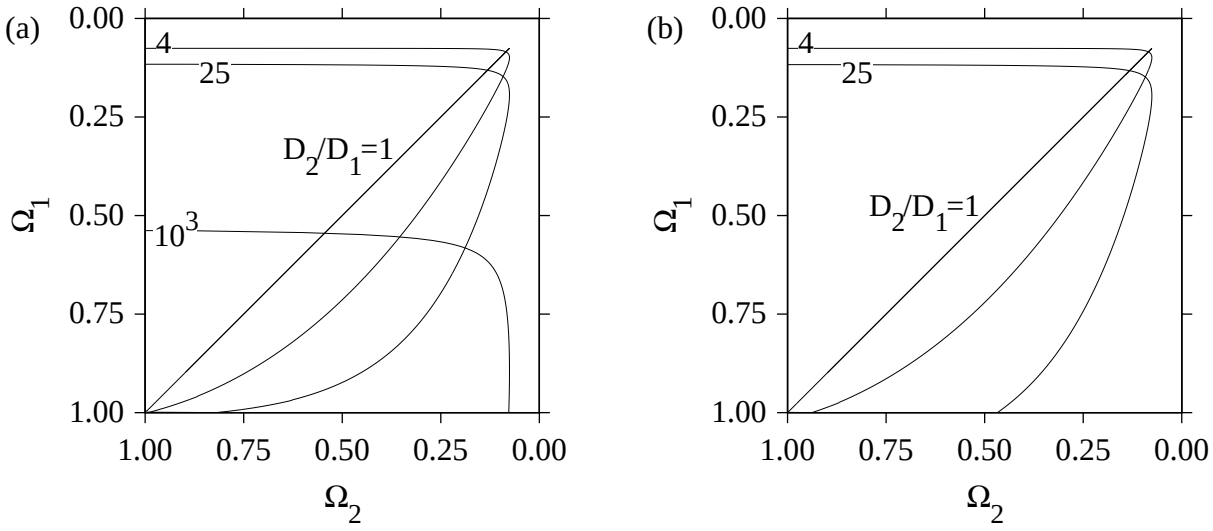

Fig. 5.12: Plate IS contours for $r/r_c = 100$ and $q =$ (a) 10, (b) 1.

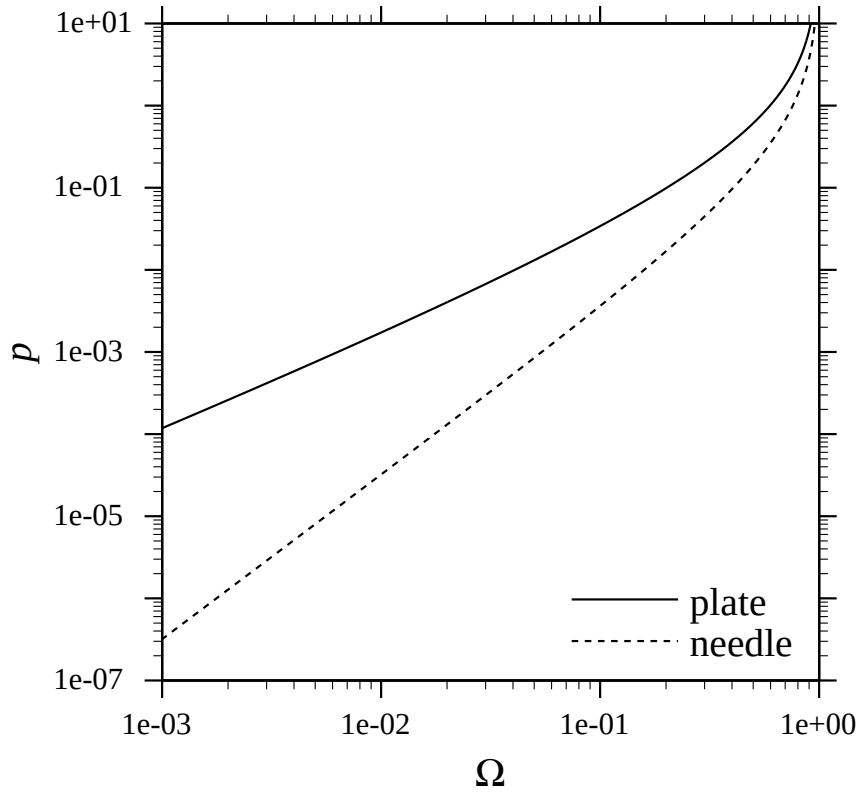

Fig. 5.13: Isoconcentrate boundary values of p against Ω for plate and needle–shaped particles.

5.6 Application of the theory to Fe-C-Mo

To illustrate the use of the theory, it has been applied to calculate the lengthening rate of Mo_2C needle–shaped precipitates growing in a ferrite matrix in a Fe–0.11C–1.95Mo alloy. Measurements on the lengthening rates and needle tip radius have been performed by Hall *et al.* [1972] for a number of temperatures, and their data are shown in Table 5.1.

T [°C]	r [Å]	g_p [m s^{-1}]
600	25	1.0×10^{-12}
650	30	1.0×10^{-11}
700	35	1.3×10^{-10}
750	40	2.2×10^{-10}

Table 5.1: Mo_2C tip radius and average Mo_2C lengthening rates in Fe–0.11C–1.95Mo [Hall *et al.*, 1972]

The diffusion coefficients of C and Mo are calculated from

$$D = D_o \exp\left\{-\frac{Q}{R_u T}\right\} \tag{5.31}$$

For molybdenum, D_o=1.1×10^{-4} m^2 s^{-1} and Q=240×10^3 J mol^{-1} [Friedberg *et al.*, 1969]. For carbon, D_o=2.2×10^{-4} m^2 s^{-1} and Q=122×10^3 J mol^{-1} [Wilkinson, 2000].

The critical radius was obtained from equation [2.18] with σ = 0.2471 J m^{-2} [Fujita and Bhadeshia, 1999], v_{C}^{β} and v_{Mo}^{β} were approximated as 1.25×10^{-29} m^3 atom^{-1}; and $c_i^{\alpha\beta}$ and $c_i^{\beta\alpha}$ were obtained from a tie–line satisfying equation [5.21], which was provided by a thermodynamical database and phase diagram software MTDATA [1995].

The values of D_2/D_1 were found to be $\sim 10^7$ (Table 5.2), and the IS contours corresponding to the values of r/r_c that intersect supersaturations Ω_{Mo}, Ω_C were chosen. The tip radii and lengthening velocities associated to these calculations are shown in Table 5.2.

T [°C]	D_2/D_1	Ω_{Mo}	Ω_C	$p_{Mo} \times 10^{-3}$	r/r_c	r [Å]	g_p [m s^{-1}]
600	2.3×10^7	0.0165	0.0149	2.25	21.6	11	2.0×10^{-12}
650	9.5×10^6	0.0159	0.0145	2.11	20.8	18	6.8×10^{-12}
700	4.3×10^6	0.0150	0.0139	1.92	20.1	30	1.8×10^{-11}
750	2.1×10^6	0.0132	0.0130	1.60	19.6	49	4.0×10^{-11}

Table 5.2: Results of the application of the theory to the lengthening of Mo_2C

On comparison of Tables 5.1 and 5.2, it is shown that the predicted and measured tip radius and lengthening velocity are quite close. This model, however, neglects the effects of cementite, which is present in the initial states of precipitation, and dissolves, providing solute for Mo_2C growth. This will be added in a model to predict the kinetics in a next chapter.

5.7 Summary

The theory to treat growth of precipitates in an ideal multicomponent Henrian solution is presented. It is assumed that the precipitating particles approach spheres, paraboloids of revolution (needles) or parabolic cylinders (plates). It has been observed that the effect of capillarity in spheres is to reduce the thickening rate, such that a particle that would grow under a regime where there is no long–range partitioning of the slow diffuser, can be shifted into a regime where such partitioning is necessary. The main result for needles and plates was to demonstrate that the maximum velocity hypothesis cannot be sustained in the multicomponent scenario, and that the supersaturations are bounded for lower and upper values when capillarity and interface kinetic effects are prominent, respectively.

A methodology to calculate the lengthening rate for the referred geometries was presented, and it proved good accuracy for Mo_2C lengthening in a secondary hardening steel. Both the theory, and the solution method prove that the maximum velocity hypothesis is not required.

CHAPTER 6

Capillarity and Growth in non–ideal multicomponent systems

6.1 Introduction

Precipitation reactions commonly occur in non–ideal solutions where interactions between components occur. It would therefore be useful to develop theory to account for these. In this chapter the Gibbs–Thomson effect is generalised for non–ideal solutions where a change in the precipitate composition and chemical potential is present, and theory for the growth of spheres, plates and needles is presented in this framework.

6.2 Gibbs–Thomson effect in non–ideal systems

During precipitate growth, particles can be characterised by a curvature which alters the state of equilibrium of the system, depleting the available energy for growth. This is the so–called Gibbs–Thomson effect [Christian, 1975], which induces concentration shifts in the matrix as the energy of the precipitate is increased by $\sigma(dO/dn)$ as shown in Fig. 2.4. This situation can be expressed mathematically in a molar basis as:

$$(c^{\beta\alpha} - c^{\alpha\beta})\frac{\partial^2 G^\alpha}{\partial c^2}(c_r^{\alpha\beta} - c^{\alpha\beta}) = \frac{2\sigma V_m}{r} \tag{6.1}$$

where G^α is the α phase molar volume.

Equation [6.1] has recently been generalised for a multicomponent system by Morral and Purdy [1994]; however this leads to a violation of the condition of chemical equilibrium at the interface, as demonstrated by Trivedi [1975], and Kulkarni and DeHoff [1997], and discussed next. Expressing the chemical potential of α phase as

$$\mu^\alpha = G^\alpha + (1 - c^{\alpha\beta})\frac{\partial G^\alpha}{\partial c}$$

then †

$$\frac{\partial^2 G^\alpha}{\partial c^2} = \frac{1}{1 - c^{\alpha\beta}}\frac{\partial \mu^\alpha}{\partial c} \tag{6.2}$$

which can be substituted in equation [6.1] to give

$$\frac{c^{\beta\alpha} - c^{\alpha\beta}}{1 - c^{\alpha\beta}}\frac{\partial \mu^\alpha}{\partial c}dc^{\alpha\beta} = 2\sigma V_m dH \tag{6.3}$$

† Note that the term $(\mu^\alpha - G^\alpha)/(1 - c^{\alpha\beta})^2$ vanishes by choosing a reference state such that $\mu^\alpha = G^\alpha$.

where equation [6.1] is now expressed in terms of increments of composition $dc^{\alpha\beta} = c_r^{\alpha\beta} - c^{\alpha\beta}$ and H is the curvature of the particle. Note that for a sphere $H = 1/r$, whereas for a particle with variable curvature at the interface, *e.g.* a parabola $H = 1/\overline{R}$, where $\overline{R}$ is the mean parabolic interface radius. The following derivations are for spheres, but their application to particles of variable curvature is straightforward. The case of needles will be discussed in more detail in Chapter 8.

Equation [6.3] can be expressed as

$$\frac{c^{\beta\alpha} - c^{\alpha\beta}}{1 - c^{\alpha\beta}}(\mu^{\alpha}\{H\} - \mu^{\alpha}\{H = 0\}) = 2\sigma V_m H \tag{6.4}$$

for a curvature increment from $H = 0$ to $H = 1/r$. However, from thermodynamic theory [DeHoff, 1993]

$$\frac{\partial \mu^{\alpha}}{\partial c} dc^{\alpha\beta} = \frac{\partial \mu^{\beta}}{\partial c} dc^{\beta\alpha} + 2\sigma \overline{V}^{\beta} H \tag{6.5}$$

where μ^{β} is the chemical potential of β phase and $dc^{\beta\alpha} = c_r^{\beta\alpha} - c^{\beta\alpha}$ where $c_r^{\beta\alpha}$ is the capillarity corrected composition of β in equilibrium with α and $\overline{V}^{\beta}$ is the partial molar volume of the β phase. By analogy to equation [6.4], equation [6.5] can be expressed as:

$$\mu^{\alpha}\{H\} - \mu^{\alpha}\{H = 0\} = (\mu^{\beta}\{H\} - \mu^{\beta}\{H = 0\}) + 2\sigma \overline{V}^{\beta} H \tag{6.6}$$

for sufficiently small increments of composition, i.e. $|dc^{\alpha\beta}| \ll |c^{\beta\alpha} - c^{\alpha\beta}|$ and $|dc^{\beta\alpha}| \ll |c^{\beta\alpha} - c^{\alpha\beta}|$ which is the same assumption implicit in the form of the Gibbs–Thomson equation that appears in literature [Kulkarni and DeHoff, 1997]; the increase in chemical potential can be approximated as:

$$2\sigma \overline{V}^{\beta} H = \frac{1 - c^{\alpha\beta}}{c^{\beta\alpha} - c^{\alpha\beta}} 2\sigma V_m H$$

which can be substituted in equation [6.6] to give

$$\frac{c^{\beta\alpha} - c^{\alpha\beta}}{1 - c^{\alpha\beta}}(\mu^{\alpha}\{H\} - \mu^{\alpha}\{H = 0\}) = \frac{c^{\beta\alpha} - c^{\alpha\beta}}{1 - c^{\alpha\beta}}(\mu^{\beta}\{H\} - \mu^{\beta}\{H = 0\}) + 2\sigma V_m H \tag{6.7}$$

Thus, if equation (6.4) is substituted in equation [6.7] we see that

$$\mu^{\beta}\{H\} = \mu^{\beta}\{H = 0\} \tag{6.8}$$

But equilibrium demands that

$$\mu^{\alpha}\{H = 0\} = \mu^{\beta}\{H = 0\} \tag{6.9}$$

Combining equation [6.8] and [6.9] we obtain $\mu^{\beta}\{H\} = \mu^{\alpha}\{H = 0\}$, which can be substituted in equation [6.4] to give $\mu^{\alpha}\{H\} \neq \mu^{\beta}\{H\}$, which violates the equilibrium condition when a

curvature is present. The origin of such a contradiction is that the term $\partial\mu^\beta/\partial c$ in equation [6.5] is lacking in equation [6.3]. Note that the Gibbs–Thomson equation is correct in the context it was derived: liquid–gas equilibria in unary and binary systems, but it has been assumed to be valid for condensed phase equilibria in unary, binary and multicomponent systems. An extension of the Gibbs–Thomson equation has been given by Morral and Purdy for multicomponent systems [1994], which implicitly contains the same approximation.

Kulkarni and DeHoff [1997] demonstrated that the same violation to the equilibrium condition ($\mu^\alpha\{H\} \neq \mu^\beta\{H\}$) is present in a unary solid–liquid system when the Gibbs–Thomson equation is used. They concluded that this is due to the pressure change of the α phase is neglected, and demonstrated this has a significant effect in the chemical potential shifts in solid–liquid interfaces.

Chaix, Eustathopoulos and Allibert [1986] have studied the effect of curvature on the Gibbs energy for a binary two phase system, in terms of the interactions between the system components where the term $\partial\mu^\beta/\partial c$ is not neglected in equation [6.5], but their results are limited to the first order development of the chemical potentials of each component. Chaix and Allibert [1986] have extended the previous work to ternary systems but still using the first order development of the chemical potentials, assuming a main constituent and a negligible solubility of another one, i.e. pseudo–binary behaviour.

Kuehmann and Voorhees [1996] have presented an elegant method to predict the capillarity shifts in a ternary two phase system, but it is limited to the first order terms of the chemical potentials, and is applied just to spherical particles.

It is thus required to develop theory to obtain the chemical potential shifts in multicomponent and multiphase systems, taking into account $\partial\mu^\beta/\partial c$ in the chemical potential equilibrium equations. DeHoff has followed the same method to calculate the composition shifts due to capillarity in a binary system [DeHoff, 1993], but the final expressions he obtains are different to the ones presented in the next section.

6.3 Gibbs–Thomson effect in binary systems

In this section, the Gibbs-Thomson effect will be extended to include the term $(\partial\mu^\beta/\partial c)dc^\beta$ in equation [6.6], for binary systems. In deriving expressions for chemical potential and composition shifts, it is assumed that the effects of elastic fields on the morphological stability of precipitates growing from a solid solution can be neglected [Leo and Serka, 1989, Cahn and Larché, 1982], as they appear to be small when the particles are small [Calderón *et al.*, 1994,

Nishimori and Onuki, 1991], which is the case when capillarity effects are prominent; thus it is assumed that the particles are shape–preserving. Furthermore, no variation of the interfacial energy per unit area with composition is assumed. The recent work from Miyazaki and co–workers has proved that this can actually be true by inducing a macroscopic concentration gradient in several binary alloys [Miyazaki *et al.*, 1996, Miyazaki, 1999]. Bearing the above assumptions in mind, the equilibrium conditions for a binary system where a curvature change dH is present require [DeHoff, 1993]:

$$dT^{\beta} = dT^{\alpha} \tag{6.10}$$

$$dP^{\beta} = dP^{\alpha} + \sigma w dH \tag{6.11}$$

$$d\mu_i^{\beta} = d\mu_i^{\alpha} \tag{6.12}$$

for components $i = 1, 2$ where T^{β}, P^{β} and T^{α}, P^{α} are the temperatures and pressures of β and α phases, respectively, and μ_i^{β}, μ_i^{α} are the chemical potentials of component i in β and α phases, respectively, w is the order of curvature of the particle, *e.g.* $w = 2,\ 1,\ 0$ for a sphere, cylinder and a flat surface. A differential change in chemical potential of component i in α can be expressed as

$$d\mu_i^{\alpha} = -\overline{S}_i^{\alpha} dT^{\alpha} + \overline{V}_i^{\beta} dP^{\alpha} + \mu_{i2}^{\alpha} dc_2^{\alpha\beta} \tag{6.13}$$

where the component 2 is chosen as the independent composition variable. $\overline{S}_i^{\alpha}$ and $\overline{V}_i^{\alpha}$ are the component i partial molar entropy and volume, respectively, and

$$\mu_{ij}^{\alpha} \equiv \left(\frac{\partial \mu_i^{\alpha}}{\partial c_j} \right)_{T,P,c_i} \tag{6.14}$$

is the change in chemical potential of component i with c_j composition. Analogous expressions to equation [6.13] can be obtained for μ_i^{β}, thus, equation [6.12] can be expressed as

$$-\Delta\overline{S}_1 dT + \Delta\overline{V}_1 dP^{\alpha} - w\sigma\overline{V}_1^{\beta} dH + \mu_{12}^{\alpha} dc_2^{\alpha\beta} - \mu_{12}^{\beta} dc_2^{\beta\alpha} = 0 \tag{6.15}$$

$$-\Delta\overline{S}_2 dT + \Delta\overline{V}_2 dP^{\alpha} - w\sigma\overline{V}_2^{\beta} dH + \mu_{22}^{\alpha} dc_2^{\alpha\beta} - \mu_{22}^{\beta} dc_2^{\beta\alpha} = 0 \tag{6.16}$$

where $\Delta\overline{V}_i = \overline{V}_i^{\alpha} - \overline{V}_i^{\beta}$ and $\Delta\overline{S}_i = \overline{S}_i^{\alpha} - \overline{S}_i^{\beta}$.

To assess the effect of capillarity, temperature and pressure are fixed. Note that assuming $dP^{\alpha} = 0$ seems to be reasonable in the context of solid–solid transformations where, as the particle nucleates (when capillarity effects are prominent) the strain fields are small. Using the Gibbs–Duhem equation $c_1 d\mu_1 + c_2 d\mu_2 = 0$, μ_{22} can be expressed as

$$\mu_{22} = -\frac{c_1}{c_2}\mu_{12}$$

Thus, equations [6.15, 6.16] can be expressed as

$$\mu_{12}^{\alpha}\left(\frac{dc_2^{\alpha\beta}}{dH}\right) - \mu_{12}^{\beta}\left(\frac{dc_2^{\beta\alpha}}{dH}\right) = w\sigma\overline{V}_1^{\beta} \tag{6.17}$$

$$-\frac{c_1^{\alpha\beta}}{c_2^{\alpha\beta}}\mu_{12}^{\alpha}\left(\frac{dc_2^{\alpha\beta}}{dH}\right) + \frac{c_1^{\beta\alpha}}{c_2^{\beta\alpha}}\mu_{12}^{\beta}\left(\frac{dc_2^{\beta\alpha}}{dH}\right) = w\sigma\overline{V}_2^{\beta} \tag{6.18}$$

The solution to the previous system is

$$\frac{dc_2^{\alpha\beta}}{dH} = w\sigma\left(c_1^{\beta\alpha}\overline{V}_1^{\beta} + c_2^{\beta\alpha}\overline{V}_2^{\beta}\right)\frac{c_2^{\alpha\beta}}{\mu_{12}^{\alpha}\left(c_1^{\beta\alpha}c_2^{\alpha\beta} - c_1^{\alpha\beta}c_2^{\beta\alpha}\right)} \tag{6.19}$$

$$\frac{dc_2^{\beta\alpha}}{dH} = w\sigma\left(c_1^{\alpha\beta}\overline{V}_1^{\beta} + c_2^{\alpha\beta}\overline{V}_2^{\beta}\right)\frac{c_2^{\beta\alpha}}{\mu_{12}^{\beta}\left(c_1^{\beta\alpha}c_2^{\alpha\beta} - c_1^{\alpha\beta}c_2^{\beta\alpha}\right)} \tag{6.20}$$

Assuming that $c_1^{\alpha\beta},\ c_2^{\beta\alpha} \to 1$ and $c_1^{\beta\alpha},\ c_2^{\alpha\beta} \to 0$, and that the solution obeys Henry's law in spherical particles, the variation of concentration with curvature (equations [6.19, 6.20]) can be expressed as:

$$c_{r2}^{\alpha\beta} = c_2^{\alpha\beta}\exp\left\{\frac{w\sigma\overline{V}_2^{\beta}}{R_uT}H\right\} \tag{6.21}$$

$$c_{r1}^{\beta\alpha} = c_1^{\beta\alpha}\exp\left\{-\frac{w\sigma\overline{V}_1^{\beta}}{R_uT}H\right\} \tag{6.22}$$

From which the exponential in equation [6.21] can be expanded in power series to give

$$c_{r2}^{\alpha\beta} = c_2^{\alpha\beta}\left(1 + \frac{w\sigma\overline{V}^{\beta}}{R_uT}\frac{1 - c_2^{\alpha\beta}}{c_2^{\beta\alpha} - c_2^{\alpha\beta}}H\right) \tag{6.23}$$

which is equivalent to the expression for concentration shifts in a Henrian solution given by equation [2.11], when $w = 2$.

DeHoff [1993] used the same method described in this section, and obtained equations [6.17–6.18], but when solved them simultaneously, the equations he obtains are different to [6.19–6.20] for unknown reasons to the author. The validity of equations [6.19–6.20] can be corroborated by direct substitution in [6.17–6.18].

6.4 Multicomponent and multiphase systems

6.4.1 Two phase systems

For a two phase system, where α is the matrix phase and β the precipitate, and $i = 1, 2, ..., C$ components, the equilibrium conditions are given by equations [6.10–6.12]. Equation [6.12] can be expressed as

$$-\Delta\overline{S}_i dT + \Delta\overline{V}_i dP^{\alpha} - w\sigma\overline{V}_i^{\beta}dH + \sum_{k=1}^{C-1}\mu_{ik}^{\alpha}dc_k^{\alpha\beta} - \sum_{k=1}^{C-1}\mu_{ik}^{\beta}dc_k^{\beta\alpha} = 0 \tag{6.24}$$

Keeping temperature and pressure constant, equation [6.24] can be expressed as:

$$\sum_{k=1}^{C-1} \mu_{ik}^{\alpha} \frac{dc_k^{\alpha\beta}}{dH} - \sum_{k=1}^{C-1} \mu_{ik}^{\beta} \frac{dc_k^{\beta\alpha}}{dH} = w\sigma \overline{V}_i^{\beta} \tag{6.25}$$

which can be solved for $dc_k^{\alpha\beta}/dH$ and $dc_k^{\beta\alpha}/dH$ for $k = 1, 2, ..., C-1$ whose numerical integration provides the solute concentration shifts. Equation [6.25] is reduced to the binary system of equations [6.17–6.18] for $C = 2$.

To illustrate the solution of the system given by equation [6.25], consider a ternary steel the type Fe-C-X where a β phase precipitates in an α matrix phase. Being that temperature and pressure are fixed, there are four variables, say $c_{\rm C}^{\beta\alpha}$, $c_{\rm C}^{\alpha\beta}$, $c_{\rm X}^{\beta\alpha}$ and $c_{\rm X}^{\alpha\beta}$, and three equations given by [6.25] for $i =$ Fe, C, X, thus, consistent with Gibbs phase rule there is one degree of freedom. Say $c_{\rm X}^{\alpha\beta}$ is chosen to vary, then for an increment dH^{β} there is just one value $dc_{\rm X}^{\alpha\beta}$ that satisfies equations given by [6.25], and $dc_{\rm X}^{\beta\alpha}$, $dc_{\rm C}^{\alpha\beta}$ and $dc_{\rm X}^{\beta\alpha}$ are given by the phase diagram. This process can be followed for incremental values of dH^{β} until $c_{r{\rm X}}^{\alpha\beta} = \overline{c}_{\rm X}$, where the critical radius for nucleation is determined. The values of $\mu_{ik}^{\alpha\beta}$ and $\mu_{ik}^{\beta\alpha}$ may be obtained from a thermodynamical database such as MTDATA [1995].

6.4.2 Multiphase systems

In a system of $i = 1, 2, ..., C$ components and $j = I, II, ..., {\rm P}$ precipitate phases ($j \neq \alpha$, which is the matrix phase), the equilibrium conditions are given by:

$$dT^{I} = dT^{II} = ... = dT^{\alpha} = ... = dT^{\rm P} \tag{6.26}$$

$$d\mu_i^{I} = d\mu_i^{II} = ... = d\mu_i^{\alpha} = ... = d\mu_i^{\rm P} \tag{6.27}$$

The mechanical equilibrium condition is extracted from the balance of forces per unit area along the interface of each particle:

$$P^j = P^{\alpha} + w^j \sigma^j H^j \quad \Rightarrow \quad dP^j = dP^{\alpha} + w^j \sigma^j dH^j \tag{6.28}$$

for $j = I, II, ..., {\rm P}$, $j \neq \alpha$, where w^j is the order of curvature of the j precipitate, σ^j is its matrix–j particle interfacial energy per unit area, and dH^j its curvature.

Setting $dT^j = 0$ and $dP^{\alpha} = 0$, the chemical potential shifts are given by

$$d\mu_i^{\alpha} = \sum_{k=1}^{C-1} \mu_{ik}^{\alpha} dc_k^{\alpha j} \tag{6.29}$$

$$d\mu_i^{j} = \sum_{k=1}^{C-1} \mu_{ik}^{j} dc_k^{j\alpha} + w^j \sigma^j \overline{V}_i^j dH^j \tag{6.30}$$

for $j = I, II, ..., \mathrm{P}, j \neq \alpha$. The term $dc_k^{\alpha j}$ is the shift in the composition of α in equilibrium with β, which will produce an equal shift in chemical potential $\mu_{ik}^{\alpha} dc_k^{\alpha j}$ for a system in equilibrium (equation [6.27]) regardless of the selection of j. Expressions [6.29] and [6.30] can be substituted in [6.27] to give

$$\sum_{k=1}^{C-1} \mu_{ik}^{I} dc_k^{I\alpha} + w^I \sigma^I \overline{V}_i^I dH^I = ... = \sum_{k=1}^{C-1} \mu_{ik}^{\mathrm{P}} dc_k^{\mathrm{P}\alpha} + w^{\mathrm{P}} \sigma^{\mathrm{P}} \overline{V}_i^{\mathrm{P}} dH^{\mathrm{P}} = \sum_{k=1}^{C-1} \mu_{ik}^{\alpha} dc_k^{\alpha j}$$

or

$$\sum_{k=1}^{C-1} \mu_{ik}^{I} \frac{dc_k^{I\alpha}}{dH^I} + w^I \sigma^I \overline{V}_i^I = \sum_{k=1}^{C-1} \mu_{ik}^{II} \frac{dc_k^{II\alpha}}{dH^I} + w^{II} \sigma^{II} \overline{V}_i^{II} \frac{dH^{II}}{dH^I} = ... =$$

$$\sum_{k=1}^{C-1} \mu_{ik}^{\mathrm{P}} \frac{dc_k^{\mathrm{P}\alpha}}{dH^I} + w^{\mathrm{P}} \sigma^{\mathrm{P}} \overline{V}_i^{\mathrm{P}} \frac{dH^{\mathrm{P}}}{dH^I} = \sum_{k=1}^{C-1} \mu_{ik}^{\alpha} \frac{dc_k^{\alpha j}}{dH^I} \tag{6.31}$$

for $i = 1, 2, ..., C$. The derivatives dH^{II}/dH^I, dH^{III}/dH^I,...,dH^{P}/dH^I and can be obtained from the particle growth equations as will be shown in the following sections. When these are set, there are $C - \mathrm{P}$ degrees of freedom, the solution of [6.31] comes from the iteration of those composition differentials until the equations are met for increments of curvature dH^I until the interface composition of each particle equals the average composition of the alloy at the critical radius. The significance of the derivatives dH^j/dH^I ($j = II, III, ..., \mathrm{P}$) is that a change in curvature in any of the present phases will induce changes in the remaining for the system to maintain equilibrium.

From equations [6.31], any composition shift caused by a curvature change from $H^j = 0$ to $H^j = 1/r$ can be approximated as

$$c_{rk}^{j\alpha} - c_k^{j\alpha} = f_k^{j\alpha} H^j \tag{6.32}$$

$$c_{rk}^{\alpha j} - c_k^{\alpha j} = f_k^{\alpha j} H^j \tag{6.33}$$

for averaged values of $dc^{j\alpha}/dH^j$ and $dc_k^{\alpha j}/dH^j$. The case of a Henrian solution is when

$$f_k^{\alpha j} = c_k^{\alpha\beta} \frac{w\sigma \overline{V}^{\beta}}{R_u T} \frac{1 - c_k^{\alpha\beta}}{c_k^{\beta\alpha} - c_k^{\alpha\beta}}$$

as given by equation [6.23].

6.5 Precipitate growth with capillarity effects

The methods described in the previous sections can be employed to obtain the local equilibrium concentrations for particle growth. This task will be done in the present section. The

procedure to obtain particle lengthening rate expressions in a diffusion–controlled growth process can be described in steps as follows: 1. The diffusion equation for each solute is written in an appropriate coordinate system. 2. Each equation is solved under boundary conditions that account for capillarity. 3. The solutions are substituted in a mass balance equation for each solute written in the appropriate coordinate system, from which the lengthening rate expression is extracted. This procedure is followed next for three different particle morphologies, removing the usual dilute solution assumption, and developing for multicomponent systems. No variation of diffusion coefficient with concentration is assumed, and interdiffusion coefficients are neglected.

6.5.1 Spherical particles

In a multicomponent system, the diffusion equation in a spherical coordinate system can be written as (equation [2.39]):

$$\frac{\partial c_i}{\partial t} = \frac{D_i}{R^2}\frac{\partial}{\partial R}\left\{R^2\frac{\partial c_i}{\partial R}\right\} \tag{6.34}$$

for $i = 1, 2, ..., C$ components. The solution is of the type

$$r = \alpha_{3i}\sqrt{D_i t} \tag{6.35}$$

where r is the spherical particle radius and α_{3i} growth parameter related to component $i = 1, 2, ..., C$. The boundary conditions to solve equation [6.34] are:

$$c\{t = 0, R\} = \overline{c}_i \qquad \text{and} \qquad c\{t, r\} = c_{ri}^{\alpha\beta} \tag{6.36}$$

where $\overline{c}_i$ is the average concentration of solute $i = 1, 2, ..., C$ in the alloy, and $c_{ri}^{\alpha\beta}$ is the concentration of solute i in the matrix (α) in equilibrium with a β precipitate for a curved interface. In analogy to equation [3.7] an approximate solution that satisfies equation [6.34] is

$$c_i\{t, R\} = \overline{c}_i + \left[c_{ri}^{\alpha\beta} - \overline{c}_i\right]\frac{\phi\{R/\sqrt{D_i t}\}}{\phi\{\alpha_{3i}\}} \tag{6.37}$$

where

$$\phi\{\alpha_{3i}\} = \frac{1}{\alpha_{3i}}\exp\left\{-\frac{\alpha_{3i}^2}{4}\right\} - \frac{\sqrt{\pi}}{2}\mathrm{erfc}\left\{\frac{\alpha_{3i}}{2}\right\} \tag{6.38}$$

and $c_{ri}^{\alpha\beta}$ accounts for the capillarity corrected concentration shift of a non–Henrian solution.

Mass balance at the interface is mathematically expressed as

$$g\left[c_{ri}^{\beta\alpha} - c_{ri}^{\alpha\beta}\right] = D_i\frac{\partial c_i}{\partial R}\bigg|_{R=r} \tag{6.39}$$

where $g = \partial r/\partial t$ is the spherical particle growth rate. When equation [6.37] is substituted in equation [6.39] we obtain

$$\Omega_{si} = \frac{1}{2}\alpha_{3i}^3 \exp\left\{\frac{1}{4}\alpha_{3i}^2\right\}\phi\{\alpha_{3i}\} \tag{6.40}$$

where

$$\Omega_{si} = \frac{\overline{c}_i - c_{ri}^{\alpha\beta}}{c_{ri}^{\beta\alpha} - c_{ri}^{\alpha\beta}}$$

The concentrations $c_{ri}^{\beta\alpha}$ and $c_{ri}^{\alpha\beta}$ are given by the solution to the system of equations [6.31], once obtained, equations [6.40] can be solved simultaneously for $i = 1, 2, ..., C$ providing values of α_{3i} consistent with equation [5.12], from which $g = \frac{1}{2}\alpha_{3i}\sqrt{D_i/t}$ is extracted for a given curvature $H = 1/r$.

As discussed in Chapter 3, the analytical solution presented above is theoretically inconsistent, although its accuracy may be tolerated for kinetic calculations in many cases. If larger accuracy is required, the finite element solution can be invoked when extended for multicomponent systems as shown next.

For i components, equation [3.13] can be written in the form of finite differences as

$$\frac{c_{i,n}^{j+1} - c_{i,n}^{j}}{\Delta t} = \frac{N_0 - n}{L - r} \times \frac{c_{i,n+1}^{j} - c_{i,n-1}^{j}}{2} \times g^{j+1}$$

$$+D_i \times \frac{c_{i,n+1}^{j} - 2c_{i,n}^{j} + c_{i,n-1}^{j}}{(L-r)^2/N_0^2} + \frac{D_i}{r + \frac{(n)(L-r)}{N_0}} \times \frac{c_{i,n+1}^{j} - c_{i,n-1}^{j}}{(L-r)/N_0} \tag{6.41}$$

where $i = 1, 2, ..., C$ and $n = 0, 1, 2, ..., N_0$ are the nodes that divide the matrix phase in N elements each of length ΔR (Fig. 3.6), j is a time interval, $c_{i,n}^{j}$ is the i solute concentration in node n at the time interval j, Δt is the increment in time, L is the zero mass transfer boundary at the matrix, *i.e.* where $c_{i,N_o}^{j} = c_{i,N_0+1}^{j}$, and g^{j+1} the interface velocity at the time interval $j + 1$.

For i components, the mass transfer equation [3.15] is similarly expressed as

$$\frac{r^{j+1} - r^{j}}{\Delta t} = \frac{D_i}{c_{ri}^{\beta\alpha} - c_{i,0}^{j}} \times \frac{-c_{i,2}^{j} + 4c_{i,1}^{j} - 3c_{i,0}^{j}}{2(L-r)/N_0} \tag{6.42}$$

where $i = 1, 2, ..., C$, r^j is the particle radius at time interval j and $c_{i,0}^{j} = c_{ri}^{\alpha\beta}$.

The numerical solution for spherical precipitates comes from the simultaneous solution of equations [6.41, 6.42, 5.12] for successive time intervals with

$$\Delta t \leq 0.25\frac{\Delta R^2}{D_i} \tag{6.43}$$

for non–oscillatory solutions [Tanzilli and Heckel, 1968]. The equilibrium concentrations $c_{ri}^{\beta\alpha}$ and $c_{ri}^{\alpha\beta}$ are obtained from the method described previously.

6.5.2 Plate-type particles

Assuming that the particles approach a parabolic cylinder, the diffusion equation is expressed in terms of the parabolic coordinates η and ξ, and the Péclet number $p_i = g_p r/2D_i$ where g_p is the interface velocity, and r the plate tip radius [Trivedi, 1970b]:

$$\frac{\partial^2 c_i}{\partial \xi^2} + \frac{\partial^2 c_i}{\partial \eta^2} + 2p_i\left[\xi\frac{\partial c_i}{\partial \xi} - \eta\frac{\partial c_i}{\partial \eta}\right] = 0 \tag{6.44}$$

From equation [6.33], the concentration at the interface can be expressed as:

$$c_i = c_i^{\alpha\beta} + f_i^{\alpha\beta}\underbrace{(1/r)[1+\eta^2]^{-3/2}}_{a} \tag{6.45}$$

where term a accounts for the curvature change along the interface. The concentration at the tip of the plate, where the curvature is maximum, is obtained from the solution of the system of equations given by [6.31] with $w = 1$; the variation of concentration along the interface is approximated by the product of constant $f_i^{\alpha\beta}$ (equation [6.33]) and the interface curvature $(1/r)[1+\eta^2]^{-3/2}$. By analogy to equation [2.35], the solution to equation [6.44] is given by

$$c_i - c_i' = \sum_{m=0}^{\infty} A_{2m}\frac{I_{2m}\mathrm{erfc}\{\sqrt{p_i}\xi\}}{I_{2m}\mathrm{erfc}\{\sqrt{p_i}\}}H_{2m}\{\sqrt{p_i}\eta\} \tag{6.46}$$

where

$$c_i' = \overline{c}_i + (c_i^{\alpha\beta} - \overline{c}_i)\frac{\mathrm{erfc}\{\sqrt{p_i}\xi\}}{\mathrm{erfc}\{\sqrt{p_i}\}}$$

is the isoconcentrate boundary solution given by Ivanstov [1947]. The value of the coefficient A_{2m} is obtained from the boundary condition along the interface $\xi = 1$, giving

$$\sum_{m=0}^{\infty} A_{2m}H_{2m}\{\sqrt{p_i}\eta\} = (f_i^{\alpha\beta}/r)[1+\eta^2]^{-3/2}$$

Following Trivedi's analysis, the properties of Hermite polynomials are invoked [Trivedi, 1970b], so the coefficient is expressed as:

$$A_{2m} = \frac{2f_i^{\alpha\beta}}{r}\frac{p_i^{3/2}}{\pi}\frac{(-1)^m}{(2m)!}\Gamma_D\{m+1/2\}\Gamma_D\{m+3/2\}\Psi\{m+3/2, 2, p_i\}$$

The mass balance equation is expressed in analogy to the binary case as

$$2p_i\left[c_{ri}^{\beta\alpha} - \left(c_i^{\alpha\beta} + \frac{f_i^{\alpha\beta}}{r}\right)\right] = \left(\frac{\partial c}{\partial \xi}\right)_{\substack{\xi=1\\ \eta=0}} \tag{6.47}$$

in which equation [6.46] can be substituted to give

$$2p_i\left[c_{ri}^{\beta\alpha} - \left(c_i^{\alpha\beta} + \frac{f_i^{\alpha\beta}}{r}\right)\right] = 2(\overline{c}_i - c_i^{\alpha\beta})\sqrt{\frac{p_i}{\pi}}\frac{\exp\{-p_i\}}{\mathrm{erfc}\{\sqrt{p_i}\}} + \frac{f_i^{\alpha\beta}}{r}M_2\{p_i\} \tag{6.48}$$

where

$$M_2\{p_i\} = \frac{4p_i^2}{\pi}\sum_{n=0}^{\infty}\Gamma_D\{n+\tfrac{3}{2}\}\frac{I_{2n+1}\mathrm{erfc}\{\sqrt{p}_i\}}{I_{2n}\mathrm{erfc}\{\sqrt{p}_i\}}\Psi\{n+\tfrac{3}{2},2,p_i\}$$

has been presented in Fig. 4.2. Equation [6.48] can be re-arranged to obtain

$$\Omega_{pi} = \sqrt{\pi p_i}\exp\{p_i\}\mathrm{erfc}\{\sqrt{p_i}\}\left[1+\underbrace{\frac{c_{ri}^{\alpha\beta}-c_i^{\alpha\beta}}{c_{ri}^{\beta\alpha}-c_i^{\alpha\beta}}S_2\{p_i\}}_{b}\right] \tag{6.49}$$

where

$$\Omega_{pi} = \frac{\overline{c}_i - c_i^{\alpha\beta}}{c_{ri}^{\beta\alpha}-c_i^{\alpha\beta}}$$

$$S_2\{p_i\} = \frac{1}{2p_i}M_2\{p_i\} - 1$$

Equation [6.49] shows that when capillarity vanishes ($c_{ri}^{\alpha\beta} - c_i^{\alpha\beta} \to 0$), this is reduced to Ivanstov solution as $b \to 0$. Furthermore, when the difference $c_{ri}^{\alpha\beta} - c_i^{\alpha\beta}$ is expressed using the Henrian solution approximation (equation [5.7]), Trivedi's equations extended for the multicomponent scenario [5.19] are recovered.

6.5.3 Needle-like particles

It is assumed that needle–like particles approach a paraboloid of revolution, where the tip radius is defined by r, in which case the diffusion equation is expressed in terms of the parabolic coordinates γ, δ as

$$\frac{\partial^2 c_i}{\partial\gamma^2} + \left(\frac{1}{\gamma}+2p_i\gamma\right)\frac{\partial c_i}{\partial\gamma} + \frac{\partial^2 c_i}{\partial\delta^2} + \left(\frac{1}{\delta}-2p_i\delta\right)\frac{\partial c_i}{\partial\delta} = 0 \tag{6.50}$$

The interface concentration provides the boundary condition

$$c_i = c_i^{\alpha\beta} + f_i^{\alpha\beta}\underbrace{(1/r)\frac{2+\delta^2}{(1+\delta^2)^{3/2}}}_{d} \tag{6.51}$$

where d term accounts for the curvature change along the interface, and the concentration shift $f_i^{\alpha\beta}$ is obtained from (6.31) with $w = 2$. The general solution of the diffusion equation [6.50] is

$$c_i - c_i' = \sum_{n=0}^{\infty} A_n \frac{\exp\{-p_i\gamma^2\}\Psi\{n+1,1,p_i\gamma^2\}}{\exp\{-p_i\}\Psi\{n+1,1,p_i\}}L_i^o\{p_i\delta^2\} \tag{6.52}$$

where

$$c_i' = \overline{c}_i + (c_i^{\alpha\beta} - \overline{c}_i)\frac{E_1(p_i\gamma^2)}{E_1(p_i)}$$

where c_i' is the isoconcentrate boundary solution provided by Ivanstov [1947] and Horvay and Cahn [1961]. The coefficient A_n is obtained when the boundary concentration (equation [6.51]) is equated with the concentration field expression (equation [6.52]) for $\gamma = 1$, giving

$$A_n = \frac{f_i^{\alpha\beta}}{r} \exp\{p_i\} \left[2p_i I_{2n+1}\mathrm{erfc}\{\sqrt{p_i}\} + \sqrt{p_i} \frac{\Gamma_D(n+\frac{1}{2})}{\Gamma_D(n+1)} I_{2n}\mathrm{erfc}\sqrt{p_i} \right] \tag{6.53}$$

The interface mass flux balance can now be obtained

$$2p_i \left[c_{ri}^{\beta\alpha} - \left(c_i^{\alpha\beta} + \frac{f_i^{\alpha\beta}}{r} \right) \right] = \frac{2(\overline{c}_i - c_i^{\alpha\beta})}{\exp\{p_i\} E_1\{p_i\}} + \frac{f_i^{\alpha\beta}}{r} N_2\{p_i\} \tag{6.54}$$

where

$$N_2\{p_i\} = 2p_i^{3/2} \exp\{p_i\} \sum_{n=0}^{\infty} \frac{\Psi\{n+1,2,p_i\}}{\Psi\{n+1,1,p_i\}} \left[2\sqrt{p_i} I_{2n+1}\mathrm{erfc}\{\sqrt{p_i}\} + \frac{\Gamma_D\{n+\frac{1}{2}\}}{\Gamma_D\{n+1\}} I_{2n}\mathrm{erfc}\{\sqrt{p_i}\} \right]$$

is shown in Fig. 4.2.

Equation [6.54] can be re-arranged as:

$$\Omega_{pi} = p_i \exp\{p_i\} E_1\{p_i\} \left[1 + \underbrace{\frac{c_{ri}^{\alpha\beta} - c_i^{\alpha\beta}}{c_{ri}^{\beta\alpha} - c_i^{\alpha\beta}} R_2\{p_i\}}_{e} \right] \tag{6.55}$$

where

$$R_2\{p_i\} = \frac{1}{2p_i} N_2\{p_i\} - 1$$

By analogy to equation [6.49], equation [6.55] will approach to the isoconcentrate solution when the term e vanishes, and to Trivedi's expressions for Henrian solutions when $c_{ri}^{\alpha\beta} - c_i^{\alpha\beta}$ is calculated through equation [5.7].

6.6 Summary

The thermodynamic equilibrium relationships for non–ideal multicomponent and multiphase systems has been presented when capillarity is introduced. A method to predict the equilibrium concentrations as a function of curvature is described. This has been applied to obtain relationships to determine the growth rate of particles approaching spheres, paraboloids of revolution and parabolic cylinders, which have been shown to be consistent with the theory for particle growth which obeys Henry's law.

CHAPTER 7

Precipitate coarsening in multicomponent systems

7.1 Introduction

The latest theory of precipitate coarsening is capable to deal with multicomponent effects in non–ideal solutions [Umanstev and Olson, 1993], and off–diagonal terms of the diffusivity, which have been recently included by Morral and Purdy [1994]. However, those theories use a form of the Gibbs–Thomson equation that neglects changes in chemical potential of the precipitate phase (section 6.2) to obtain the composition shifts due to capillarity.

This chapter presents an extension of the Ostwald ripening theory introduced in section 2.6 that incorporates the generalised form of the Gibbs–Thomson equation given in previous chapter.

7.2 Gibbs–Thomson effect in coarsening

From equation [6.25], it is possible to express the Gibbs–Thomson effect as:

$$\sum_{k=1}^{C} \mu_{ik}^{\alpha} dc_k^{\alpha\beta} - \sum_{k=1}^{C} \mu_{ik}^{\beta} dc_k^{\beta\alpha} = w\sigma \overline{V}_i^{\beta} dH \tag{7.1}$$

When coarsening of particles occur, their curvature is expected to be large, thus it becomes possible to express equation [7.1] in terms of composition increments and a curvature $H = 1/r$:

$$\sum_{k=1}^{C} \mu_{ik}^{\alpha} \Delta c_k^{\alpha} - \sum_{k=1}^{C} \mu_{ik}^{\beta} \Delta c_k^{\beta} = \frac{w\sigma \overline{V}_i^{\beta}}{r} \tag{7.2}$$

where $\Delta c_k^{\alpha} = c_k^{\alpha\beta}\{r\} - c_k^{\alpha\beta}$ and $\Delta c_k^{\beta} = c_k^{\beta\alpha}\{r\} - c_k^{\beta\alpha}$.

From the definition of partial molar properties [DeHoff, 1993], it is possible to express the molar volume of β phase as

$$V_m = \sum_{i=1}^{C} c_i^{\beta\alpha} \overline{V}_i^{\beta} \tag{7.3}$$

Thus, when the sum of i equations given by [7.2] is multiplied by $c_i^{\beta\alpha}$, it can be expressed in terms of the molar volume of the β phase:

$$\sum_{i=1}^{C} \left[\sum_{k=1}^{C} c_i^{\beta\alpha} \mu_{ik}^{\alpha} \Delta c_k^{\alpha} - \sum_{k=1}^{C} c_i^{\beta\alpha} \mu_{ik}^{\beta} \Delta c_k^{\beta} \right] = \frac{w\sigma V_m}{r} \tag{7.4}$$

In the notation used next, a matrix **A** can be expressed as (A], [A] or [A), which refer to a row, square or column matrix. Thus, the Gibbs–Thomson effect (equation [7.4]) can be written as:

$$(c^{\beta\alpha}][\mu^{\alpha}][\Delta c^{\alpha}) = (c^{\beta\alpha}][\mu^{\beta}][\Delta c^{\beta}) + \frac{2\sigma V_m}{r} \tag{7.5}$$

where

$$[\mu^{\alpha}] = \left(\frac{\partial \mu_i^{\alpha}}{\partial c_j}\right)_{T,P,c_k}, \quad [\mu^{\beta}] = \left(\frac{\partial \mu_i^{\beta}}{\partial c_j}\right)_{T,P,c_k} \tag{7.6}$$

Equation [7.4] and the forthcoming equations can be reduced to $C-1$ independent variables by setting

$$\sum_{i=1}^{C} c_i = 1 \tag{7.7}$$

.

7.3 Coarsening rate

The method to obtain the equations that describe the kinetics of coarsening can be summarised as follows [Umanstev and Olson, 1993]: 1. The mass balance condition at the interface is set using the appropriate concentrations as these are modified by capillarity. 2. Conservation of each solute component is set by balancing this with the initial supersaturation of the alloy, and accounting for particle growth and dissolution. 3. The continuity equation is applied to the particle size distribution. 4. The expressions provided by former steps are simultaneously solved. This method is applied next for coarsening of spherical particles ($w = 2$); this rests no generality to the analysis presented here as the actual shape of the particles may be taken into account by adjusting certain numerical constants in the relevant formulae [Lifshitz and Slyozov, 1961].

Interface mass conservation

Following Morral and Purdy [1994], the mass conservation condition at the interface of a particle of radius r yields

$$[\Delta c^{\alpha\beta}) \times \frac{dr}{dt} + \frac{[D][\Delta \overline{c}^{\alpha})}{r} = 0 \tag{7.8}$$

where $[\Delta c^{\alpha\beta}) = [c^{\beta\alpha}\{r\} - c^{\alpha\beta}\{r\})$, $[\Delta \overline{c}^{\alpha}) = [c^{\alpha\beta}\{r\} - \overline{c})$ where $[\overline{c})$ is the matrix far field concentration and $[D] = D_{ij}$ is the square diffusivity matrix. Equation [7.8] can be obtained from the mass conservation condition applied at the interface of a growing sphere (equation [5.9]) when off–diagonal terms of the diffusivity matrix are incorporated and the concentration shifts are taken as increments. Equation [7.8] can be multiplied by $(c^{\beta\alpha}][\mu^{\alpha}][D]^{-1}$ form which

the term $(c^{\beta\alpha}][\mu^{\alpha}][\Delta\overline{c}^{\alpha})$ can be obtained from the Gibbs–Thomson equation [7.5] when this is expressed as

$$(c^{\beta\alpha}][\mu^{\alpha}][\Delta\overline{c}^{\alpha}) + (c^{\beta\alpha}][\mu^{\alpha}][\Delta\overline{c}^{\alpha\beta}) = (c^{\beta\alpha}][\mu^{\beta}][\Delta c^{\beta}) + \frac{2\sigma V_m}{r} \tag{7.9}$$

where $[\Delta\overline{c}^{\alpha\beta}) = [\overline{c} - c^{\alpha\beta})$, this can be substituted in equation [7.8] to give

$$(c^{\beta\alpha}][\mu^{\alpha}][D]^{-1}[\Delta c^{\alpha\beta})\frac{dr}{dt} = \frac{1}{r}\left((c^{\beta\alpha}][\mu^{\alpha}][\Delta\overline{c}^{\alpha\beta}) - (c^{\beta\alpha}][\mu^{\beta}][\Delta c^{\beta}) - \frac{2\sigma V_m}{r}\right) \tag{7.10}$$

it is seen that the critical radius at which a particle dissolves is given by

$$r_c = \frac{2\sigma V_m}{(c^{\beta\alpha}][\mu^{\alpha}][\Delta\overline{c}^{\alpha\beta}) - (c^{\beta\alpha}][\mu^{\beta}][\Delta c^{\beta})} \tag{7.11}$$

which includes the term $(c^{\beta\alpha}][\mu^{\beta}][\Delta c^{\beta})$ in the denominator which is lacking in Umanstev and Olson's [1993] expression for critical radius, this accounts for the β phase energy contribution to keep the particle in equilibrium with the matrix as a curvature is present.

To solve equation [7.10] it is recognised that $\Delta\{t\} = (c^{\beta\alpha}][\mu^{\alpha}][\Delta\overline{c}^{\alpha\beta})$ is a function of time [Umanstev and Olson, 1993] and $(c^{\beta\alpha}][\mu^{\beta}][\Delta c^{\beta})$ depends on r only; the functional dependence of the last term can be approximated as

$$(c^{\beta\alpha}][\mu^{\beta}][\Delta c^{\beta}) = (c^{\beta\alpha}][\mu^{\beta}][\Delta c_r^{\beta})\frac{\overline{r}_r}{r} \tag{7.12}$$

where $\overline{r}_r$ is an average reference particle radius and $[\Delta c_r^{\beta})$ the difference in concentration between a β particle of this radius and that of an infinite radius or $[\Delta c_r^{\beta}) = [c^{\beta\alpha}\{\overline{r}_r\} - c^{\beta\alpha})$. The validity of equation [7.12] lies on approximating the change in composition of β phase during the coarsening process as

$$[\Delta c^{\beta}) = [c^{\beta\alpha}\{r\} - c^{\beta\alpha}) = [c^{\beta\alpha}\{\overline{r}_r\} - c^{\beta\alpha})\frac{\overline{r}_r}{r} \tag{7.13}$$

which represents a curve in a C dimensional space where the initial point is given by

$$[c^{\beta\alpha}\{r\}) = [c^{\beta\alpha}\{\overline{r}_r\} - c^{\beta\alpha})\frac{\overline{r}_r}{r} + [c^{\beta\alpha})$$

and the final point is the composition of β in equilibrium with α for a flat interface $[c^{\beta\alpha}\{r = \infty\}) = [c^{\beta\alpha})$. The approximation used here is not general as the variation of $c^{\beta\alpha}$ with r is strictly given by the phase diagram, but during the coarsening regime the equilibrium particle radii are expected to be large, and an average particle radius $\overline{r}_r$ when coarsening starts is large, thus, the range of error should be small. Rigorously, $[\Delta c^{\beta})$ in equation [7.10] must be expressed as a function that describes the $\beta/\beta + \alpha$ boundary in the phase diagram as r is varied, which complicates the analysis as it will produce different expressions for the coarsening kinetics

for each system; therefore, equation [7.13] is employed as a first approach. In substitution of equation [7.13] in equation [7.10] it is obtained:

$$\Phi \frac{dr}{dt} = \frac{1}{r}\left(\Delta\{t\} - \frac{\Omega^I}{r}\right) \tag{7.14}$$

where $\Phi = (c^{\beta\alpha}][\mu^{\alpha}][D]^{-1}[\Delta c^{\alpha\beta})$ characterises the coarsening resistance of the material and $\Omega^I = 2\sigma V_m + (c^{\beta\alpha}][\mu^{\beta}][\Delta c_r^{\beta})\overline{r}_r$ the total energy increase of β phase as a curvature is present.

Solute concentration

The second element of the theory is mass balance of the alloy, this can be expressed as

$$c_j^0 = (1-\varphi_v)\overline{c}_j + \varphi_v c_j^{\beta\alpha}\{r\}, \quad \varphi_v = \frac{4\pi}{3V_m}\int_0^{\infty} r^3 f\{r,t\}dr \tag{7.15}$$

for $j = 1, 2, ..., C$ components, where φ_v is the volume fraction of β phase and $f\{r,t\}$ the particle radius distribution function. Subtracting $c_i^{\alpha\beta}$ from equation [7.15] and multiplying it by $c^{\beta\alpha}\mu_{ij}^{\alpha}$ it is obtained

$$c_i^{\beta\alpha}\mu_{ij}^{\alpha}(c_j^0 - c_j^{\alpha\beta}) = (1-\varphi_v)c_i^{\beta\alpha}\mu_{ij}^{\alpha}(\overline{c}_j - c_j^{\alpha\beta}) + \varphi_v c_i^{\beta\alpha}\mu_{ij}^{\alpha}(c_j^{\beta\alpha} - c_j^{\alpha\beta}) + \varphi_v c_i^{\beta\alpha}\mu_{ij}^{\alpha}(c_j^{\beta\alpha}\{r\} - c_j^{\beta\alpha})$$

or

$$\Delta_0 = (1-\varphi_v)\Delta\{t\} + \varphi_v\Gamma_C + \varphi_v\Lambda \tag{7.16}$$

where $\Delta_0 = (c^{\beta\alpha}][\mu^{\alpha}][\overline{c}_0^{\alpha\beta})$ is the initial cumulative supersaturation of the alloy before precipitation starts, $\Gamma_C = (c^{\beta\alpha}][\mu^{\alpha}][\Delta c^{\alpha\beta})$ is a time–independent scalar that accounts for the interactions of the system at equilibrium [Umanstev and Olson, 1993], $\Lambda = (c^{\beta\alpha}][\mu^{\alpha}][\Delta c^{\beta})$ characterises the binary interactions of the solute concentration increment in β phase as curvature changes, this is a function of curvature and can be approximated for a reference radius and composition shift as

$$\Delta_0 = (1-\varphi_v)\Delta\{t\} + \varphi_v\Gamma_C + \varphi_v\Lambda_r\frac{\overline{r}_r}{r} \tag{7.17}$$

where $\Lambda_r = (c^{\beta\alpha}][\mu^{\alpha}][\Delta c_r^{\beta})$.

After long time coarsening, excess solute will vanish in the matrix as the particles thicken to large radii, causing the volume fraction to tend to the limiting value $\overline{\varphi} = \Delta_0/\Gamma_C$.

Continuity equation

The last element of the theory is the application of the continuity equation to the particle radius distribution function $f\{r,t\}$:

$$\frac{\partial f}{\partial t} + \frac{\partial}{\partial r}\left\{f\frac{\partial r}{\partial t}\right\} = 0 \tag{7.18}$$

Equations [7.14, 7.17, 7.18] can now be solved using the methods of LS or MR assuming a small precipitate volume fraction, leading to the next expressions for average particle size $\overline{r}\{t\}$, supersaturation $\Delta\{t\}$ and number N of precipitate particles. When the method of MR is employed, a time scaling technique is used to derive the power law dependence and distribution function for the size of the precipitating particles; this will produce the expressions:

$$\overline{R}^3\{t\} = (2/3)^2 Kt + \mathrm{O}\{1\}, \quad K = \Omega^I/\Phi \tag{7.19}$$

$$\Delta\{t\} = (3\sigma V_m)^{2/3}\Phi^{1/3}t^{-1/3} + \mathrm{O}\{t^{-2/3}\} \tag{7.20}$$

$$N\{t\} = (3\overline{\varphi}\Phi/4\pi\sigma)t^{-1} + \mathrm{O}\{t^{-4/3}\} \tag{7.21}$$

Where the terms of the type $\mathrm{O}\{x\}$ can be obtained from expanding to higher order terms the distribution function for the size of the precipitates [Marqusee and Ross, 1983]; for large values of t these will vanish in equations [7.20] and [7.21], reducing to LS approximation. Term $\mathrm{O}\{1\}$ in equation [7.19] can be adjusted if the initial average radius in known.

To assess the effects of adding $(c^{\beta\alpha}][\mu^\beta][\Delta c^\beta)$ in the Gibbs–Thomson equation and in coarsening kinetics, it is first recognised that the product of the vectors $(c^{\beta\alpha}]$ and $[\mu^\beta][\Delta c^\beta)$ represents a dot product which accounts for the change on the Gibbs energy of the β phase projected in the composition $(c^{\beta\alpha}]$; similarly, $(c^{\beta\alpha}][\mu^\alpha][\Delta c^\alpha)$ represents the Gibbs energy change of the α phase projected in the composition $(c^{\beta\alpha}]$. The generalised form of the Gibbs–Thomson equation is shown schematically in Fig. 7.1, showing that the satisfaction of equation [7.5] requires a negative value of $(c^{\beta\alpha}][\mu^\beta][\Delta c^\beta)$; this represents the energy "stored" in the β phase when a curvature is present, and "released" upon precipitation as thickening occurs.

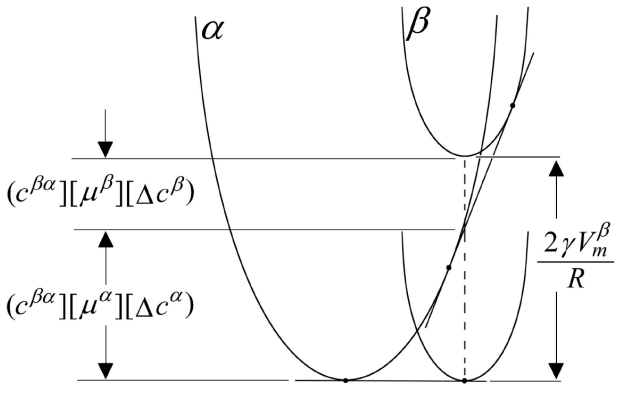

Fig. 7.1 *Schematic representation of the equilibrium conditions required by equation [7.5].*

Equations [7.11] and [7.19] show that for $(c^{\beta\alpha}][\mu^{\beta}][\Delta c^{\beta}) > 0$, r_c and K are larger, and the opposite is true for $(c^{\beta\alpha}][\mu^{\beta}][\Delta c^{\beta}) < 0$. Furthermore, equations [7.14] and [7.19] show that coarsening in a multicomponent system is not independent of the solution thermodynamics followed by the continuous phase due to the term $[\Delta c^{\beta})$ represents a curve in an C dimensional space which connects the initial and final states of the β composition with their corresponding α concentrations as coarsening progresses. This is consistent with Gibbs phase rule, which requires that for a 2 phase system where the pressure and temperature are set, the number of degrees of freedom is $C - 2$. Previous investigations have reached opposite conclusions when the thermodynamics of β phase are neglected [Umanstev and Olson, 1993, Morral and Purdy, 1994].

7.4 Summary

Expressions for the average particle radius, matrix composition and number of particles have been obtained when allowing for changes in chemical potential and composition shifts of the product phase in the coarsening regime. As opposed to previous theories, the results show dependence on the solution thermodynamics followed by the continuous phase.

CHAPTER 8

Model for needle–shaped precipitates in multicomponent alloys

8.1 Introduction

This chapter introduces a computational model for overall kinetics that incorporates the concepts of needle–shaped particle growth presented in Chapters 4, 5 and 6. Rigorous thermodynamic equilibrium of each particle is taken into account, and coarsening is incorporated. The model is then applied to obtain the kinetics of precipitation in a secondary hardening steel. The information cast includes the number distribution of particles characterised by a given needle equilibrium tip radius, length and thickness during growth and coarsening regimes. This information is simply not available from previous models, which assume a constant aspect ratio, and it may be an aid to the design of alloys with improved mechanical properties.

8.2 Model

The model presented here is aimed at predicting the precipitation and coarsening kinetics of carbides in the secondary hardening steel Fe–0.11C–1.95Mo wt.%, which was studied originally by Hall *et al.* [1972]. They obtained the isothermal lengthening rate of Mo_2C needle–shaped precipitates for temperatures ranging from 600 to 750°C.

During the first stages of heat–treatment, cementite, which is kinetically favoured, is assumed to form by a paraequilibrium mechanism from ferrite. The cementite first enriches in substitutional solutes and later dissolves as the more stable Mo_2C precipitation gathers pace, and grows and coarsens until equilibrium is reached. In the present work it is assumed that the interfacial energy per unit area (σ) of Mo_2C in ferrite remains constant as precipitation proceeds, and that the Mo_2C particles remain in thermodynamic equilibrium with ferrite, whose concentration is updated at each stage of growth. The details of the model are discussed next.

8.2.1 Cementite enrichment and dissolution

Cementite, which forms as a result of tempering, is known to form rapidly by a mechanism which involves the diffusion only of substitutional atoms. Thus, the ratio of iron to substitutional solute atoms does not change during this paraequilibrium transformation [Bhadeshia, 1985a].

Since cementite forms rapidly in supersaturated ferrite, the starting microstructure for the purposes of Mo_2C formation is assumed to contain cementite precipitates. These cementite particles change in composition during the ageing process. Bhadeshia [1989] has presented a theory of cementite enrichment where the composition variation of a cementite particle is given by

$$t_c = \frac{\pi[x_\theta(\overline{c} - c^\theta)]^2}{16D(c^{\alpha\theta} - \overline{c})^2} \tag{8.1}$$

where c^θ is the concentration of solute in cementite (θ), $\overline{c}$ is the average concentration of solute in the alloy, $c^{\alpha\theta}$ is the concentration of solute in ferrite (α) in equilibrium with θ, and x_θ is the cementite particle thickness. D is the solute diffusion coefficient in the matrix and t_c the time required for the cementite to reach a concentration c^θ.

Cementite will eventually dissolve when the average concentration of solute at the Mo_2C needle interface of each particle $c_R^{\alpha\beta}$ (where β stands for the Mo_2C precipitate) is lower than $c^{\alpha\theta}$. The dissolution velocity v_c, is given by

$$v_c(c^{\theta\alpha} - c_r^{\alpha\beta}) = D\frac{c^{\alpha\theta} - c_R^{\alpha\beta}}{\overline{d}} \tag{8.2}$$

where $\overline{d}$ is the average distance between particles. To obtain $c_R^{\alpha\beta}$ consider first the parabola shown in Fig. 4.1a, which can be described as

$$x_p^2 = 4f_p(f_p - z_p) \tag{8.3}$$

through the transformation $x_p = X/r$, $z_p = Z/r$, $f_p = f_o/r$ where x_p, z_p are adimensional parabolic coordinates, f_p the adimensional focal distance, r the tip radius, and $f_o = r/2$ is the focal distance. Following Horvay and Cahn [1961], the radius of curvature at any point X of the parabola is

$$R_{XZ} = -2f_p r\left[1 + \left(\frac{x_p}{2f_p}\right)^2\right]^{3/2}$$

or

$$R_{XZ} = -r\left[1 + x_p^2\right]^{3/2} \tag{8.4}$$

where the mean value theorem can be applied to obtain the averaged parabolic radius of curvature at the interface as

$$\overline{R} = -\frac{r}{d/2r}\int_0^{d/2r}\left[1 + x_p^2\right]^{3/2} dx_p \tag{8.5}$$

where d is the needle thickness. The integration of equation [8.5] gives [Gradshtein, 1965]

$$\overline{R} = \frac{r}{d_p}\left[\frac{1}{4}d_p u^3 + \frac{3}{8}d_p u + \frac{3}{8}\ln\{d_p + u\}\right] \tag{8.6}$$

where $d_p = d/2r$ and $u = (1 + d_p^2)^{1/2}$. Following the approximation of equation [6.45], where the matrix interface composition is assumed to be proportional to the curvature along the parabolic surface, the average concentration of a needle–shaped particle of tip radius r is given by

$$c_R^{\alpha\beta} = c_r^{\alpha\beta}\frac{\overline{R}}{r} \tag{8.7}$$

Referring to equation [8.2], the term $\overline{d}$ has traditionally been calculated as [Robson and Bhadeshia, 1997a, Fujita and Bhadeshia, 1999]:

$$\overline{d} = \frac{1}{2}(N_\theta + N_\beta)^{-1/3} \tag{8.8}$$

But this accounts for the average distance between the totality of N_θ and N_β particles that are not distinguished, as shown in Fig. 8.1, where particles separated by an approximate distance of $\overline{d}$ are marked. However, dissolution of cementite (θ) in favour of Mo_2C (β) requires the average distance between θ and β particles. In order to do this, first consider a distribution of particles denoted by $\bullet$ and $\circ$ (Fig. 8.2). If there are many more $\bullet$ particles that dissolve in favour of $\circ$ (Fig. 8.2a), and these are characterised by $N_\bullet$ and $N_\circ$ particles per unit length, the average distance between $\bullet$ and $\circ$ is

$$\overline{d} = \frac{\int_0^{N_\circ^{-1}/2} N_\bullet X\, dX}{\int_0^{N_\circ^{-1}/2} N_\bullet\, dX} = \frac{N_\circ^{-1}}{4} \tag{8.9}$$

If the density of $N_\bullet$ is much lower than for $\circ$ ($N_\bullet \ll N_\circ$) as shown in Fig. 8.2b it can be assumed that a $\bullet$ particle dissolves in favour of its nearest $\circ$ particle within a radius of $N_\circ/2$. It is important to remark that $\overline{d}$ in equation [8.9] depends only on $N_\circ$.

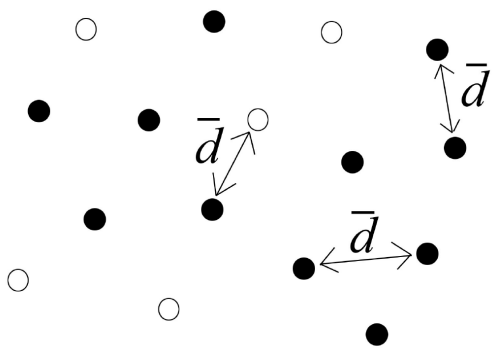

Fig. 8.1: To show that the average distance given provided by equation [8.8] is the same regardless of the nature of the particle.

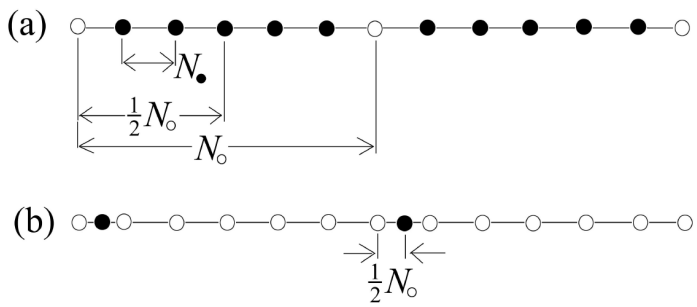

Fig. 8.2: Average distances between particles for (a) $N_\circ > N_\bullet$, and (b) $N_\bullet > N_\circ$.

In the three dimensional case, the average distance of θ dissolving in favour of β is

$$\overline{d} = \frac{\int_0^{\frac{1}{2}(N_\beta)^{-1/3}} N_\theta r(4\pi r^2 dr)}{\frac{4}{3}\pi\left(\frac{1}{2}(N_\beta)^{-1/3}\right)^3 N_\theta} = \frac{3}{8}(N_\beta)^{-1/3} \tag{8.10}$$

which shows dependence on N_β only. It is seen that the use of equation [8.10] instead of (8.8) at early stages of cementite dissolution, when N_β is several orders of magnitude lower than N_θ, produces a large difference in $\overline{d}$.

In obtaining the dissolution velocity of cementite as provided by equation [8.2], the thickness of cementite particles was considered to be of 20 nm by those precipitated within the martensite laths, and of 50 nm for those particles at the lath boundaries [Fujita, 1999, 2000].

The concentration used in equation [8.1] is that of Mo, since this component enriches the cementite. In equation [8.2] the Mo concentration is used as well, due to it is characterised by a much smaller diffusion coefficient than C, and thus is assumed to control the rate of cementite dissolution.

8.2.2 Nucleation of Mo_2C

Classical theory [Christian, 1975] is used to estimate the nucleation rate I for Mo_2C

$$I = N_\beta \frac{kT}{h} \exp\left\{-\frac{G^* + Q^*}{kT}\right\} \tag{8.11}$$

where

$$G^* = \frac{16\pi\sigma^3}{3(\Delta G_v)^3} \tag{8.12}$$

where h and k are the Planck and Boltzmann constants, respectively, Q^* is the activation energy for the transfer of atoms across the nucleus/precipitate interface, assumed to be one half of the activation energy for Mo diffusion [Christian, 1975].

Referring to equation [8.12], σ is the surface energy per unit area and ΔG_v is the chemical free energy change per unit volume. ΔG_v was obtained by subtracting the Gibbs energy of a particle that nucleates at a critical radius r^* and that of a particle of infinite radius as

$$\Delta G_v = \frac{1}{V_m}\left[\left(c^{\beta\alpha}_{\rm Mo}\mu_{\rm Mo}\{r^*\} + c^{\beta\alpha}_{\rm C}\mu_{\rm C}\{r^*\} + c^{\beta\alpha}_{\rm Fe}\mu_{\rm Fe}\{r^*\}\right)\right.$$
$$\left. -\left(c^{\beta\alpha}_{\rm Mo}\mu_{\rm Mo}\{\infty\} + c^{\beta\alpha}_{\rm C}\mu_{\rm C}\{\infty\} + c^{\beta\alpha}_{\rm Fe}\mu_{\rm Fe}\{\infty\}\right)\right] \qquad (8.13)$$

where V_m is the molar volume of β phase and $\mu_{\rm C}$, $\mu_{\rm Mo}$ and $\mu_{\rm Fe}$ are the chemical potentials of C, Mo, and Fe, respectively, and which are evaluated at a critical radius r^* or an infinite radius (flat interface).

8.2.3 Growth of Mo_2C

To obtain the lengthening rate of Mo_2C needle–shaped particles, it is necessary to solve equation [6.55] for i =C, Mo. The matrix composition $\overline{c}_i$ is updated with time, and appropriate values of $c^{\alpha\beta}_{r\rm Mo}$, $c^{\alpha\beta}_{r\rm C}$, $c^{\alpha\beta}_{\rm Mo}$, $c^{\alpha\beta}_{\rm C}$, $c^{\beta\alpha}_{r\rm Mo}$, $c^{\beta\alpha}_{r\rm C}$, g_p and r have to be substituted in [6.55]. This complicated task is enormously simplified if it is recognised that the Mo_2C composition $c^{\beta\alpha}_i$ is not significantly altered by curvature (i.e. $c^{\beta\alpha}_{ri} \simeq c^{\beta\alpha}_i$), and thus equation [6.55] can be written as

$$\Omega_{pi} = p_i \exp\{p_i\} E_1\{p_i\}\left[1 + \frac{1}{s_i}\Omega_{pi} R_2\{p_i\}\right] \qquad (8.14)$$

where

$$s_i = \frac{\overline{c}_i - c^{\alpha\beta}_i}{c^{\alpha\beta}_{ri} - c^{\alpha\beta}_i} \qquad (8.15)$$

is the shift of the i solute composition, which has been defined in analogy to the term r/r_c in equation [5.19] and ranges from zero to infinity for a flat interface. Note that Ω_{pi} in [8.14] is reduced to Ω_i for $c^{\beta\alpha}_{ri} = c^{\beta\alpha}_i$.

To solve equation [8.15] for i =C, Mo consider Fig. 8.3, this shows that for given supersaturations of Mo and C, $\Omega_{\rm Mo}$ and $\Omega_{\rm C}$, respectively, the solutions for the Péclet number of Mo and C, range between two values denoted by $p^A_{\rm Mo}$ and $p^B_{\rm Mo}$ for Mo, and $p^A_{\rm C}$ and $p^B_{\rm C}$ for C. $s = 6$ gives the minimum value of $s_{\rm Mo}$ and Péclet number, which combined with $p^A_{\rm Mo}$ solves equation [8.14] for Mo, whereas $s \to \infty$ will provide the maximum value of $s_{\rm Mo}$ and Péclet number which, combined with $p^B_{\rm Mo}$ solves [8.14]. Thus, in this case $s_{\rm Mo}$ ranges between 6 and infinity. $s_{\rm C}$ is got from the intersection of $p_{\rm C} = p_{\rm Mo} D_{\rm Mo}/D_{\rm C}$ and $\Omega_{\rm C}$, as shown in Fig. 8.3. But there is a collection of values of $s_{\rm C}$, $s_{\rm Mo}$ that solve equation [8.15], each pair of $s_{\rm C}$, $s_{\rm Mo}$ defines a needle tip radius. The one that provides the maximum lengthening rate through

$$g_p = \frac{2p_{\rm Mo}D_{\rm Mo}}{r} = \frac{2p_{\rm C}D_{\rm C}}{r}$$

was considered. Note that Fig. 8.3 shows that there are minimum values of $s_{\rm C}$ and $s_{\rm Mo}$ for needle equilibrium growth, from equation [8.15] it is seen that these set the compostions $c_{ri}^{\alpha\beta}$ (i =Mo, C) that are closest to the matrix concentration, and thus set the minimum radius at which the needle tip can form under the present shape preserving assumption.

In this computational model, all the needle particles characterised by different tip radii are updated in their equilibrium compositions with the matrix at any stage of growth.

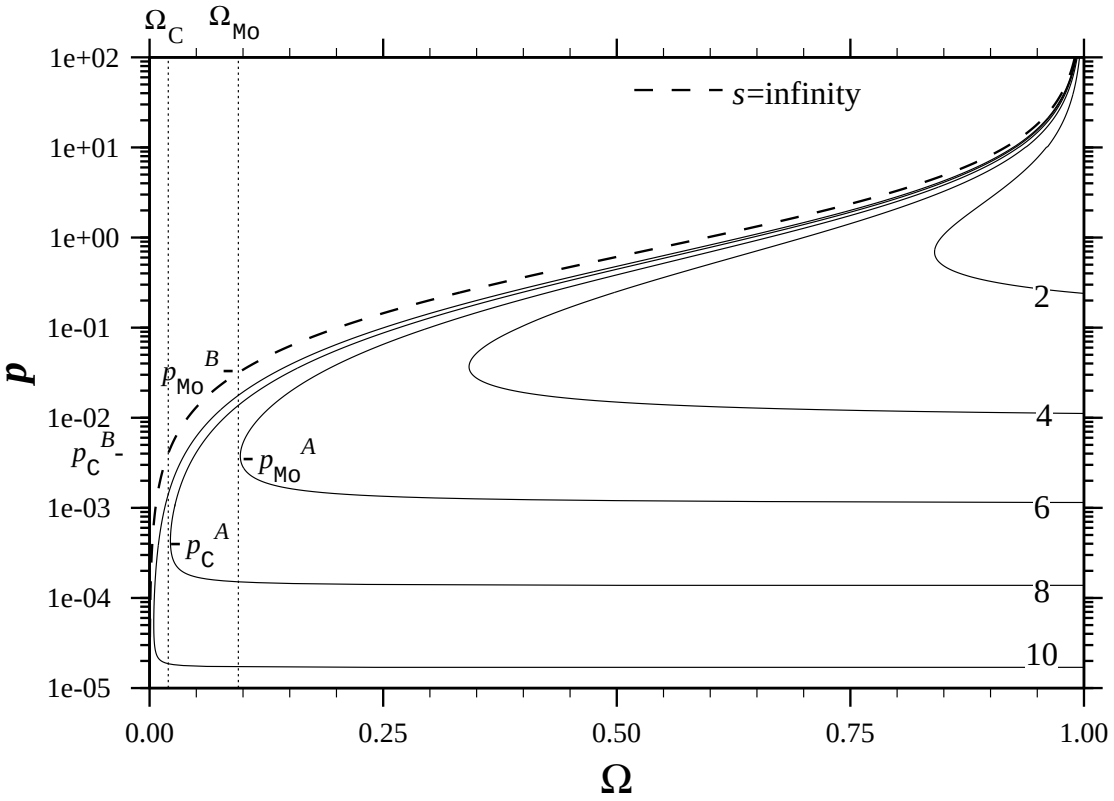

Fig. 8.3: IS contours to show solution to equation [8.15] for the shown values of Ω_C and Ω_{Mo}. The solution involves a range of values from p_C^A, p_{Mo}^A to p_C^B, p_{Mo}^B, and the corresponding values of s, which approximately range from $6 \leq s_{Mo} \leq \infty$, and $8 \leq s_C \leq \infty$.

8.2.4 Precipitate coarsening and dissolution

Normally there is an arbitrary division between growth and coarsening, which is not necessary when capillarity is taken into account. However, for needles, small and large particles have the same tip radius with the assumption of the shape–preserving solution. Therefore, there can be no coarsening if the difference in tip concentrations is assumed to provide the driving force for coarsening.

Coarsening must involve spherodization of the needles. Therefore, in this model it is

assumed that growth continues until a critical amount of solute is removed from the matrix, after which equilibrium growth requires a very large needle tip raduis, which demands an amount of solute in the precipitate inconsistent with mass balance. At this stage coarsening is introduced, particles of a smaller average interface radius will dissolve in favour of those of larger average interface radius due to a concentration gradient is present. The average interface radius of a particle is obtained through equation [8.6], and the rate of dissolution is given by:

$$v_d(c^{\beta\alpha s} - c_r^{\alpha\beta s}) = D\frac{c_R^{\alpha\beta l} - c_R^{\alpha\beta s}}{\overline{d}} \tag{8.16}$$

where $c^{\beta\alpha s}$ is the solute concentration of the Mo_2C small precipitate in equilibrium with the matrix, which is assumed to be constant along the parabolic interface, $c_R^{\alpha\beta s}$ and $c_R^{\alpha\beta l}$ are the average interface solute concentrations of the matrix in equilibrium with the precipitate of the small and large particles, respectively. $\overline{d}$ holds the same form as in equation [8.10]; it is defined in terms of large particles as

$$\overline{d} = \frac{3}{8}(N_\beta^l)^{-1/3} \tag{8.17}$$

where N_β^l is the number density of large Mo_2C particles per unit volume.

In order to calculate the rate of particle thickening, it is necessary to obtain expressions for the parabola length and thickness. From equation [8.3], it is possible to express the parabola as

$$X = \sqrt{2Zr} \tag{8.18}$$

by locating the needle tip at $Z = 0$ and rotating 180°. A differential volume element of the needle normal to its main axis is $dV_N = \pi X^2 dZ = 2\pi Z r dZ$. If l is the needle length, then the volume can be calculated by integration as

$$V_N = 2\pi r\left(\frac{l}{2}\right)^2 \tag{8.19}$$

and the needle thickness d can be calculated as

$$d = 2\sqrt{lr} \tag{8.20}$$

In this model, the dissolution of a needle (small particle) is supposed to decrease its length, keeping its thickness constant, whereas thickening of a (large) particle is assumed to increase its thickness, keeping its length constant; this means that small particles will evolve to spheres of a decreasing radius of curvature, until they disapear, whereas large particles evolve to spheres of an increasing radius. From equations [8.19, 8.20], and assuming mass balance, *i.e.* that the

solute removed from the dissolving particle is equal to that incorporating in the coarsening particle, the expressions for the change in volume of the small and large particles are given by

$$\frac{dV_s/dt}{\frac{1}{8}\pi d^2}(c^{\beta\alpha s} - c_r^{\alpha\beta s}) = D\frac{c_R^{\alpha\beta l} - c_R^{\alpha\beta s}}{\overline{d}} \tag{8.21}$$

$$dV_l/dt\sqrt{\frac{2}{\pi l V_l}}(c^{\beta\alpha l} - c_r^{\alpha\beta l}) = D\frac{c_R^{\alpha\beta l} - c_R^{\alpha\beta s}}{\overline{d}} \tag{8.22}$$

where V_s and V_l are the volumes of small and large particles, respectively.

In coarsening regime, the independent interaction of all particles of different radii is accounted for, and the volume of each updated accordingly. In analogy to cementite dissolution, Mo controls the dissolution and thickening of particles in this regime.

8.2.5 Mass balance

At every time step, solute mass balance is taken into account by updating the C and Mo matrix composition as

$$\overline{c}_i\{t\} = \overline{c}_i\{t=0\} - \frac{\sum_j V_j^\beta (c_{ji}^{\beta\alpha} - \overline{c}_{ji}\{t=0\}) + \sum_k V_k^\theta (c_{ki}^\theta - \overline{c}_{ki}\{t=0\})}{1 - \sum_j V_j^\beta - \sum_k V_k^\theta} \tag{8.23}$$

where i =C, Mo and the subscripts j and k label the particles of Mo_2C characterised by different average interface radius, and

$$\sum_j V_j^\beta = V^\beta \tag{8.24}$$

$$\sum_k V_k^\theta = V^\theta \tag{8.25}$$

account for the total transformed volumes of β and θ phases, respectively, $c_{ji}^{\beta\alpha}$, c_{ki}^θ are the i concentrations of j–Mo_2C and k–cementite particles, respectively, and $\overline{c}_i\{t=0\}$, $\overline{c}_i\{t\}$ are the matrix concentrations of i solute when precipitation starts and at time t, respectively.

8.3 Computational model: results and discussion

The computational model requires six parameters to be considered, the surface energy per unit area of Mo_2C/ferrite interface (σ), the initial number density (N_β) of Mo_2C nucleation sites per unit volume, the diffusivity of Mo and C in ferrite ($D_{o\mathrm{Mo}}$ and $D_{o\mathrm{C}}$, respectively), and the activation energy for diffusion of Mo and C (Q_{Mo} and Q_{C}, respectively). The values of

Parameter	Value
σ	0.0339 J m^{-2}
N_β	1×10^{6} m^{-3}
D_{Mo}	1.1×10^{-4} m^2 s^{-1}
Q_{Mo}	240×10^{3} J mol^{-1}
D_C	2.2×10^{-4} m^2 s^{-1}
Q_C	122×10^{3} J mol^{-1}

Table 8.1: Parameters used in the calculations

σ and N_β are fitted empirically to adjust the results to the observations of Hall *et al.* [1972], whereas the diffusivity and activation energy for Mo are those reported by Fridberg *et al.* [1969], and the diffusivity and activation energy for C have been provided by Wilkinson [2000]. These data are shown in Table 8.1.

Additionally it is required to obtain the cementite paraequilibrium and equilibrium compositions for cementite enrichment and dissolution, these are extracted from MTDATA [1995] for temperatures ranging between 600 to 750 °C as shown in Table 8.2.

Cementite stage	Temperature/° C	C	Mo	Fe
equilibrium	600	0.25	0.0698784	Bal.
paraequilibrium	600	0.25	0.0085927	Bal.
equilibrium	650	0.25	0.0614924	Bal.
paraequilibrium	650	0.25	0.0085927	Bal.
equilibrium	700	0.25	0.0545462	Bal.
paraequilibrium	700	0.25	0085927	Bal.
equilibrium	750	0.25	0.0485998	Bal.
paraequilibrium	750	0.25	0.0085927	Bal.

Table 8.2: Equilibrium and paraequilibrium cementite compositions

As described in previous sub–section, the Gibbs energy for particle nucleation (ΔG_v in equation [8.12]) is a function of time and curvature through the composition of each precipitate characterised by a different tip radius (equation [8.13]). ΔG_v was extracted from MTDATA through a computer program (Appendix 5) that varies the composition of C, Mo and curvature,

and obtains the chemical potential of each component in the form of tables. Those tables were used as input data of a program (Appendix 6) that obtains the overall kinetics (nucleation–growth–coarsening) of Fe–0.11C–1.95Mo wt.%.

The results for particle length are shown in Fig. 8.4, where the solid line represents the length of the longest particle at a given time, the dots are the measurements of the longest needle performed by Hall *et al.* [1972], the dotted line joins the average particle length obtained by the model at those times, and the error bars represent 1.3 standard deviations around the average length, to account for 90% of the particles. The measurements performed by Hall *et al.* were done in lots for at least 100 particles, so it is expected that their measurements lie inside the ranges given by the error bars. At 700 and 750 °C (Figs. 8.4c,d) the agreement between the measurements and the maximum length obtained by the model is extremely good, but at 600 and 650 °C this appears to be lower. To interpret these data, it must be considered that at the longer tempering times associated with lower temperatures there is a much wider range of particle lengths, therefore, the probability of finding the longest particle particle described by the solid line is much lower; the fact that the experimental measurements lie within the error bars is a proof that the model is capable to predict the existence of particles characterised by the lengths experimentally observed. A surface energy per unit area of 0.0339 J m^{-2} was selected so that the agreement at higher temperatures is best due to their measurements are considered to be more accurate.

Fig. 8.5 shows the length of the particles that nucleate first. Consistent with the Trivedi's theory for Henrian solutions, Fig. 8.5 reveals that there is an approximately linear relation of particle length with time, this is not the case for particle thickness, whose rate of growth decreases with time (Fig. 8.6), as expected with the shape preserving solution, where thickness should be proportional to $t^{1/2}$.

The needle aspect ratio (length/thickness) for the particles that lengthen from the first time step is shown in Fig. 8.7; the values well agree with the measured aspect ratios of Mo_2C from Fujita [2000], which lie between 10 and 20.

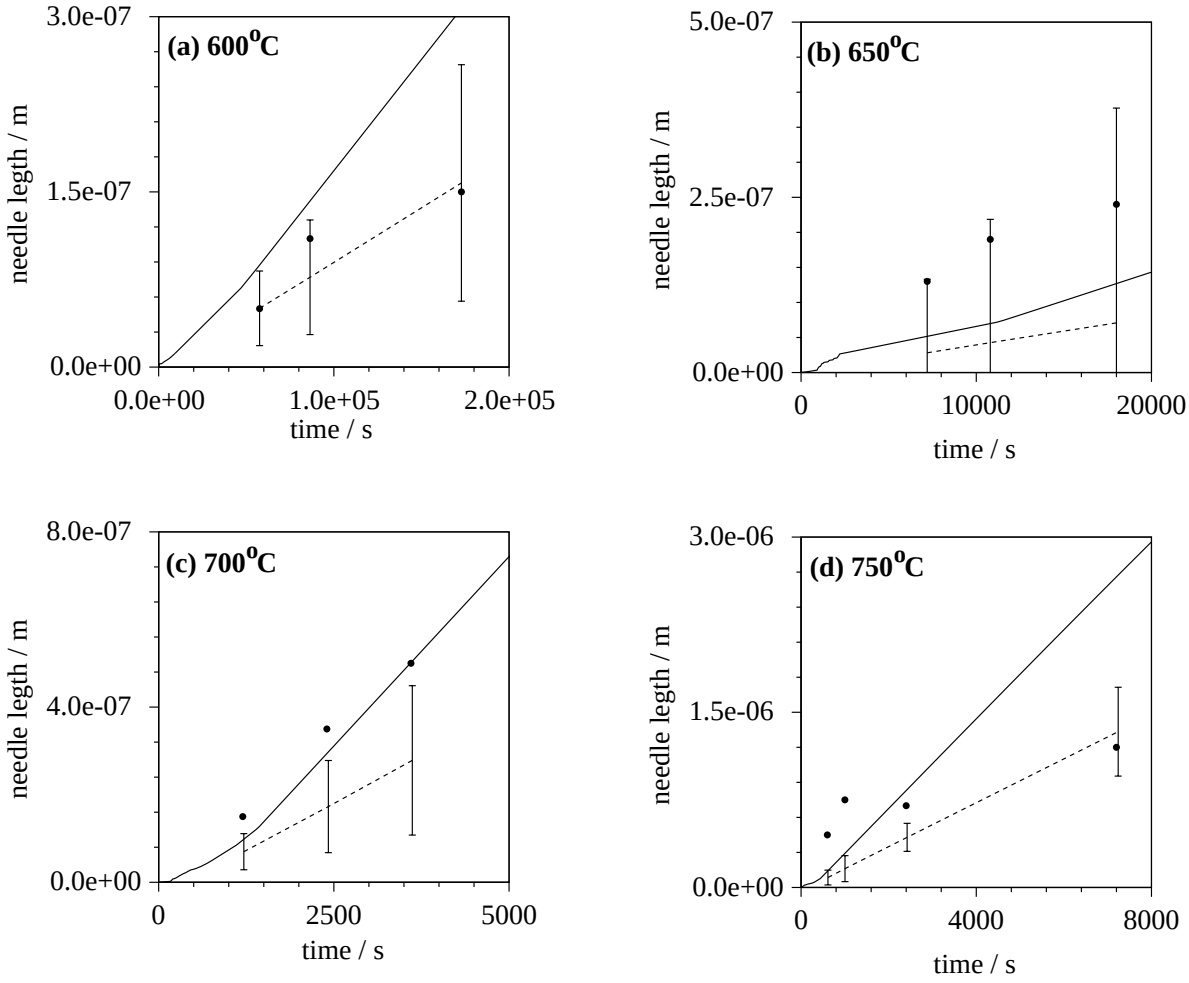

Fig. 8.4: Length of the longest particle (solid line) and average length (dotted line) as a function of time. The dots represent the experimental measurements by Hall *et al.* [1972], and the error bars 1.3 standard deviations around the average length calculated.

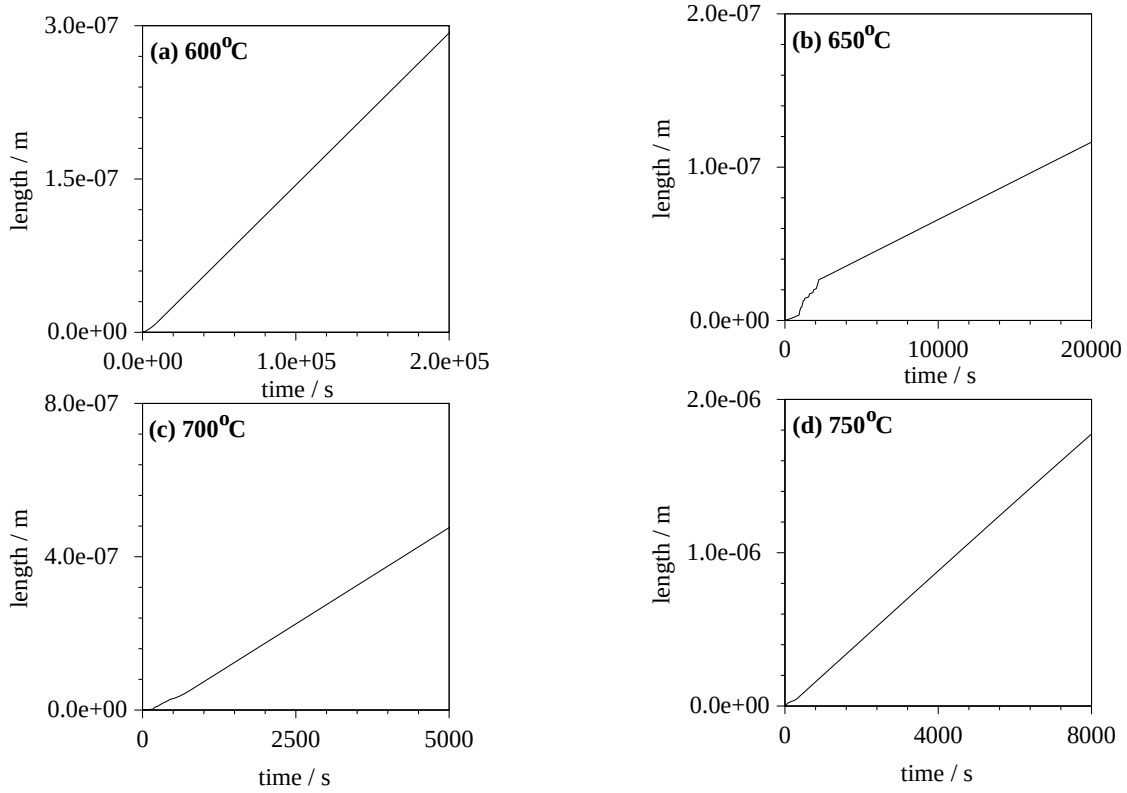

Fig. 8.5: Calculated length of the particles that nucleate in the first time step.

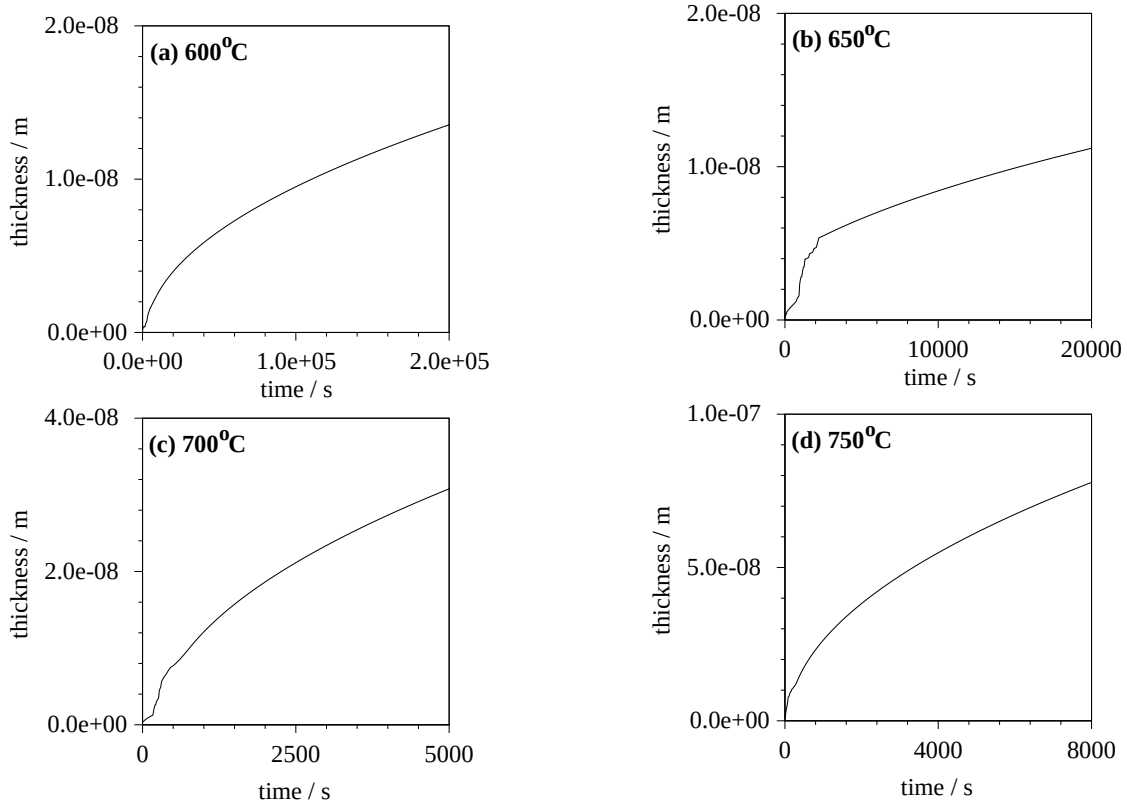

Fig. 8.6: Calculated thickness of the particles that nucleate in the first time step.

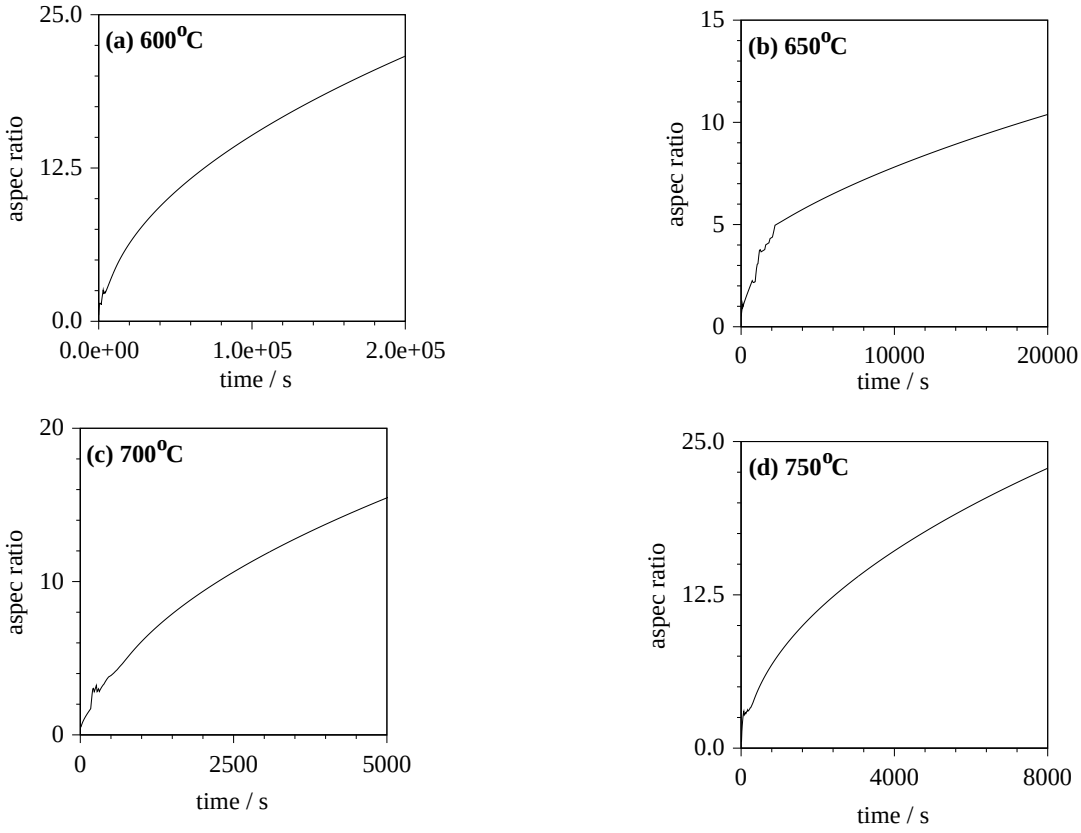

Fig. 8.7: Calculated aspect ratio of the particles that nucleate in the first time step.

During the growth process, cementite eventually will dissolve and Mo_2C particles will reach a maximum length prior to thickening, this situation is shown in Fig. 8.8, where the dotted line represents the volume fraction of cementite, and the solid line that of Mo_2C.

The behaviour of the needle tip radius of the particle that lengthens from the first time step is shown in Fig. 8.9. Its variation depends on the matrix solute content, which is affected by cementite dissolution, growth and coarsening of other particles. Consistent with the observations of Hall *et al.* [1972], it is increased with temperature, and as expected from the depletion of solute in the matrix, it increases with time.

During the coarsening regime, the average number of particles is reduced by several orders of magnitude (Marqusee and Ross [1983]), this is confirmed in Fig. 8.10.

LSW theory predicts that the coarsening regime is accompanied by an average particle radius increase in proportion to $t^{1/3}$, an effect shown in Fig. 8.11 with the aid of the grid lines.

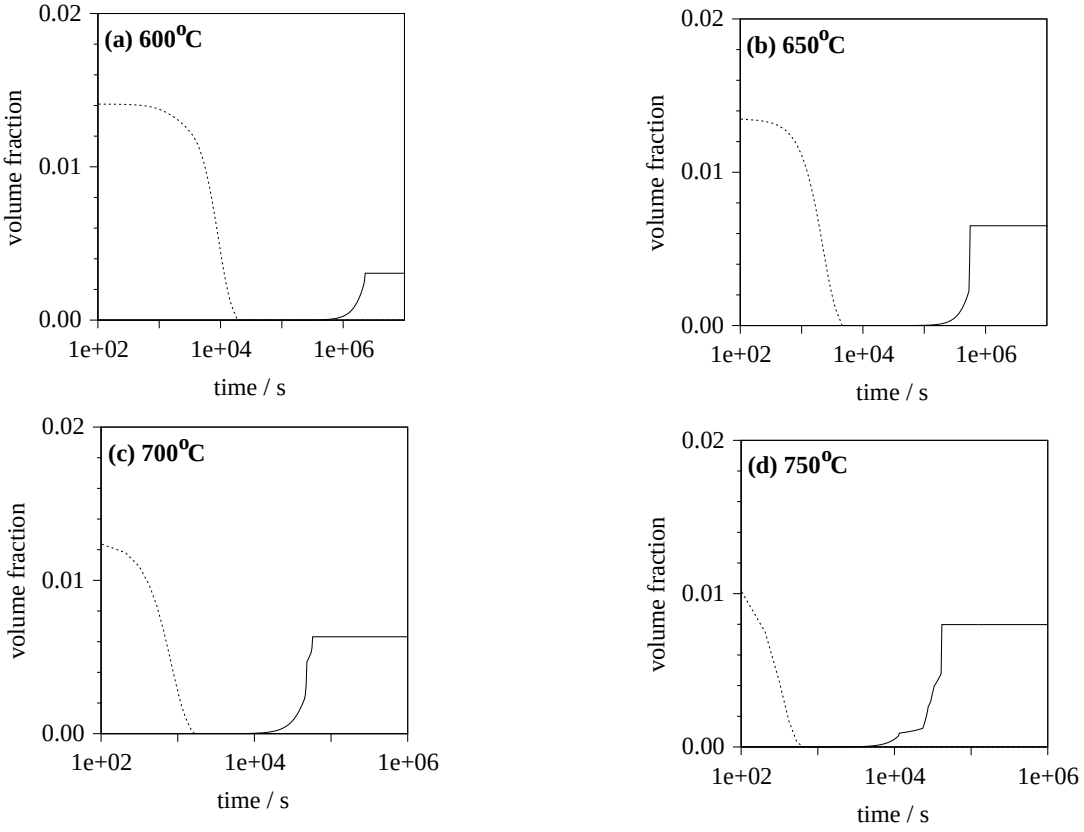

Fig. 8.8: Calculated volume fraction of cementite (dotted line) and Mo_2C (solid line) as a function of time.

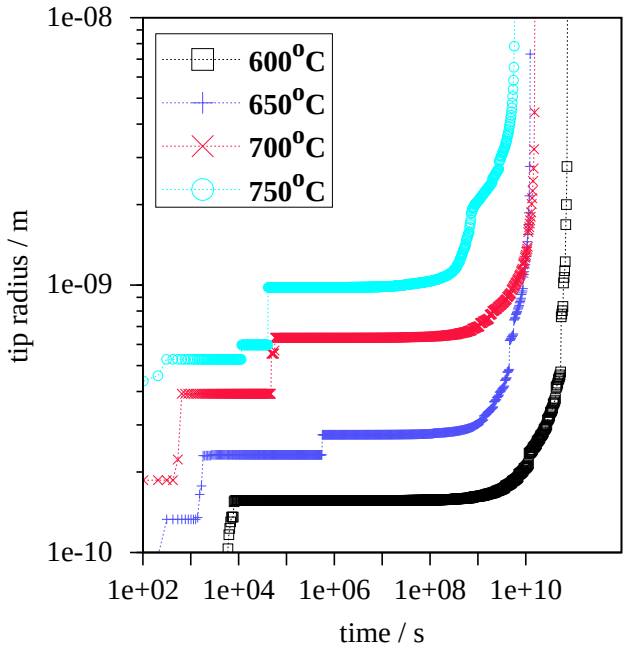

Fig. 8.9: Variation of needle tip radius with time.

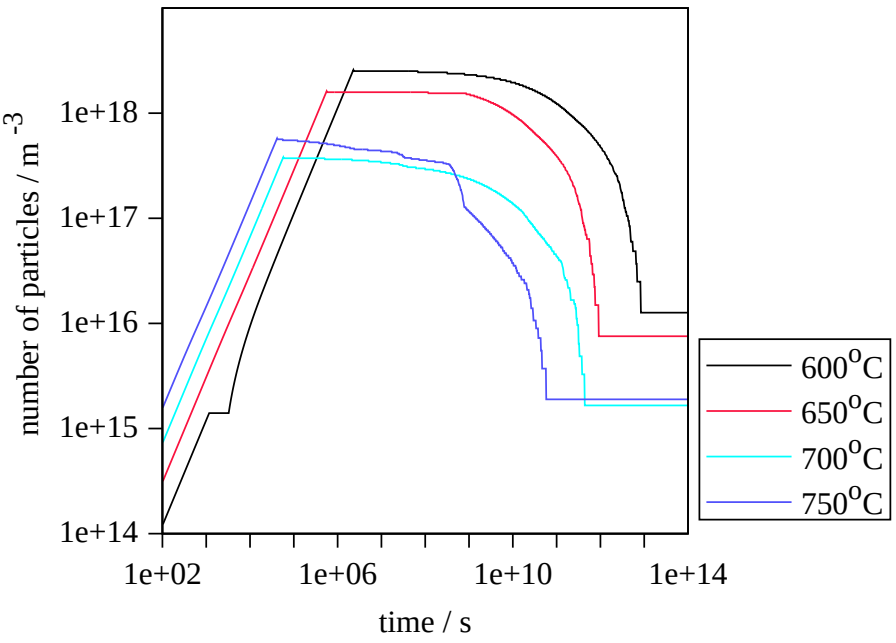

Fig. 8.10: Calculated total number of Mo_2C particles during growth (straight line) and coarsening.

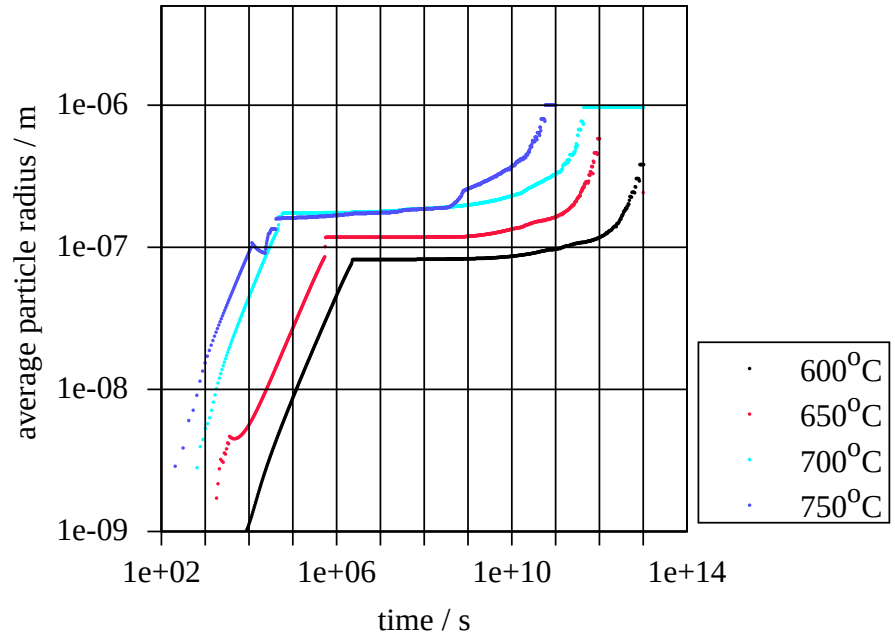

Fig. 8.11: Calculated particle average radius during growth and coarsening.

8.4 Critical assessment and conclusions

A new model to predict the overall kinetics of cementite dissolution and Mo_2C growth and coarsening has been presented. This model rigorously deals with multicomponent capillarity and diffusion effects, and treats individually each particle for thermodynamic equilibrium with

the matrix, accounting for dissolution or thickening. From Fig. 8.3, it is seen that its extension to more than three diffusing components is immediate and just depends on finding the ratio between diffusion coefficient of the components, the values of s_i, and hence obtaining the compositions and tip radius.

The agreement with measured data is good, and the method is capable of predicting particle length and thickness, and hence aspect ratio, along with the distribution of particles characterised by these. This information is essential for alloy design as mechanical properties change due to dislocation interactions with the precipitates.

This model assumes no variation of precipitate composition with curvature, this is justified for Mo_2C kinetics, but is not general. Furthermore, it has been assumed, with no justification, that coarsening starts immediately after growth, while Fig. 8.10 seems to suggest that combined growth and coarsening may occur during late growth stages due to the number of particles decrease immediately after the straight–line growth regime; however, the error seems to be small due to a small decrease in the number of particles after growth requires several orders of magnitude of time increase.

CHAPTER 9

Conclusions and suggestions for further work

A solution for the growth of spherical precipitates with capillarity in dilute ideal solutions was presented, showing that the overall effect of capillarity was to reduce the growth rate of the particle. The solution was extended to incorporate multicomponent effects in concentrated solutions.

A solution for the growth of needle and plate–shaped precipitates with small supersaturations was presented. This was extended to incorporate multicomponent diffusion, interface kinetics and capillarity effects in Henrian and concentrated solutions. The solution showed that the maximum velocity hypothesis cannot be sustained for Henrian solutions in the multicomponent scenario, and that upper and lower bounds are imposed in the Péclet number when interface kinetics and capillarity effects become prominent, respectively. The concept of interface saturation contours has been introduced in order to demonstrate that when two components of different diffusion coefficient are present in the alloy, the supersaturations required for equilibrium growth are limited depending on the curvature of the particle and interface kinetics. A methodology to simultaneously solve the mass balance equations has been presented. The method was extended for concentrated solutions.

Theory for coarsening of particles has been developed to account for composition shifts in the precipitated phase. As opposed to previous theories, the results showed that coarsening in a multicomponent system is not independent of the solution thermodynamics followed by the continuous phase.

A computational method to apply the theory for multicomponent growth of needles in concentrated alloys was presented, and applied to obtain the precipitation kinetics of Mo_2C in a secondary hardening steel of composition Fe–0.11C–1.95Mo wt.%. The results predicted by the program are in good agreement with experimental observations, and new information was cast such as the change of the needle aspect ratio and the particle size dispersion with time. This information, which was not available from previous models, will be an aid to develop alloys of improved mechanical properties.

The theory presented here can be applied to obtain the kinetics of precipitation when any number of phases and components are present; thus, it is required to extend the computational method presented here for this scenario. In doing this, the accuracy of the predictions can be improved if the surface energy is experimentally obtained via the concentration gradient

method presented by Miyazaki [1999]. A correlation between mechanical properties such as yield strength, composition and heat treatment can now be obtained through application of the dislocation theory [Dieter, 1988].

The coarsening theory presented in Chapter 7 can be experimentally validated through the study of particles whose composition significantly varies as coarsening progresses.

APPENDIX 1

This appendix presents the computer programs described in Chapter 3 that obtain the variation of the growth parameter with supersaturation (Figs. 3.2, 3.3) and the variation of the growth parameter with the particle radius (Figs. 3.4, 3.5).

The programs can be downloaded from http://www.msm.cam.ac.uk/map/mapmain.html.

1. Program MAP_ZENER_CAPI

1.1. Provenance of Source Code

P. E. J. Rivera Díaz del Castillo,
Phase Transformations and Complex Properties Group,
Department of Materials Science and Metallurgy,
University of Cambridge,
Cambridge, U.K.

1.2. Purpose

To obtain the variation of growth parameter α_3 as a function of Ω supersaturation.

1.3. Specification

This is a self-contained program written in FORTRAN 77.

1.4. Description

The program solves equation [3.11] as supersaturation is varied, and for given values of r/r_c, casting the data utilised to plot Figs. 3.2, 3.3.

1.5. References

1. Rivera-Díaz-del-Castillo, P. E. J. and Bhadeshia, H. K. D. H. [2001], *Theory for growth of spherical precipitates with capillarity effects*, *Materials Science and Technology*, **17**, 30–32.

2. Chapter 3.

1.6. Parameters

Input parameters

R - double precision

value of r/r_c.

Output parameters

O - double precision

Ω supersaturation.

GP - double precision

α_3 growth parameter.

1.7. **Error Indicators**

None.

1.8. **Accuracy**

No information supplied.

1.9. **Further Comments**

The program is set to write the results to file 'res1.d'.

1.10. **Example**

1. Program data

The data can be found in the program.

2. Program results

See sample results file 'res1.d'.

1.11. **Auxiliary Routines**

The subroutines called by this program are:

ERROR

1.12. **Keywords**

capillarity, sphere, growth, parabolic growth

2. Program MAP_ZENER_CAPI1

2.1. **Provenance of Source Code**

P. E. J. Rivera Díaz del Castillo,

Phase Transformations and Complex Properties Group,
Department of Materials Science and Metallurgy,
University of Cambridge,
Cambridge, U.K.

2.2. **Purpose**

To obtain the variation of growth parameter α_3 with adimensional sphere radius variation r/r_c.

2.3. **Specification**

This is a self-contained program written in FORTRAN 77.

2.4. **Description**

The program solves equation [3.11] as r/r_c is varied and for given values of supersaturation, casting the data utilised to plot Figs. 3.4, 3.5.

2.5. **References**

1. Rivera-Díaz-del-Castillo, P. E. J. and Bhadeshia, H. K. D. H. [2001], *Theory for growth of spherical precipitates with capillarity effects*, *Materials Science and Technology*, **17**, 30–32.

2. Chapter 3.

2.6. **Parameters**

Input parameters

O - double precision

Ω supersaturation.

Output parameters

R - double precision

value of r/r_c.

GP - double precision

α_3 growth parameter.

2.7. **Error Indicators**

None.

2.8. **Accuracy**

No information supplied.

2.9. **Further Comments**

The program is set to write the results to file 'res1.d'.

2.10. **Example**

1. Program data

The data can be found in the program.

2. Program results

See sample results file 'res1.d'.

2.11. **Auxiliary Routines**

The subroutines called by this program are:

ERROR

2.12. **Keywords**

capillarity, sphere, growth, parabolic growth

APPENDIX 2

This appendix presents the finite differences computer program described in Chapter 3 that obtains the variation of the growth parameter with supersaturation. The solution presented here is described in section 3.3, and produces data to obtain Fig. 3.7. The program presented here is set to calculate the parameters for $\Omega = 0.75$.

The program can be downloaded from http://www.msm.cam.ac.uk/map/mapmain.html.

1. Program MAP_READ75

1.1. Provenance of Source Code

P. E. J. Rivera Díaz del Castillo,
Phase Transformations and Complex Properties Group,
Department of Materials Science and Metallurgy,
University of Cambridge,
Cambridge, U.K.

1.2. Purpose

To obtain the variation of growth parameter α_3 as a function of r/r_c for different values of Ω supersaturation.

1.3. Specification

This is a self–contained program written in FORTRAN 77.

1.4. Description

The program solves equations [3.13–3.16] as r/r_c is varied and for given values of Ω, producing data utilised to plot Fig. 3.7.

1.5. References

1. Chapter 3.

1.6. Parameters

Input parameters

none

Output parameters

AL - double precision array of size 50

α_3 growth parameter for small growth rates.

IC - double precision array of size 50×2

$g \times r_c/D$ for small growth rates.

RHOR - double precision

r/r_c adimensional radius.

PRALPH - double precision

α_3 growth parameter.

PRSP - double precision

$g \times r_c/D$.

1.7. Error Indicators

None.

1.8. Accuracy

No information supplied.

1.9. Further Comments

The program is set to write the results to file 'read75.d'.

1.10. Example

1. Program data

The data can be found in the program.

2. Program results

See sample results file 'read75.d'.

1.11. Auxiliary Routines

The subroutines called by this program are:

ZENER

ERROR

AC

1.12. Keywords

capillarity, sphere, growth, parabolic growth, finite differences, numerical solution

APPENDIX 3

This appendix presents the computer programs referred in Chapter 4 that obtain the functions S_1, S_2 and R_1, R_2 for plate and needle growth, respectively, which have been plotted in Fig. 4.2, 4.3.

The programs can be downloaded from http://www.msm.cam.ac.uk/map/mapmain.html.

1. Program MAP_PARAMETER_S1

1.1. Provenance of Source Code

P. E. J. Rivera Díaz del Castillo,
Phase Transformations and Complex Properties Group,
Department of Materials Science and Metallurgy,
University of Cambridge,
Cambridge, U.K.

1.2. Purpose

To obtain the variation of functions S_1, S_2 with Péclet number p.

1.3. Specification

This is a self-contained program written in FORTRAN 77.

1.4. Description

The program obtains the variation of S_1, S_2 functions defined in section 4.3.

1.5. References

1. Rivera-Díaz-del-Castillo, P. E. J. and Bhadeshia, H. K. D. H. [2001], *Growth of needle and plate shaped particles: theory for small supersaturations, maximum velocity hypothesis*, *Materials Science and Technology*, **17**, 25–29.

2. Chapter 4.

1.6. Parameters

Input parameters

none

Output parameters

N1, N2 - double precision

M_1, M_2 functions.

S1, S2 - double precision

S_1, S_2 functions.

P - double precision

Péclet number p.

1.7. **Error Indicators**

None.

1.8. **Accuracy**

No information supplied.

1.9. **Further Comments**

The program is set to write the results to files 'res1.d', 'res2.d'.

1.10. **Example**

1. Program data

The data can be found in the program.

2. Program results

See sample results file 'res1.d', 'res2.d'.

1.11. **Auxiliary Routines**

The subroutines called by this program are:

ERROR

GAMMA

LGAMA

CHGU

PSI

1.12. **Keywords**

capillarity, interface kinetics, plate, growth, Trivedi

2. Program MAP_PARAMETER_R1

2.1. Provenance of Source Code

P. E. J. Rivera Díaz del Castillo,

Phase Transformations and Complex Properties Group,

Department of Materials Science and Metallurgy,

University of Cambridge,

Cambridge, U.K.

2.2. Purpose

To obtain the variation of functions R_1, R_2 with Péclet number p.

2.3. Specification

This is a self-contained program written in FORTRAN 77.

2.4. Description

The program obtains the variation of R_1, R_2 functions defined in section 4.2.

2.5. References

1. Rivera-Díaz-del-Castillo, P. E. J. and Bhadeshia, H. K. D. H. [2001], *Growth of needle and plate shaped particles: theory for small supersaturations, maximum velocity hypothesis*, *Materials Science and Technology*, **17**, 25–29.

2. Chapter 4.

2.6. Parameters

Input parameters

none

Output parameters

N1, N2 - double precision

N_1, N_2 functions.

R1, R2 - double precision

R_1, R_2 functions.

P - double precision

Péclet number p.

2.7. Error Indicators

None.

2.8. Accuracy

No information supplied.

2.9. Further Comments

The program is set to write the results to files 'res1.d', 'res2.d'.

2.10. Example

1. Program data

The data can be found in the program.

2. Program results

See sample results file 'res1.d', 'res2.d'.

2.11. Auxiliary Routines

The subroutines called by this program are:

ERROR

GAMMA

LGAMA

CHGU

CHGUS

CHGUL

CHGUBI

CHGUIT

INTE

PSI

2.12. Keywords

capillarity, interface kinetics, needle, growth, Trivedi

APPENDIX 4

This appendix presents the computer programs referred in Chapter 4 that obtain the variation of supersaturation with Péclet number and tip radius for plates and needles.

The programs can be downloaded from http://www.msm.cam.ac.uk/map/mapmain.html.

1. Program MAP_PLATE2

1.1. Provenance of Source Code

P. E. J. Rivera Díaz del Castillo,
Phase Transformations and Complex Properties Group,
Department of Materials Science and Metallurgy,
University of Cambridge,
Cambridge, U.K.

1.2. Purpose

To obtain the variation of Ω with Péclet number p and the ratio of the plate tip radius and the critical radius for nucleation r/r_c. The output of this program is plotted in Figs. 4.6, 4.7.

1.3. Specification

This program reads the value of q, and a table with the variation of M_1 and M_2 with p from the input data file 'indat11.d', and writes the output in the file 'res1.d'. The code is written in FORTRAN 77.

1.4. Description

The program obtains the variation of Ω with p and r/r_c by simultaneously solving equations [4.9] and [4.10].

1.5. References

1. Rivera-Díaz-del-Castillo, P. E. J. and Bhadeshia, H. K. D. H. [2001], *Growth of needle and plate shaped particles: theory for small supersaturations, maximum velocity hypothesis*, *Materials Science and Technology*, **17**, 25–29.

2. Chapter 4.

1.6. **Parameters**

Input parameters

Q - double precision

q, characterises relative importance of interface kinetics and diffusion effects.

PEC - double precision array of size 6053

Péclet number p.

N1, N2 - double precision arrays of size 6053

M_1, M_2 functions.

Output parameters

O - double precision

Supersaturation Ω.

RRR - double precision

Value of r/r_c.

P - double precision

Péclet number p.

1.7. **Error Indicators**

None.

1.8. **Accuracy**

No information supplied.

1.9. **Further Comments**

The program is set to write the results to file 'res1.d'.

1.10. **Example**

1. Program data

See input data file 'indat11.d'.

2. Program results

See sample results file 'res1.d'.

1.11. **Auxiliary Routines**

The subroutines called by this program are:

ERROR

1.12. **Keywords**

capillarity, interface kinetics, plate, growth, Trivedi

2. Program MAP_PLATE3

2.1. **Provenance of Source Code**

P. E. J. Rivera Díaz del Castillo,
Phase Transformations and Complex Properties Group,
Department of Materials Science and Metallurgy,
University of Cambridge,
Cambridge, U.K.

2.2. **Purpose**

To obtain the variation of small values of Ω with Péclet number p and the ratio of the plate tip radius and the critical radius for nucleation r/r_c. The output of this program is plotted in Figs. 4.10, 4.11.

2.3. **Specification**

This program reads the value of q, and a table with the variation of M_1 and M_2 with p from the input file 'indat11.d', and writes the output in the file 'res1.d'. The code is written in FORTRAN 77.

2.4. **Description**

The program obtains the variation of Ω with p and r/r_c by simultaneously solving equations [4.9] and [4.10].

2.5. **References**

1. Rivera-Díaz-del-Castillo, P. E. J. and Bhadeshia, H. K. D. H. [2001], *Growth of needle and plate shaped particles: theory for small supersaturations, maximum velocity hypothesis*, *Materials Science and Technology*, **17**, 25–29.

2. Chapter 4.

2.6. **Parameters**

Input parameters

Q - double precision

q, characterises relative importance of interface kinetics and diffusion effects.

PEC - double precision array of size 6053

Péclet number p.

N1, N2 - double precision arrays of size 6053

M_1, M_2 functions.

Output parameters

O - double precision

Supersaturation Ω.

RRR - double precision

Value of r/r_c.

P - double precision

Péclet number p.

2.7. Error Indicators

None.

2.8. Accuracy

No information supplied.

2.9. Further Comments

The program is set to write the results to file 'res1.d'.

2.10. Example

1. Program data

See input data file 'indat11.d'.

2. Program results

See sample results file 'res1.d'.

2.11. Auxiliary Routines

The subroutines called by this program are:

ERROR

2.12. Keywords

capillarity, interface kinetics, plate, growth, Trivedi, low supersaturations

3. Program MAP_NEEDLE2

3.1. Provenance of Source Code

P. E. J. Rivera Díaz del Castillo,
Phase Transformations and Complex Properties Group,
Department of Materials Science and Metallurgy,
University of Cambridge,
Cambridge, U.K.

3.2. Purpose

To obtain the variation of Ω with Péclet number p and the ratio of the needle tip radius and the critical radius for nucleation r/r_c. The output of this program is plotted in Figs. 4.4, 4.5.

3.3. Specification

This program reads the value of q^*, and a table with the variation of N_1 and N_2 with p from the input file 'indat11.d', and writes the output in the file 'res1.d'. The code is written in FORTRAN 77.

3.4. Description

The program obtains the variation of Ω with p and r/r_c by simultaneously solving equations [4.4] and [4.5].

3.5. References

1. Rivera-Díaz-del-Castillo, P. E. J. and Bhadeshia, H. K. D. H. [2001], *Growth of needle and plate shaped particles: theory for small supersaturations, maximum velocity hypothesis*, *Materials Science and Technology*, **17**, 25–29.
2. Chapter 4.

3.6. Parameters

Input parameters

Q - double precision

q^*, characterises relative importance of interface kinetics and diffusion effects.

PEC - double precision array of size 20010

Péclet number p.

N1, N2 - double precision arrays of size 20010

N_1, N_2 functions.

Output parameters

O - double precision

Supersaturation Ω.

RRR - double precision

Value of r/r_c.

P - double precision

Péclet number p.

3.7. Error Indicators

None.

3.8. Accuracy

No information supplied.

3.9. Further Comments

The program is set to write the results to file 'res1.d'.

3.10. Example

1. Program data

See input data file 'indat11.d'.

2. Program results

See sample results file 'res1.d'.

3.11. Auxiliary Routines

The subroutines called by this program are:

E1XB

3.12. Keywords

capillarity, interface kinetics, needle, growth, Trivedi

4. Program MAP_NEEDLE3

4.1. Provenance of Source Code

P. E. J. Rivera Díaz del Castillo,

Phase Transformations and Complex Properties Group,

Department of Materials Science and Metallurgy,

University of Cambridge,

Cambridge, U.K.

4.2. Purpose

To obtain the variation of small values of Ω with Péclet number p and the ratio of the needle tip radius and the critical radius for nucleation r/r_c. The output of this program is plotted in Figs. 4.8, 4.9.

4.3. Specification

This program reads the value of q^*, and a table with the variation of N_1 and N_2 with p from the input file 'indat11.d', and writes the output in the file 'res1.d'. The code is written in FORTRAN 77.

4.4. Description

The program obtains the variation of Ω with p and r/r_c by simultaneously solving equations [4.4] and [4.5].

4.5. References

1. Rivera-Díaz-del-Castillo, P. E. J. and Bhadeshia, H. K. D. H. [2001], *Growth of needle and plate shaped particles: theory for small supersaturations, maximum velocity hypothesis*, *Materials Science and Technology*, **17**, 25–29.

2. Chapter 4.

4.6. Parameters

Input parameters

Q - double precision

q^*, characterises relative importance of interface kinetics and diffusion effects.

PEC - double precision array of size 20010

Péclet number p.

N1, N2 - double precision arrays of size 20010

N_1, N_2 functions.

Output parameters

O - double precision

Supersaturation Ω.

RRR - double precision

Value of r/r_c.

P - double precision

Péclet number p.

4.7. **Error Indicators**

None.

4.8. **Accuracy**

No information supplied.

4.9. **Further Comments**

The program is set to write the results to file 'res1.d'.

4.10. **Example**

1. Program data

See input data file 'indat11.d'.

2. Program results

See sample results file 'res1.d'.

4.11. **Auxiliary Routines**

The subroutines called by this program are:

E1XB

4.12. **Keywords**

capillarity, interface kinetics, needle, growth, Trivedi, low supersaturations

APPENDIX 5

This appendix presents the computer program that extracts from MTDATA the thermodynamic parameters required by the model described in Chapter 8.

The program can be downloaded from http://www.msm.cam.ac.uk/map/mapmain.html.

1. Program MAP_CHEM_POT6

1.1. Provenance of Source Code

P. E. J. Rivera Díaz del Castillo,
Phase Transformations and Complex Properties Group,
Department of Materials Science and Metallurgy,
University of Cambridge,
Cambridge, U.K.

1.2. Purpose

To obtain the variation of chemical potentials and equilibrium precipitate and matrix compositions of a system at a given temperature as the pressure of the system is incremented.

1.3. Specification

This program is to be compiled and run with the aid of MTDATA [1995].

1.4. Description

The program varies the pdV or pressure term in MTDATA, and thus allows to obtain the change in equilibrium compositions of a system as the pressure or the surface energy term is varied. For each pressure value the equilibrium compositions of the matrix and precipitate are calculated, and the chemical potential of each component are obtained. The program presented here is set to run for 600°C.

1.5. References

1. Chapter 8.

1.6. Parameters

Input parameters

none

Output parameters

AVC - double precision

Average concentration of C in the alloy.

AVMO - double precision

Average concentration of Mo in the alloy.

PRESS - double precision

System pressure.

FC - double precision array of size 2500

Ferrite concentration of C.

FMO - double precision array of size 2500

Ferrite concentration of Mo.

CC - double precision array of size 2500

Mo_2C concentration of C.

CMO - double precision array of size 2500

Mo_2C concentration of Mo.

CPC - double precision array of size 2500

Chemical potential of C.

CPM - double precision array of size 2500

Chemical potential of Mo.

CPF - double precision array of size 2500

Chemical potential of Fe.

1.7. Error Indicators

None.

1.8. Accuracy

No information supplied.

1.9. Further Comments

The program is set to write the results to file 'chem.out'.

1.10. Example

1. Program data

The data can be found in the program.

2. Program results

See sample results file 'chem.out'.

1.11. Auxiliary Routines

The are no subroutines used in this program.

1.12. Keywords

thermodynamic parameters, pressure, surface energy, MTDATA

APPENDIX 6

This appendix presents the computer program associated to the computational model described in Chapter 8 and aimed to predict the kinetics of nucleation–growth–coarsening of a secondary hardening steel.

The program can be downloaded from http://www.msm.cam.ac.uk/map/mapmain.html.

1. Program MAP_CINFLE1

1.1. Provenance of Source Code

P. E. J. Rivera Díaz del Castillo,
Phase Transformations and Complex Properties Group,
Department of Materials Science and Metallurgy,
University of Cambridge,
Cambridge, U.K.

1.2. Purpose

To predict the kinetics of nucleation, growth and coarsening of Mo_2C precipitating in Fe–0.11C–1.95Mo wt.%.

1.3. Specification

This is a self–contained program written in FORTRAN 77.

1.4. Description

The program calculates the nucleation–growth–coarsening of Mo_2C particles in a ferrite matrix. The calculations are divided in time steps as precipitation progresses, and rigorously account for mass balance and thermodynamic equilibrium of each particle at every time step.

The program is set to read data from next input files:

indat11.d - table with variation of N_1, N_2 functions with p

chem.out - thermodynamic data (see Appendix 5).

The program is set to write the results in five files:

d1.d - kinetics of all the particles nucleating at any time step

d2.d - kinetics of particle that nucleates in the first step

d3.d - kinetics of needle nucleated at time step 16

d4.d - overall kinetics, total volume fractions and matrix concentration

d5.d - evolution of longest needle with time, and size distribution

1.5. References

1. Chapter 8.

1.6. Parameters

Input parameters

AC - double precision

Average concentration of C in the alloy.

AM - double precision

Average concentration of Mo in the alloy.

PR - double precision

System pressure.

CCAB - double precision array of size 100000

Ferrite concentration of C.

CMAB - double precision array of size 100000

Ferrite concentration of Mo.

CCBA - double precision array of size 100000

Mo_2C concentration of C.

CMBA - double precision array of size 100000

Mo_2C concentration of Mo.

MUC - double precision array of size 100000

Chemical potential of C.

MUM - double precision array of size 100000

Chemical potential of Mo.

MUF - double precision array of size 100000

Chemical potential of Fe.

SIG - double precision

Surface energy per unit area.

QC - double precision

Carbon activation energy for diffusion.

QM - double precision

Mo activation energy for diffusion.

NO - double precision

Initial number of Mo_2C nucleation sites.

VB - double precision

Molar volume of Mo_2C.

DOC - double precision

Diffusivity of C in ferrite.

DOM - double precision

Diffusivity of Mo in ferrite.

CTHB - double precision

Intergranular cementite plate thickness.

CTHG - double precision

Grain cementite plate thickness.

MOLC - double precision

Paraequilibrium cementite mol number.

MOLF - double precision

Paraequilibrium ferrite mol number.

TEM - double precision

Temperature.

CCCA - double precision

Paraequilibrium cementite C concentration.

MCCA - double precision

Paraequilibrium cementite Mo concentration.

CCAC - double precision

Paraequilibrium ferrite C concentration.

MCAC - double precision

Paraequilibrium ferrite Mo concentration.

Output parameters

ETIM - double precision

Time.

LEN - double precision array of size 1000×1000

Needle length.

TH - double precision array of size 1000×1000

Needle thickness.

AVRA - double precision array of size 1000

Average needle interface radius.

RRIN - double precision array of size 1000

Needle tip radius.

VE - double precision array of size 1000×1000

Needle lengthening rate.

NS - double precision array of size 10000

Number of nucleation sites.

ASRA - double precision array of size 1000×1000

Needle aspect ratio.

DACC - double precision

Instant C matrix concentration.

DACM - double precision

Instant Mo matrix concentration.

TAPR - double precision

Total average needle interface radius.

TNP - double precision

Total number of particles.

TVF - double precision

Total volume fraction.

CAR - double precision

Coarsening needle average radius.

IVFC - double precision

Instant cementite volume fraction.

MALE - double precision

Length of longest needle.

MATH - double precision

Thickness of the longest needle.

AVLE - double precision

Average particle length.

SDLE - double precision

Standard deviation of length.

1.7. Error Indicators

None.

1.8. Accuracy

No information supplied.

1.9. Further Comments

none.

1.10. Example

1. Program data

The data can be found in the program.

2. Program results

See sample results file 'chem.out'.

1.11. Auxiliary Routines

The are no subroutines used in this program.

1.12. Keywords

secondary hardening, kinetics, precipitation, Trivedi

Bibliography

Aaronson, H. I., Lee, J. K. [1978], *Proc. Symp. on Precipitation Processes in Solids: Met. Soc. AIME*, edited by Russel, K. C. and Aaronson, H. I., 31.

Abramowitz, M. [1965], *Handbook of Mathematical Functions*, *Wiley: New York.*

Akamatsu, S., Senuma, T. and Hasebe, M. [1992], *Iron and Steel Institute of Japan International*, **32**, 275.

Avrami, M. [1939], *J. Chem. Phys.*, **7**, 1103; *Ibid.* **8**, 212 [1940]; *Ibid.* **9**, 177 [1941]

Baker, R. G., Nutting, J. [1959], *J. Iron Steel Institute*, **192**, 257.

Bhadeshia, H. K. D. H. [1985a], *Progress in Mater. Sci.*, **29**, 321.

Bhadeshia, H. K. D. H. [1985b], *Mater. Sci. Technol.*, **1**, 497.

Bhadeshia, H. K. D. H. [1989], *Mater. Sci. Technol.*, **5**, 131.

Bhadeshia, H. K. D. H. [1998], *International Materials Reviews*, **43**, **2**, 45.

Bhadeshia, H. K. D. H. [1999], *Mater. Sci. Technol.*, **15**, 22.

Bolling, G. F., Tiller, W. A. [1961], *J. Appl. Phys.*, **32**, 2587.

Cahn, J. W. and Larché, F. [1982], *Acta Metall.*, **30**, 51.

Calderón, H. A. *et. al.* [1994], *Acta Metall.*, **42**, 991.

Callen, H. B. [1985], *Thermodynamics and an Introduction to Thermostatistics*, *Second Edition*, *John Wiley: New York.*

Chaix, J. M., Eustathopoulos, N. and Allibert, C.H. [1986], *Acta Metall.*, **34**, 1589.

Chaix, J. M. and Allibert, C.H. [1986], *Acta Metall.*, **34**, 1593.

Coates, D. E. [1972], *Metall. Trans.*, **3**, 1203.

Coates, D. E. [1973a], *Metall. Trans.*, **4**, 1077.

Coates, D. E. [1973b], *Metall. Trans.*, **4**, 2313.

Cottrell, A. [1995], *An Introduction to Metallurgy, Second Edition, The Institute of Materials*: London.

Christian, J. W. [1975], *Transformations in Metals and Alloys, Part I, Pergamon Press: Oxford.*

DeHoff, R. T. [1981], *Proc. Int. Conf. on Solid → Solid Phase Transformations: TMS-AIME*, Warrendale: Pennsylvania, 503.

DeHoff, R. T. [1993], *Thermodynamics in Materials Science*, McGraw–Hill, Second Edition: New York, London.

Dieter, G. E. [1988], *Mechanical Metallurgy, McGraw–Hill: London.*

Edmonds, D. V., Honeycombe, R. W. K. [1978], *Proc. Symp. on Precipitation Processes in Solids: Met. Soc. AIME*, edited by Russel, K. C. and Aaronson, H. I., 121.

Fujita, N., Bhadeshia, H. K. D. H. [1998], *Precipitation Reactions in 3Cr1.5Mo Power Plant Steel, Advanced Heat Resistant Steel for Power Generation*, edited by R. Viswanathan and J. Nutting: *Ins. of Mater.: London*, 223.

Fujita, N., Bhadeshia, H. K. D. H. [1999], *Mater. Sci. Technol.*, **15**, 627.

Fujita, N., Bhadeshia, H. K. D. H. [2000], *Ph. D. Thesis*, University of Cambridge.

Fujita, N., Bhadeshia, H. K. D. H. [2001], *Mater. Sci. Technol.*, **17**, 403.

Fridberg, J., Torndahl, L., Hillert, M. [1969], *Jerkontorets Ann.*, **153**, 263.

Gradshtein, I. S. [1965], *Table of Integrals, series and products, Academic Press*, 86.

Greenwood, G. W. [1956], *Acta Metall.*, 4, 243.

Gustafson, Å., Höglund, L. and Ågren, J. [1998], *Advanced Heat Resistant Steel for Power Generation*, ed. Viswanathan, R. and Nutting, J., The Institute of Materials 270.

Hall, M. G., Kinsman, K. R., Aaronson, H. I. [1972], *Metall. Trans.*, **3**, 1320.

Hillert, M. [1957], *Jernkontorets Ann.*, **141**, 757.

Honeycombe, R. W. K. [1976], *Metall. Trans. A*, **7A**, 915.

Horvay, G., Cahn, J. W. [1961], *Acta Metall.*, **9**, 695.

Ivanstov, G. P. [1947], *Dokl. Akad. Nauk, SSSR*, **58**, 567.

Johnson, W. A. and Mehl, R. F. [1939], *Transactions of the American Institute of Mining and Metallurgical Engineers*, **135**, 416.

Kasuya, T., Ichikawa, K., Fuji, M., Bhadeshia, H. K. D. H., [1999], *Mater. Sci. Technol.*, **15**, 471.

Kotler, G. R., Tarshis, L. A. [1969], *Journal of Crystal Growth*, **5**, 90.

Kuenmann, C. J. and Voorhees, P. W. [1996], *Metall. and Mater. Trans. A*, **27A**, 937.

Kulkarni, N. and DeHoff, R. T. [1997], *Acta Mater.*, **45**, 4963.

Lee, H. M., Allen, S. M. and Grujicic M.. [1991a], *Metall. Trans. A*, **22A**, 2863.

Lee, H. M., Allen, S. M. and Grujicic M. [1991b], *Metall. Trans. A*, **22A**, 2869.

Lee, H. M. and Allen, S. M. [1991c], *Metall. Trans. A*, **22A**, 2877.

Leo, P.H. and Sekerka, R.F. [1989], *Acta Metall.*, **37**, 3139.

Liu, W. J. and Jonas, J. J. [1988], *Metall. Transactions*, **19A**, 1403.

Lupis, C. H. P. [1983], *Chemical Thermodynamics of Materials*, *New York: North-Holland.*

Lifshitz, I. M. and Slyozov, V. V. [1961], *J. Phys. Chem. Solids*, **19**, 35.

Marqusee J. A. and Ross J. [1983], *J. Chem. Phys.*, **79**, 373.

Miyazaki, T., Koyama, T., Kobayashi, S. [1996], *Metall. and Materials Trans. A*, **27A**, 945.

Miyazaki, T. [1999], *Solid–solid phase transformations '99, Japan Institute of Metals*, ed. by Koiowa, M., Otsuka, K. and Miyazaki, T., Japan, 15.

Miyahara, K., Hwang, J. H., Shimoide, Y., Iwamoto, T. and Hosoi, Y. [1991], *Journal of Japan Institute of Metals*, **59**, 512.

Morral, J. E. and Purdy, G. R. [1994], *Scripta Metall. et Materialia*, **30**, 905.

"MTDATA: Metallurgical and thermochemical databank", National Physical Laboratory, Teddington, Middx, UK, 1995.

Nishimori, H. and Onuki, A. [1991], *J. Phys. Soc. Japan*, **60**, 1208.

Okamoto, R. and Suehiro, H. [1998], *Tetsu to Hagane*, **84**, 12.

Olson, G. B. [1997], *Science*, **277**, 1237.

Purdy, G. R. [1971], *Metall. Sci. J.*, **5**, 81.

Robson, J.D., Bhadeshia, H. K. D. H. [1996], *A New Model for Simultaneous Transformation Kinetics in Power Plant Steels*, *Proceedings of Creep '96: Creep Resistant Metallic Materials*, *Vítkovice, Ostrava, Czech Republic*, 83.

Robson, J. D., Bhadeshia, H. K. D. H. [1997a], *Mater. Sci. Tecnol.*, **13**, 631.

Robson, J. D., Bhadeshia, H. K. D. H. [1997b], *Mater. Sci. Tecnol.*, **13**, 640.

Robson, J. D., Bhadeshia, H. K. D. H. [1997c], *Microstructural Development and Stability in High Chromium Ferritic Power Plant Steels*, *Microstructure of High Temperature Materials*, *CALPHAD*, *Institute of Materials*, 179.

Robson, J. D., Bhadeshia, H. K. D. H. [1997d], *Microstructural Development and Stability in High Chromium Ferritic Power Plant Steels*, *Kinetics of Precipitation Reactions in Ferritic Power Plant Steels*, *CALPHAD*, *Institute of Materials*, 395.

Robson, J. D., Bhadeshia, H. K. D. H. [1997e], *Kinetics of Precipitation in Power Plant Steels* *CALPHAD*, *Institute of Materials*, 447.

Saito, Y., Shiga, C. and Enami, T. [1988], *Proceedings of International Conference on Physical Metallurgy of Thermochemical Processing of Steel and Other Metals*, ed. Tamura, I., Japan **2** 753.

Simoen, E. P. and Trivedi, R. [1977], *Acta Metall.*, **25** 945.

Tanzilli, R. A. and Heckel, R. W. [1968], *Transactions of the Metallurgical Society of AIME*, **242** 2313.

Temkin, D. E. [1960], *Dok. Akad. Nauk SSSR*, **132** 1307.

Tilman, C. J., Edmonds, D. V. [1974], *Mater. Sci. Technol.*, 456.

Trivedi, R. and Pound, G. M. [1969], *Journal of Applied Physics*, **40**, 4293.

Trivedi, R. [1970a], *Acta Metall.*, **18**, 237.

Trivedi, R. [1970b], *Acta Metall.*, **1**, 921.

Trivedi, R. [1975], *Lectures on the Theory of Phase Transformations*, ed. Aaronson, H. I., *New York: AIME.*

Umanstev, A. and Olson G. B. [1993], *Scripta Metall. Mater.*, **29**, 1135.

Wagner, C. [1961], *Z. Electrochem.*, **65**, 581.

Wilson, E. A. [1983], *Worked Examples in the Kinetics and Thermodynamics of Phase Transformations*, *The Institution of Metallurgists: London.*

Wilkinson, D. [2000], *Mass Transport in Solids and Fluids*, *Cambridge University Press.*

Zhang, S. [1996], *Computation of Special Functions*, *New York: Wiley.*

Zener, C. [1946], *Trans. AIME*, **167**, 550.

Zener, C. [1949], *Journal of Applied Physics*, **20**, 950.

Zwillinger, D. [1998], *Handbook of Differential Equations*, Third Edition, *Academic Press.*